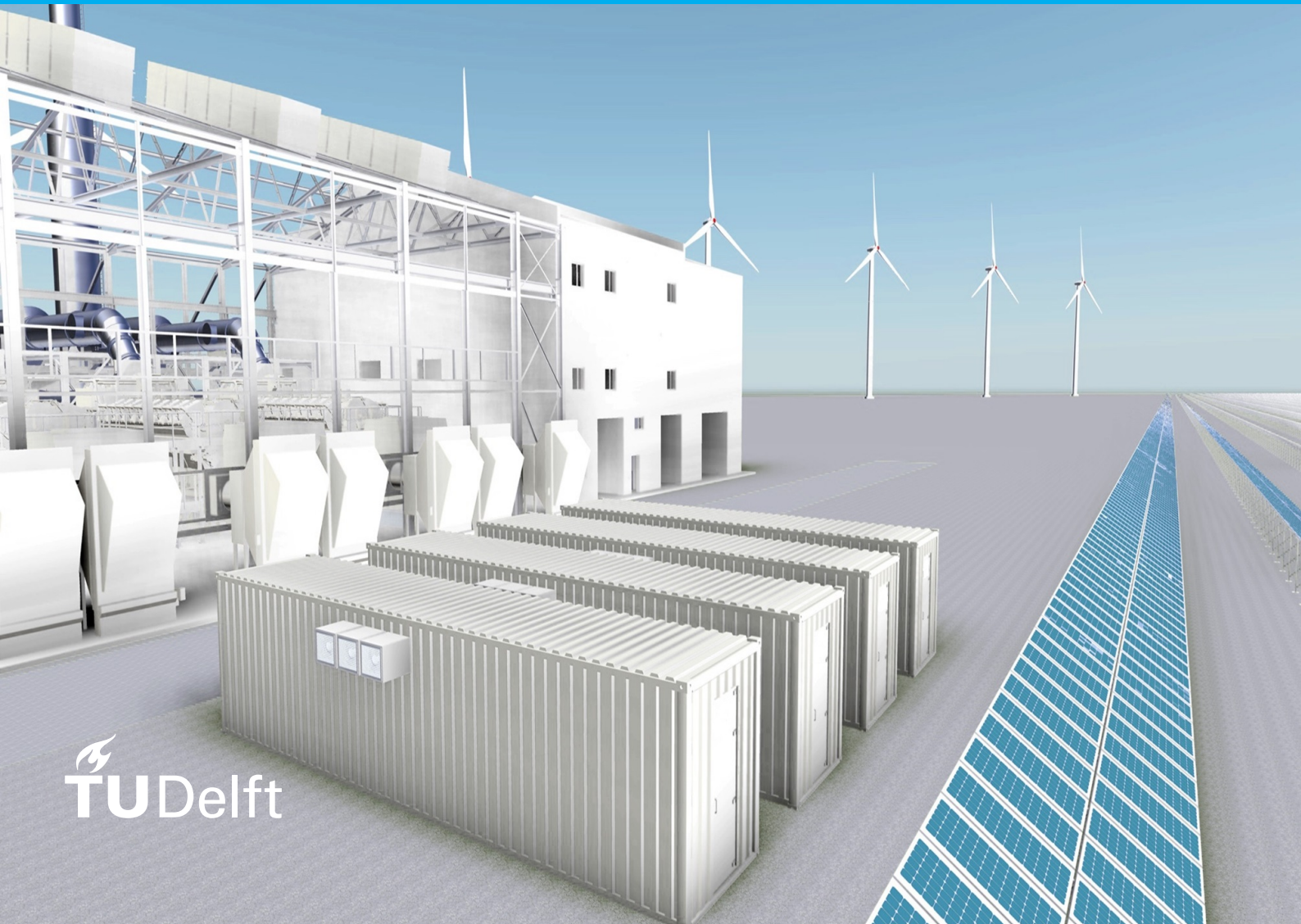


Investigating Hidden Flexibilities Provided by Power-to-X Consid- ering Grid Support Strategies

Master Thesis

B. Caner Yağcı

Intelligent Electrical Power Grids



Investigating Hidden Flexibilities Provided by Power-to-X Considering Grid Support Strategies

Master Thesis

by

B. Caner Yağcı

to obtain the degree of Master of Science
at the Delft University of Technology,
to be defended publicly on Tuesday August 26, 2020 at 15:00.

Student number: 4857089
Project duration: December 2, 2019 – August 26, 2020
Thesis committee:
Dr. Milos Cvetkovic, TU Delft, supervisor
Dr. ir. J. L. Rueda Torres, TU Delft
Dr. L. M. Ramirez Elizando TU Delft

This thesis is confidential and cannot be made public until August 26, 2020.

An electronic version of this thesis is available at <http://repository.tudelft.nl/>.



Preface

First of all, I would like to thank PhD. Digvijay Gusain and Dr. Milos Cvetkovic for not only teaching me the answers through this journey, but also giving me the perception of asking the right questions that lead simple ideas into unique values.

I would also like to thank my family Alican, Huriye, Uğur, Gökhan who have been supporting me from the beginning of this journey and more. You continue inspiring me to find my own path and soul, even from miles away. Your blessing is my treasure in life... My friends, Onurhan and Berke. You encourage me and give me confidence to be my best in any scene. You are two extraordinary men who, I know, will always be there when I need.

Finally, I would like to thank TU Delft staff and my colleagues in TU Delft for making this journey entertaining and illuminative for me.

*B. Caner Yağız
Delft, August 2020*

Contents

List of Figures	vii
List of Tables	ix
1 Introduction	1
1.1 Background	1
1.2 Literature Review	3
1.2.1 Flexibility	3
1.2.2 Multi-Energy Systems	4
1.2.3 Energy Management of Multi-Energy Systems	7
1.3 Problem Definition	8
1.4 Previous Work	9
1.5 Research Questions & Objective	9
1.6 Research Approach	10
1.7 Outline	11
2 Considered Energy System	13
2.1 Energy Production	13
2.2 Energy Demand	15
2.3 Agent Based Hierarchical Control	16
2.4 Input Data	17
2.5 Analysis	19
2.5.1 Multi-Energy System Analysis	19
2.5.2 Power-to-X Model Analysis	20
2.5.3 Power System Analysis	20
2.6 Simulation Tools	20
2.6.1 OpenModelica	21
2.6.2 Pandapower	21
2.6.3 EnergySim	21
3 Modelling	23
3.1 Industrial Loads	23
3.1.1 Power-to-Gas	23
3.1.2 Power-to-Heat	28
3.1.3 Electrical Base Load	33
3.2 Electrical Network & Optimal Power Flow	33
3.2.1 Formulation of the Optimization Problem	33
3.3 Co-simulation Setup	34
4 Results & Discussions	37
4.1 Model Validation	37
4.2 Analysis	39
4.2.1 Multi-Energy System Analysis	39
4.2.2 Power-to-X Model Analysis	40
4.2.3 Power System Analysis	43
5 Conclusion & Future Work	49
5.1 Conclusion	49
5.2 Contributions	50
5.3 Recommendations for future work	50

A Historical Data Processing & Probabilistic Weather	51
B Wind Farm & PV Farm Data	53
C Ambient Temperature & Energy Demand Data	57
D R134a Pressure - Enthalpy Table	59
E Key Modelling Assumptions	61
E.1 Power-to-Gas	61
E.2 Power-to-Heat	61
E.3 Multi-Energy System	61
F Modelica Power-to-Gas Model Parameters	63
G Modelica Power-to-Heat Model Parameters	65
Bibliography	67

List of Figures

1.1 Energy-related carbon dioxide emissions with current policies compared to accelerated uptake of renewables (REmap), 2010–2050 [29]	2
1.2 Sources of power system flexibility [63]	4
1.3 An exemplary flexible load measure with the corresponding parameters [59]	5
1.4 Schematic illustration of main inputs, products, processes and technologies of different Power-to-X process chains and their classification [31]	6
1.5 Interconnections of power-to-heat options with electricity and district heating networks [9]	7
1.6 Shares of renewables in the energy mix of the power sector, the transport sector, and heat [53]	8
1.7 Communication between simulation tools	11
2.1 Electrical side of the MES	13
2.2 Location of the 100 MW wind park in Maasvlakte	14
2.3 Location of the 100 MW solar park in Maasvlakte	14
2.4 Coupled multiphysic phenomena involved in an electrolysis stack [44]	15
2.5 Heating Cycle of Water	16
2.6 Flow chart of higher control level of MES	17
2.7 The relation between ambient temperature and hydrogen & heat demand [68]	18
3.1 Power-to-gas model in OM	24
3.2 Electrolyser model "A" (upper) and model "B" (lower) in OM	27
3.3 Adjustable power level controller in OM	29
3.4 Power-to-heat model in OM	30
3.5 Theoretical Single-Stage Vapor Compression Refrigeration Cycle ($C = \text{Constant}$) [17]	30
3.6 COP vs. T_{ambient} , $T_{\text{condenser}} = 70^\circ\text{C}$	32
3.7 COP vs. T_{ambient} , $T_{\text{condenser}} = 50^\circ\text{C}$	32
3.8 Co-simulation flow chart	34
3.9 Co-simulation synchronization	35
4.1 PEM Electrolyser cell voltage vs. current density	38
4.2 Coefficient of performance (COP) vs. evaporating temperature for $T_{\text{cond}} = 40^\circ\text{C}$	38
4.3 Power capacity of renewable energy sources	39
4.4 Flexible capacity of multi-energy system	39
4.5 Operational temperature comparison of electrolyser models vs. time	40
4.6 Efficiency comparison of electrolyser models vs. time	40
4.7 $P_{\text{Load},\text{PtG}}$ of electrolyser models vs. time	41
4.8 Ambient temperature vs. time	41
4.9 COP results of heat pump models vs. time	42
4.10 $P_{\text{Load},\text{PtH}}$ of heat pump models vs. time	42
4.11 Active power consumption for Model "B" of PtG & PtH vs. time	43
4.12 Flexible active power demand of MES on 07.02.2019 for base case	43
4.13 Flexible active power demand of MES on 07.02.2019 for case 1	44
4.14 Hydrogen production of PtG models on 07.02.2019 for case 1	44
4.15 Heat production of PtH models on 07.02.2019 for case 1	45
4.16 Levelized cost of PtX for case 2	45
4.17 PtX active power consumption and Excess RE for case 2	46
A.1 Historical data processing	51

List of Tables

1.1 Final energy consumption by sector, fuel (Mtoe) [3]	2
2.1 Ambient temperature - demand relation parameters	18
2.2 Cost considerations for PtG & PtH	19
2.3 Selected days for historical data	20
3.1 Modelling considerations of electrolyser	23
3.2 Hydrogen & Oxygen characteristics at 80 °C	28
3.3 COP results for various ambient and condenser temperatures	29
3.4 Modelling considerations of heat pump	31
3.5 5 th order polynomial fuction parameters for $T_{condenser} = 50, 70^{\circ}\text{C}$	32
3.6 Power-to-Heat storage parameters	33
3.7 Constraints	34
3.8 Co-simulation parameters	35
4.1 Active power dispatch for optimal deployment of flexibility & priority assumptions	47
4.2 Total operational cost for optimal deployment of flexibility priority assumptions	47

1

Introduction

The effects of climate change is clearly visible. Evolution to sustainable world is an urgent challenge that must be dealt by humankind for a better life. One of the best solutions of humankind to this problem is supplying energy demand by renewable energy sources (RES) such as wind, solar, etc. These energy sources have low carbon emission for electrical power generation. However, stochastic nature of RES puts reliability of existing electrical power system in great danger and introduces a new challenge for grid operators to match the energy demand and supply in power networks. As a result, flexibility of the electrical power system must be increased in order to allow larger percentage of RES in generation units and enhance reliability of the electrical power system.

1.1. Background

Zero-carbon emission is the ultimate goal of countries. For this reason, significant amount of renewable energy sources are integrated to the electricity network and more expected to be accommodated. Figure 1.1 shows energy-related carbon dioxide (CO_2) emissions today, with current policies, and expected reduction in CO_2 emissions with increased number of renewables until 2050. It is important to note, from this figure, that renewable energy with electrification and energy efficiency can provide up to 94% reduction in energy related CO_2 emissions. Renewable energy with electrification is using RE as the primary energy source for energy sector and energy efficiency is reduction in energy losses by physical system improvements. According to Paris Agreement [64], made by UN members, substantial greenhouse gas emission reductions are required across all sectors to mitigate the effects of climate change. The objective of the countries, by this agreement, is to keep the global temperature increase below 2 °C and pursue efforts to keep it below 1.5 °C for climate-neutral economy with net-zero greenhouse gas emissions. In order to reach this objective, a worldwide effort to decarbonization the energy system, especially in industrial areas, is required.

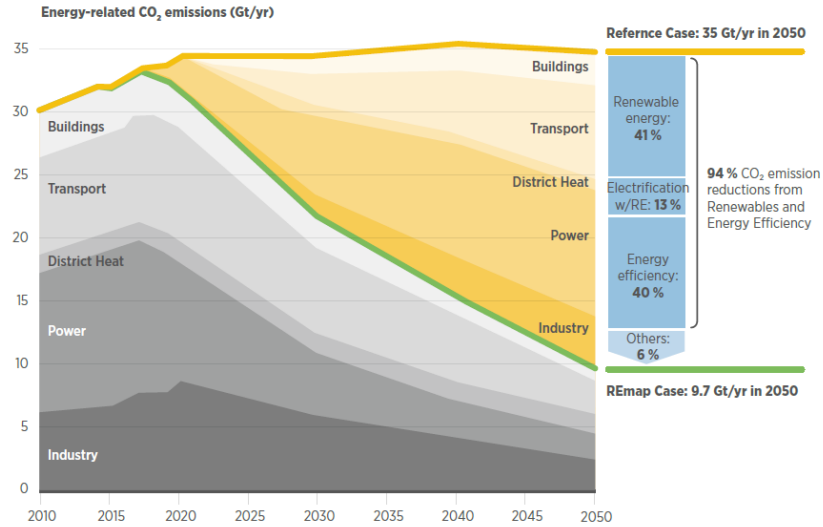


Figure 1.1: Energy-related carbon dioxide emissions with current policies compared to accelerated uptake of renewables (REmap), 2010–2050 [29]

Today, 35% of total energy demand is from industrial sectors globally [3]. Energy consumption per actor in industrial areas is much greater than that in residential or commercial areas. Electrification of even a few processes in industries can lead to significant amounts of carbon savings. Therefore, electrification of the industry is one the key solutions to have energy transition pathway that may substantially contribute to a CO₂ neutral energy system. Conventional fossil fuel based generation units, have risen the carbon dioxide emissions dramatically. As a results, new electrically powered technologies and electrochemical processes being developed in order to increase the share of directly used clean renewable power in the power system. Table 1.1 reveals the increasing role of electricity compared to other fuels [3]. According to sustainable development scenario, electricity and direct use of renewables are expected to have increasing interest in 2040. Growing role of hydrogen in the future is also indicated in the table. It is mentioned in reference [3] that, this is due to increasing industrial gas demand and advantageous of hydrogen as an energy carrier, as explained in section ??). It is also noted from table 1.1 that, industry already has the largest final energy consumption among sectors, and this will continue in 2040. Thus, electrification of the industry is the most promising way to increase energy system flexibility.

Table 1.1: Final energy consumption by sector, fuel (Mtoe) [3]

			Sustainable Development	
	2000	2018	2030	2040
By sector [Mtoe]				
Industry	1 881	2 898	2 949	2 904
Transport	1 958	2 863	2 956	2 615
Buildings	2 446	3 101	2 735	2 709
Other	758	1 092	1 264	1 272
By fuel [Mtoe]				
Electricity	1 092	1 915	2 349	2 902
District heat	248	296	264	224
Hydrogen	0	0	6	65
Direct use of renewables	271	482	887	1 142
Natural gas	1 127	1 615	1 816	1 719
Oil	3 124	4 043	3 695	2 838
Coal	542	984	746	533
Solid biomass	638	620	140	75

Power-to-X (PtX) is the sector coupling technologies used for the electrification of the industry. It consists of electricity conversion and energy storage technologies such as electrolyzers, heat pumps, electric vehicles, batteries, compressed gas tanks, etc. These technologies allow coupling of electricity into various energy domains such as gas, heat, chemicals, etc. Larger share of electricity from RES, especially from sun and wind, is increasing the flexibility demand of power system [4], and PtX is the solution to increasing power system flexibility demand. They are especially favorable in energy systems with high shares of RES, and for ambitious decarbonization targets [35, 49]. With integration of PtX into electrical power system, excess power of RES can be converted into various forms of energy, and it can be stored in the final form. This way storage would provide opportunities for demand side management [48, 58], and also the produced energy would have zero or low contribution to greenhouse gas emissions.

These demand technologies, PtXs, also require as much attention as RES have [4]. This implies PtX also needs detailed technical analysis before implementation. However, currently available models and methods in literature [30, 45, 58], make significant simplifications on physical conditions of device, particularly in consideration of operational temperature and pressure conditions. Some other uses generic models that highly depend on manufacturer's data [14, 33, 62] and difficult to find for an industrial application. These simplifications made during modelling may lead to lose some of the essential dynamics for flexibility analysis such as correct efficiency characterization, ramp up/down characterization, etc. In reality, performance of a PtX highly depends on operational conditions. This means modelling of PtX technologies needs to be investigated according to the requirements of flexibility analysis. As a result, in this project, additional information obtained from detailed models during flexibility analysis is defined as the hidden flexibility of PtX.

1.2. Literature Review

This section is divided into three main parts. In the first part, flexibility in the literature is reviewed and flexibility in this project is defined. In the second part, multi-energy systems (MES) and two modelled power-to-x (PtX) technologies are reviewed. Finally, in the third part, hierarchical control and optimal deployment of flexibility is reviewed with respect to multi-energy systems.

1.2.1. Flexibility

For reliable operation of electrical power system, energy balance between supply and demand must be maintained in any point of time. Electrical systems are able to deal with variability and uncertainty in both supply and demand of energy up to certain point, and this is called energy system flexibility [35]. However, integrating variable renewable energy sources such as wind or solar into electrical network increase the need for energy system flexibility.

Flexibility is quantified and classified in multiple ways depending on the nature of study being conducted. Reference [43] divides flexibility into four main parts: grid expansion, energy storage, flexibility on the supply side, and flexibility on the demand side. Supply side flexibility includes measures that can be taken to modify the output of power generation units for power balance. One of the ways for supply-side flexibility is curtailment of variable renewable energy sources. Even though, curtailment of RES might be necessary during oversupply of power, it also means losing electricity. Thus, it should be avoided by increasing the overall system flexibility from another aspect [35]. Supply-side flexibility can also be provided by load following or peaking power plants e.g. coal power plants, gas/oil fueled generators. However, these power plants operate at much higher price per kilowatt than base load power plants and more expensive than demand-side flexibility, because they are used occasionally during high demand of electricity. These fossil fuel based generation units also cause additional greenhouse gas emissions to atmosphere.

Demand-side flexibility, is considered to be the most effective measure to improve energy system flexibility [16, 47]. It is the ability of a load to vary its scheduled profile. It can be provided by electrification and intelligent control of heat, gas, transportation and other sectors. Industrial processes such as electrolysis, cement & paper mills, electric heat pump/boiler, etc. have the potential to shift their loads according to variable RES [19]. Since this operation does not require any change in electricity generation profile, it is less expensive than supply-side flexibility or grid expansion.

Reference [59] investigates industrial demand side flexibility of power consumption using generic data

models. Data model provides standard description of a flexibility service that can be considered for different objects. This approach is useful for dealing with uncertainties in energy system. Reference [63] classifies flexibility sources as illustrated in figure 1.2. They focus on operational flexibility of power system by shifting the generation and demand profiles of resources. As can be understood from figure 1.2, flexibility of a system can be increased by controlling conventional power units, increasing storage capacity, demand response or curtailment of RES. Reference [52] proposes a taxonomy for modelling flexibility. They simply define flexibility as the ability to deviate from the plan, and mention that flexibility of a given system is a unique, inherent, state and time dependent quality. Examples show that different approaches can be taken while defining flexibility metrics, in order to analyse different aspects of electrical system.

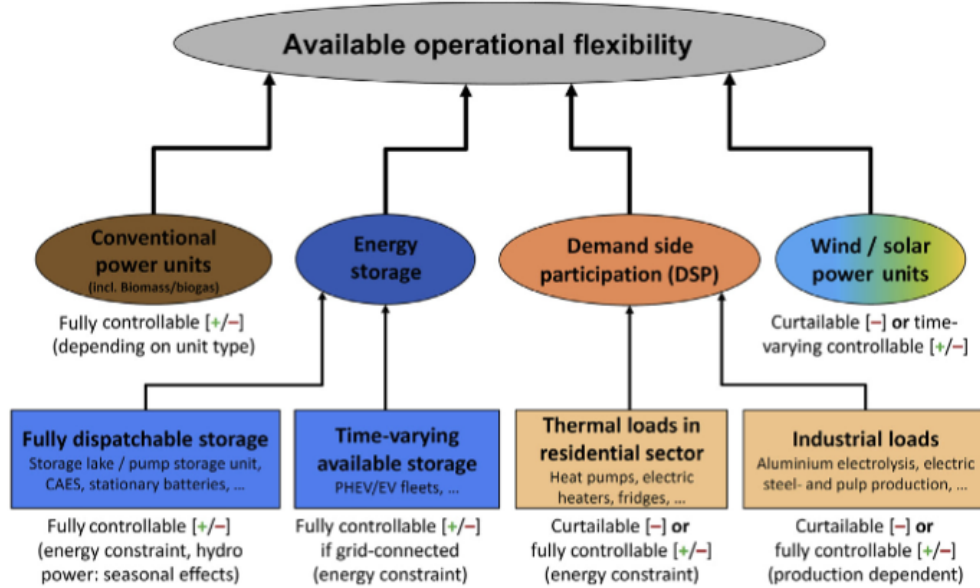


Figure 1.2: Sources of power system flexibility [63]

In this project, **flexibility is the ability of a component or a collection of components to respond power fluctuations in power systems**. Particularly, we look at the Power-to-X devices, and the flexibility offered by them to support power system. From an operational perspective, PtX flexibility becomes relevant in situations where there is excess RE supply relative to demand in the power system and, therefore, electricity prices are low. During excess RE, power set-point of PtX can be elevated in order to provide flexible response and store this excess energy for low power generation times. Increasing the power consumption of PtX during excess RE provides power balance for electrical power system and reduces operational costs for PtX owners by providing opportunities to shift demand into low electricity price time.

Reference [59] mentions that, modelling of flexibility must be standardized in such a way that, models of components must describe flexibility potential as precisely as possible. Figure 1.3 shows the power consumption of exemplary flexible load with flexibility parameters. The key figures, that characterize flexibility, considered in this project are activation duration (t_{act}), holding duration ($t_{flex, on}$), deactivation period ($t_{restore}$) and power capacity [59]. Activation duration is the amount of time to reach flexibility set-point, and deactivation period is the amount of time to return to base set point and these parameters can be modelled or decided based on the inertia of the flexible system. Holding duration is the time duration in which the chosen power state will be held. Additionally, storage level indication is inevitable for the flexibility characterization of storage models.

1.2.2. Multi-Energy Systems

In a multi-energy system, traditionally de-coupled energy vectors such as heat, electricity, gas, etc. optimally interact with each other at lower system levels, in order to enhance technical, economical and envi-

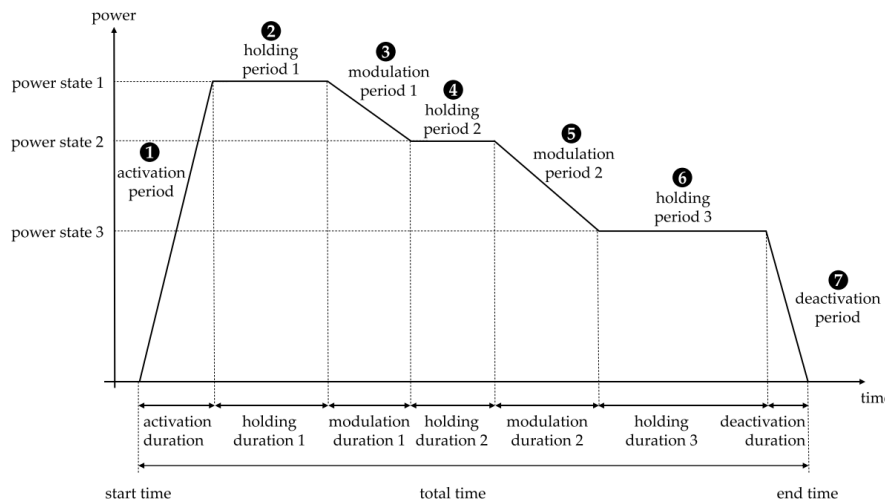


Figure 1.3: An exemplary flexible load measure with the corresponding parameters [59]

ronmental performance of the system [36]. Reference [42] defines MES as the place where the production, conversion, storage and consumption of different energy carriers takes place. It is necessary to analyze inter-dependencies between these energy carriers in order to optimally use them for sustainable, affordable and more flexible energy systems [37]. However, complex configurations of MES, with various PtX technologies available, makes this task challenging.

PtX technology is one of the key elements of MES. Figure 1.4 illustrates some of the possible PtX chains. It reveals that various PtX technologies and their combinations exist in the industry. However, electrification of the entire energy system would be too complex, or at least much more expensive than combining renewable generation with low-carbon fuels [31]. Therefore, PtX should be selected according to needs of the energy system. Reference [10] compares different combinations of MES and concludes that, a combination of power-to-gas with electric heat pumps has the best cost performance in a MES with renewables. Thus, the focus of this project is on power-to-gas (PtG) and power-to-heat (PtH) and these technologies are analyzed below.

Use of natural gas is decreasing as a result of clean energy transition. However, gases will remain crucial for a reliable, affordable and flexible energy system. Therefore, these gases must be produced with sustainable methods [34]. Hydrogen and green electrolysis may have a significant role in the production of zero-carbon gases [29]. Hydrogen offers various ways for decarbonization, and power-to-hydrogen technology currently available to produce, store, transport or use hydrogen energy in different sectors [2]. Electrolysis is an electro-chemical process that uses direct electric current to split water molecules into hydrogen and oxygen. When RES is directly used for the the production of hydrogen this is called green hydrogen due to low carbon emissions. Currently, 4-5% of hydrogen is produced from electrolysis globally and the number of electrolysis plants is increasing. It is estimated that 270,000 tons of hydrogen will be produced in Northern Netherlands, between 2017 and 2030 to provide hydrocarbons to various sectors (industry, transportation, electricity, heating, etc.) [5]. Advantages of hydrogen as an energy carrier are listed below.

- Hydrogen is the lightest fuel in the nature, this means, it can be stored at high energy density with relatively smaller storage size than other gases. Therefore, hydrogen has a significant role on revealing the flexible capacity of MES, providing demand shifting opportunities with storage.
- Hydrogen can be produced from small-scale distributed electrolysis to large-scale, central electrolysis plants that could be integrated directly to renewable energy sources.
- No greenhouse gasses or other particulates are produced by the use/production of hydrogen with renewable energy sources.
- Hydrogen can be used for transportation sector by being stored in compressed gas tanks for applications similar to gasoline or propane.

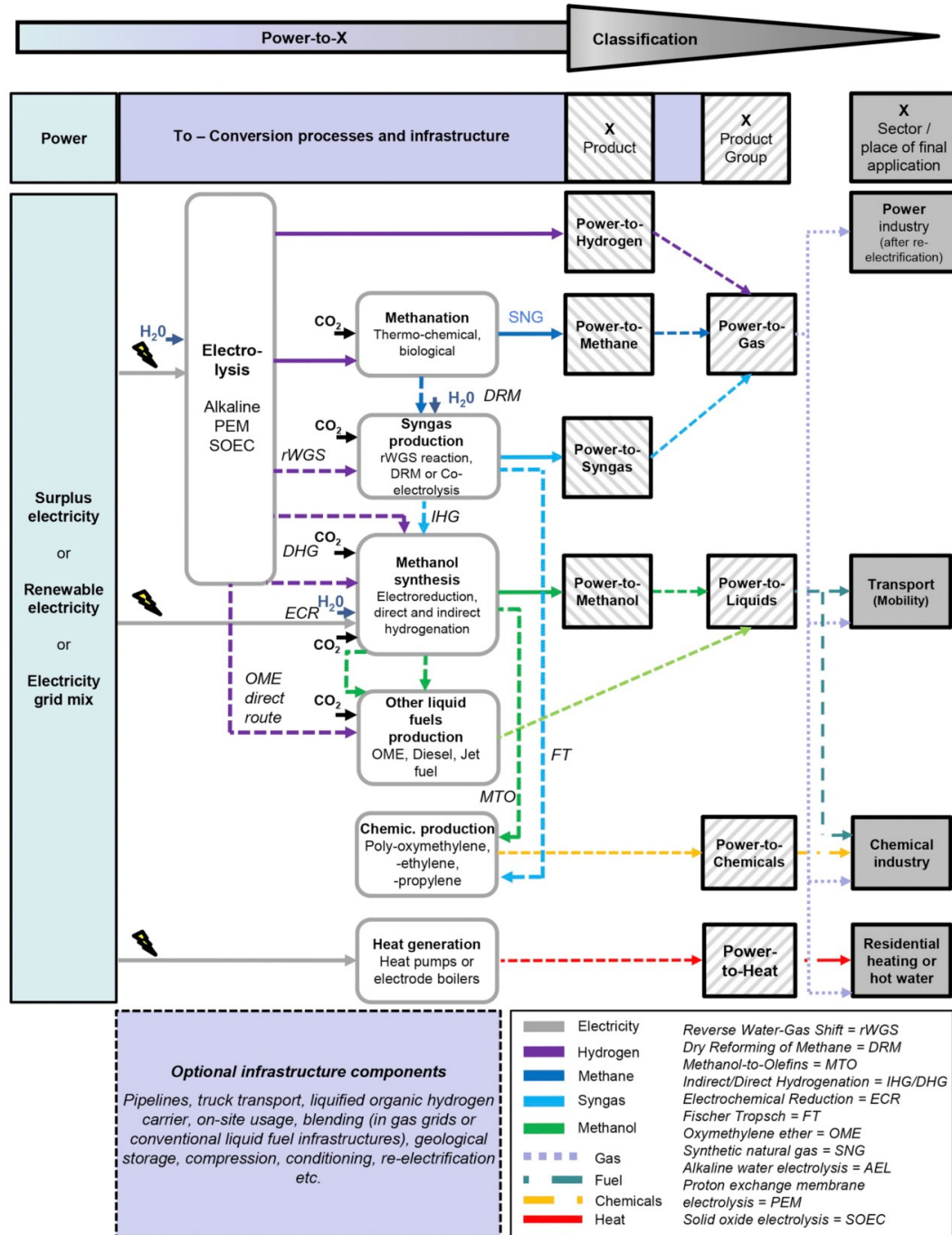


Figure 1.4: Schematic illustration of main inputs, products, processes and technologies of different Power-to-X process chains and their classification [31]

- Hydrogen can be transported or stored in the existing gas distribution networks. Therefore, it does not require additional investments for capacity enhancements.
- Hydrogen can be formed into various hydrocarbons that used in variety of sectors (chemical, petrochemical, etc.). Production of synthetic hydrocarbons from hydrogen would help greenhouse gas emission reduction by reducing the amount of fossil fuel used in that sector.

Compared to other PtX options, PtH is commonly used for high efficiency of heat pump, boiler and low heat storage cost [46]. Heat pumps are able to utilize surplus energy from variable RES at coefficient of performance (COP) values larger than four and this makes PtH an economical option [31]. Additionally, heat

capacity of the heat pump system can be increased with improved COP, if an auxiliary electric boiler is considered for PtH [12]. Electrification of district heating systems considerably improves CO_2 emission reduction, because district heating/cooling demand, which mostly based on fossil fuels, sets for 45% of the final energy consumption globally, thus provides a great opportunity for greenhouse gas emission reduction [18, 32]. Table 1.1 shows that district heating demand shifts to direct use of renewables in sustainable development scenario. Figure 1.5 illustrates various PtH options with electricity and district heating networks. While centralized/industrial PtH units are connected to the heating network, decentralized PtH units do not support the existing heat network. Reference [39] proves that, large-scale, centralized electric heat pumps for district heating are especially promising to provide additional flexibility in power system, and to reduce operational costs.

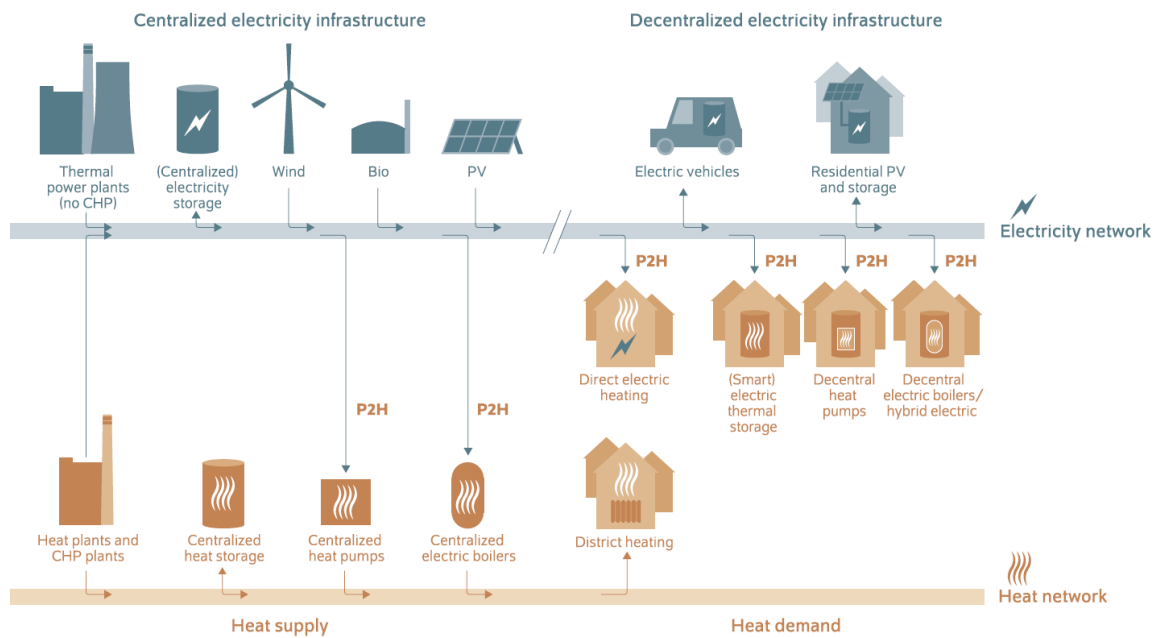


Figure 1.5: Interconnections of power-to-heat options with electricity and district heating networks [9]

In addition to district heating, improved efficiency can be reached for electrification of low or medium temperature industrial heat processes of heat pumps such as food, textile, tobacco plastics, etc [70]. Electrification of high temperature industrial processes such as steel, iron production can also be profitable depending on the application [27]. Industrial heat compose 66% of industrial energy demand and approximately 20% of global energy demand. Most of the industrial CO_2 emissions is also caused from combustion of fossil fuels [27] in heat sector. Therefore, electrification of heat sector would also contribute to significant amount of carbon emission reduction.

1.2.3. Energy Management of Multi-Energy Systems

Energy management means optimizing the energy system for the optimal use of the available resources. Due to interconnections and dependencies between previously independent energy vectors, new control strategies are necessary for MES [56]. Even though technology required for hybridization of the energy system is already available at component level, system level influence of components and their resulting effects on power system still needs to be investigated [69]. In order to provide meaningful recommendations for MES, a holistic energy management approach is required that considers both physical and operational aspects. Reference [47] states that there is an increasing attention on demand-side management (DSM) to improve flexibility and categorize DSM into: energy efficiency of device, time of use rates, demand response (including market and physical demand response) and spinning reserve. They mention that a consideration for, at least, cost/price signals and physical demand response is necessary in order to make the optimal use of the available resources. Reference [37] indicates that flexible capacity can be provided by internally shifting the energy vectors inside MES, keeping the final energy demand of MES constant. They formulate an operational

framework and optimisation problem to provide integrated ancillary services in MES.

By reason of distributed energy systems, control strategies at different levels of smart grid is essential to improve its reliability and sustainability [38]. Two or multi level configuration of energy management systems named as hierarchical control. With this approach, each component in the system considered as an agent that can communicate with the higher control level, namely community energy management system (CEMS), and CEMS can make decisions for the overall benefit of MES. A notable work on this topic is found in [13]. The authors in [13] mention that existing hierarchical management of MES models not considers energy cost of production(€/MWh). This results with unnecessary trading of electricity and increase in operational cost. Therefore, reference [13] proposes adjustable power level concept. According to adjustable power level information coming from agents, CEMS may directly control the generation amounts of PtXs in order to reduce the operational costs of MES by avoiding unnecessary trading with the utility grid.

1.3. Problem Definition

Figure 1.6 illustrates the expected share of RES in electricity, heat and transportation sectors. Although larger share of RES is expected in the future, highly volatile nature of these generation units reduces the reliability of power grid. In order to increase the percentage of RES in the electrical power system, the flexibility of the electrical network must be increased. Industrial systems are able to provide large amounts of energy and energy storage with various efficiencies, ramp up/down rates and storage duration [10]. Replacing production based on fossil fuels in heating, chemical, petrochemical, food, steel and other industries leads to more sustainable and flexible multi-energy networks. However, in order to analyze industrial MES a technical analysis including their control, available flexibility, and optimal management & deployment must be carried out.

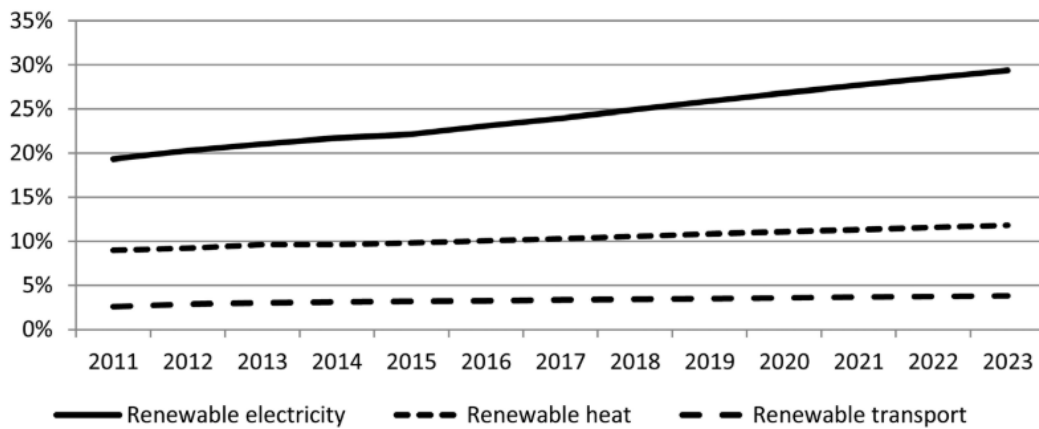


Figure 1.6: Shares of renewables in the energy mix of the power sector, the transport sector, and heat [53]

PtX models are simplified by single equations with constant or linear relation between the power input and energy output. However, operational performance of PtX such as electrolyser or electric heat pump strongly depends on operational temperature conditions. During flexibility analysis, this critical assumption leads to losing essential dynamics on simulation results. Correct efficiency characterization is crucial to understand the flexibility provided by Power-to-X, especially when a large number of these devices are present in the energy system. Inaccurate flexibility analysis of PtX may lead to increased transmission losses, higher operational costs or miscalculation of the MES capacity [59]. Due to simplifications made in model formulations, flexibilities provided by MES components to network can be concealed in the simulation results (hidden flexibility). Therefore, PtX modelling must be investigated to be optimally adapted to the requirements of flexibility analysis.

Another problem is, conventional energy management systems only consider generation side with limited amount of information. The planning and operation of multi-energy system needs to be coordinated to make optimal use of the available resources. Due to the inter-dependencies and connectivity between previously distinct energy vectors, a more holistic energy management and modelling approach must be provided

including demand side management. However, this approach requires complex simulations to be set up. Even though reference [47] suggests that, a good combination of market demand response and physical demand response is necessary to run a network optimally, many of the existing simulation models for the energy management of MES do not have any information about the energy cost of other components in the network. This approach results in unnecessary trading of electricity with the utility grid and means an increase in operational cost for PtX owners [13]. Therefore, comprehensive energy management strategies that considers economical and physical aspects is needed to find the optimum operation point of MES.

1.4. Previous Work

Power-to-X technologies, especially electrolyser and electric heat pump, have the potential to be an integral part of an efficient, renewable and interconnected multi energy system. With respect to fuel cell systems, limited number of electrolyser model develop input-output models adapted to the requirements of control and flexibility analysis [44]. The existing generic electrolyser models use an efficiency curve to simulate the transformation of energy from power to gas [62]. While generic models are easy to simulate, they are highly dependent on manufacturer data or experimental measurements that are almost impossible to find for industrial systems. Thus, a lot of effort has to be performed in the modelling of detailed design of such systems. Several projects use partial differential equations for electrolyser modelling [30, 45]. These models are commonly used for mass transport behavior characterization. Some PEM electrolyser models available in the literature use ordinary differential equation (ODE) for efficiency characterization [20, 67]. ODEs are most commonly used for practical applications of electrolyzers. Reference [20] characterize PEM electrolyzer physics and develops a detailed model of an industrial electrolyzer considering pressure, temperature, and current effects. This paper is chosen as the basis for modelling of the PEM electrolyser model.

During modelling of electric heat pump in MES, constant relation between power input and heat output is considered, assuming small variations of coefficient of performance (COP) over time [7, 8, 15, 25]. This assumption is made in order to reduce simulation complexity. However, in practice, COP of an heat pump strongly depends difference between inlet and the outlet temperature. Therefore, flexibility analysis requires more detailed electric heat pump models that considers effects of operational conditions on PtX performance. Diverse empirical approximations of heat pump's physical laws of operation can be made [66]. References [6, 12, 48] develop heat pump models with Carnot-COP, dependent on source and sink temperature. These papers are chosen as the basis for modelling of electric heat pump. The dependency of COP on both inlet and outlet temperature is taken into account by a polynomial fit in these two variables during modelling of heat pump. Additionally, several articles suggests using auxiliary electric boilers at the output of the heat pump system in order to increase the efficiency [10, 12]. The effect of auxiliary electric boiler on PtH performance is also considered during analysis.

Most of the research available on hierarchical energy management of MES do not have any information about the production cost of agents in the system. Most commonly, only excess and shortage amounts of PtX is considered, but cost signals of components in a MES are ignored during energy management analysis. Besides grid parameters and physical constraints, cost signals should also be considered in order to find the optimal operation point of MES. References [47] analyzes various types of energy management and demand-side management of intelligent energy systems. They mention that demand response (DR) of flexible load can be divided as Market DR and Physical DR, and consideration of both is required for the optimal operation of intelligent energy system. Reference [13] propose hierarchical energy management strategy based on multi energy system agents. They introduce adjustable power level concept in order to reduce operational cost.

1.5. Research Questions & Objective

The objective of this project is to investigate the impact of model fidelity of PtX devices in flexibility analysis. Additionally, impact of comprehensive energy management system to optimally control flexibility dispatch is investigated.

Research questions are divided into three main parts. First part considers PtX selection and flexible MES design. Second part is about modelling of PtX to investigate impact of model fidelity. Finally the third part is about implementing hierarchical control to investigate the optimal deployment of flexibility.

The questions addressed in this research are:

- Which technologies have the highest potential to provide flexibility?
 - Which options are available in industrial area?
 - What are the options in order to increase flexibility of an industrial grid?
- To what extent does model fidelity impact flexibility analysis?
 - Which assumptions can be made and which physical effects should be considered?
- How to manage optimal deployment of flexibility considering individual resource constraints?
 - How to combine models representing different energy vectors efficiently?
 - How complex simulations can be created for energy management of MES?

The contribution of this thesis is two fold: firstly, investigating the effect of temperature simplifications of PtX models on flexibility analysis. Effects of auxiliary components on device performance is also considered. Another contribution is the hierarchical agent based energy management approach considering levelized cost signals with co-simulation.

1.6. Research Approach

First, literature review is conducted to analyze various PtX technologies. Their pros and cons are compared. Through extensive discussion, two of the most relevant technologies are selected. Next, specific characteristics of PtX technologies are studied and modelled using OpenModelica. Later, energy management system (EMS) is designed for optimal deployment of flexibility. Agent based hierarchical energy management system is considered. The aim of agent based hierarchical control is, besides grid parameters, considering physical constraints of agents and cost signals in order to find the optimal operation point of MES. After PtX models are created in OpenModelica (OM) and electrical network model with optimal power flow problem is created in Pandapower(PP), co-simulation is used to combine these models. Energysim is used for co-simulation. It allows to combine these two simulation software and implement complex control and flexibility analysis with multiple MES agents and a higher control level.

Modelling objective is to achieve an effective energy efficiency characterization during system's operation. PEM electrolyser model is created to study the performance behaviour of electrolyser under different operating conditions. An electrochemical steady-state model is created to calculate the stack/cell voltage and the stack/cell temperature evolution from instantaneous operating conditions such as the applied current, pressure and temperature. Temperature dynamics is added for detailed model version in order to compare the efficiency and performance behaviour of electrolyser model under different modelling assumptions. Pressure - Enthalpy table of ideal heat pump cycle working fluid (r134a) is used to characterize fifth order polynomial function of heat pump COP dependent on inlet and outlet temperatures. The aim of this modelling is to evaluate the performance of the heat pump with respect to different operational temperature assumptions and auxiliary electric boiler.

The aim of the agent based hierarchical energy management is to optimize the MES operation with respect to grid parameters, hydrogen/thermal comfort and energy cost. Optimization of the considered MES is carried out by Pandapower power flow solver. Optimal power flow solver calculates the exact operation point considering cost signals within the available power range defined by the physical situation of the Modellica agents. Hierarchical energy management is achieved with co-simulation by combining OM models with Pandapower solver in Energysim as illustrated in figure 1.7.

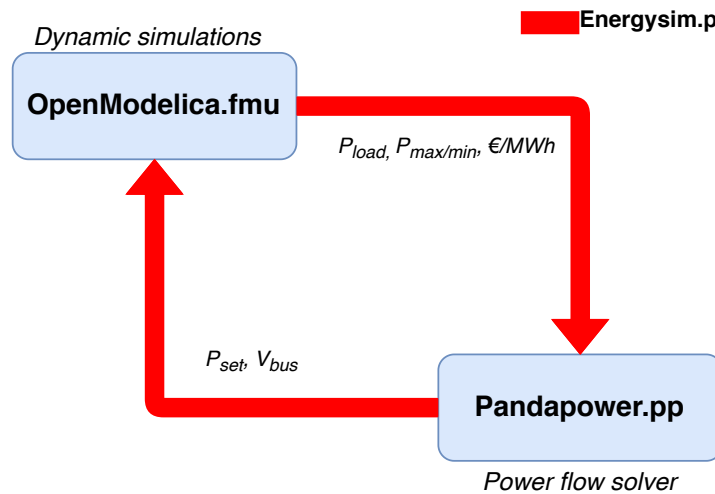


Figure 1.7: Communication between simulation tools

1.7. Outline

This report is divided into 5 chapters including introduction. Chapter 1, Introduction, explains research problem, research objectives and the literature review of the subject. Chapter 2, Methodology, describes key elements of the research approach, simulation tools and considered MES system. It also describes the input data preparation for simulations. Chapter 3, Modelling, describes the modelling of PtX and co-simulation setup. Chapter 4, Results & Discussion, presents the results obtained from models and simulation cases. Finally, chapter 5, Conclusion & Future Work, presents conclusions of the research and recommendations for future work.

2

Considered Energy System

Figure 2.1 illustrates the electrical side of the considered energy system. As can be seen, there is one industrial microgrid connected to external grid via 100 MVA transformer. Considered energy park is assumed to be 20 km away from the grid connection point. Power-to-gas consists of 50 MW proton-exchange membrane (PEM) electrolyser and simple 100 m^3 compressed hydrogen storage tank model that supplies for industrial hydrogen demand. Power-to-heat consists of 50 MW centralized electric heat pump and 2400 m^3 hot water storage tank that supplies hot water into district heating network.

Excess renewable energy from variable RES is used for hydrogen and heat production in PtG and PtH, respectively. Location and capacity of windfarm and PV farm are taken from literature. The outer contour of Maasvlakte will be installed with 36 wind turbines, as illustrated in figure 2.2, and the installed capacity will be approximately 100 MW [57]. A floating solar park will be installed in Slufter and the installed capacity of PV farm will be approximately 100 MW_p [1]. Combination of these RES with the best available PtX technologies in the industrial area is assumed to be a "Hypothetical Energy Park in Maasvlakte 2".

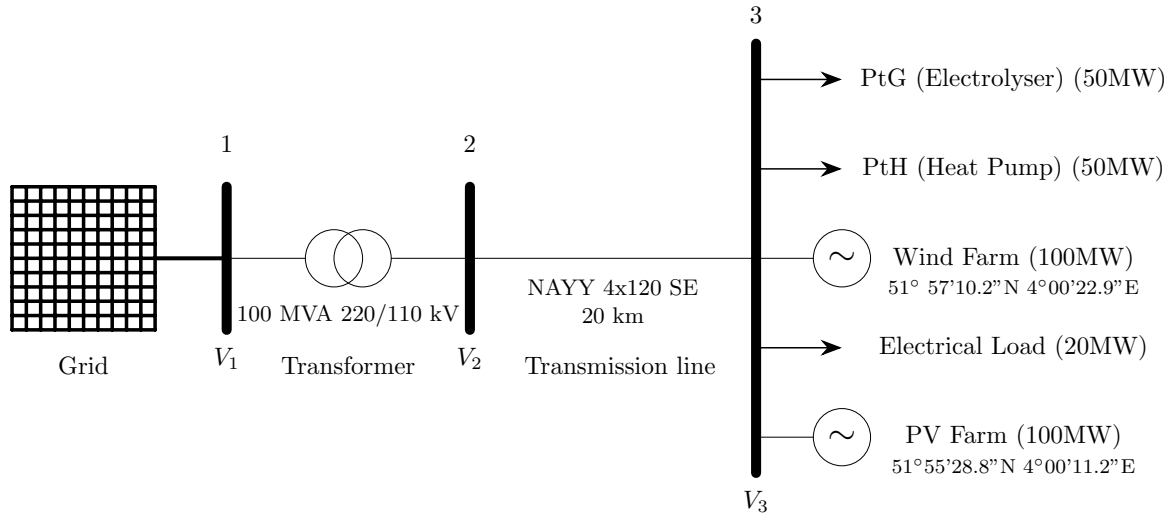


Figure 2.1: Electrical side of the MES

2.1. Energy Production

Figure 2.2 and 2.3 shows the location of the 100MW installed wind farm and the 100 MW installed PV farm respectively. The hourly power output of these RES are calculated from [53]. For generation profiles of 100 MW wind farm and PV farm in the given coordinates, the reader is referred to appendix B.

Windfarm details:

- Coordinates: 51°57'10.2"N 4°00'22.9"E
- Wind Turbine Generator: GE, 3.6MW, DFIG
- Number of wind turbines: 10 (3MW) (Harde Zeewering) + 26(3MW) (Zachte Zeewering)
- Capacity: 100-108 MW



Figure 2.2: Location of the 100 MW wind park in Maasvlakte

PV Farm details:

- Coordinates: 51°55'28.8"N 4°00'11.2"E
- PV Panel: 250 Wp
- Number of panels: 180.000<x<540.000
- Capacity: 45-135 MWp (apprx:100 MWp)



Figure 2.3: Location of the 100 MW solar park in Maasvlakte

2.2. Energy Demand

Considering large demand for heat and gas in an industrial area, and the potential to electrify these options via PtX technologies, PEM electrolyser and centralized electric heat pump is selected. Power-to-gas divided into four sub-models: PEM electrolyser, compressed hydrogen storage, adjustable power level controller and static generator. PEM Electrolyser model was developed according to the procedure used by reference [20] and the multi-physic approach illustrated in figure 2.4. It was important to have accurate model of stack polarisation curve of electrolyser. Therefore, this sub-model calculates operating stack voltage considering the active power input and stack operating temperature. The operating voltage of electrolyser cell consists of reversible voltage, that is the minimum voltage to initiate water electrolysis, and the sum of different overpotentials caused by internal losses and resistances in the cell. Developed model allows to investigate performance characteristics of electrolyser under various operating conditions. Compressed hydrogen storage model is created based on the model developed by reference [40]. A simple first order model is created considering ideal gas behaviour without losses. Energy level of the gas tank is calculated from the available volume assuming the tank pressure & temperature remains constant without losses. To control the available flexibility of PtG, adjustable power level controller is developed. This sub-model calculates minimum and maximum active power boundaries that electrolyser is able to operate. It was necessary for PtG to inform the higher control level of hierarchical control. Later, higher control level uses these constraints for finding the optimal operation point. Minimum active power ensures the continues supply of scheduled industrial hydrogen demand profile. Maximum active power demonstrates the nominal power or strictly follows minimum active power depending on the amount of stored energy. Static generator model is from iTesla Power Systems Library electrical sub-package. This sub-model provides electrical interface for PtG. Particularly, it can be improved for reactive power control and voltage regulation analysis. Modelling approach for the sub-models: storage, adjustable power level controller and static generator are similar for both PtG and PtH models.

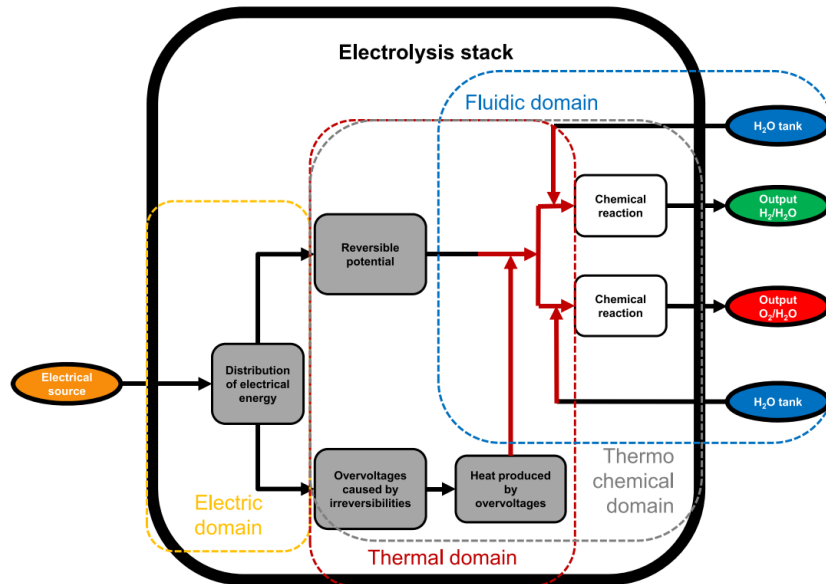


Figure 2.4: Coupled multiphysic phenomena involved in an electrolysis stack [44]

In reality, electrolyser cell is not able to provide favorable operation of electrolysis on its own. Therefore, electrolyser system must include auxiliary components for temperature regulation, input/output conditioning and power regulations. In order to investigate the effect of temperature evolution on electrolyser performance, auxiliary components are considered for the electrolyser thermal sub-model.

For power-to-heat, centralized electric heat pump and auxiliary electric boiler models are developed. It also includes hot water storage, adjustable power level controller and static generator sub-models similar to PtG. The thermal efficiency of the heat pump is characterized as coefficient of performance (COP). COP is the ratio of heat produced over input power, that is the electric compression work of heat pump. Maximum COP that can be achieved by heat pump bounded by the rankine cycle efficiency of the refrigerant inside. Refrigerant R134a, that commonly used in district heating electric heat pumps [55], is assumed to be used in

this heat pump. As a result, Pressure-enthalpy table of R134a (given in appendix D) is used for the calculation of COP at various inlet and outlet temperatures. Later, COP results are used in Matlab curve fitting in order to generate fifth order polynomial equation that calculates COP of heat pump rankine cycle (Carnot COP) depending on ambient and condenser temperature.

For district heating, hot water delivered at 70 °C and return temperature at T_{amb} are assumed. Electric heat pump is entitled as the main heat producer for all cases. For model C (explained in section 3.4), a 15MW auxiliary electric boiler is activated at full load when ambient temperature is lower than 15 °C in order to support heat pump during low ambient temperatures, by reducing the temperature difference between the inlet and outlet of heat pump for efficient operation. In this case, when the boiler is activated, heat pump outlet temperature is switched from 70 °C to 50 °C for higher COP. Hot water cycle is illustrated in figure 2.5.

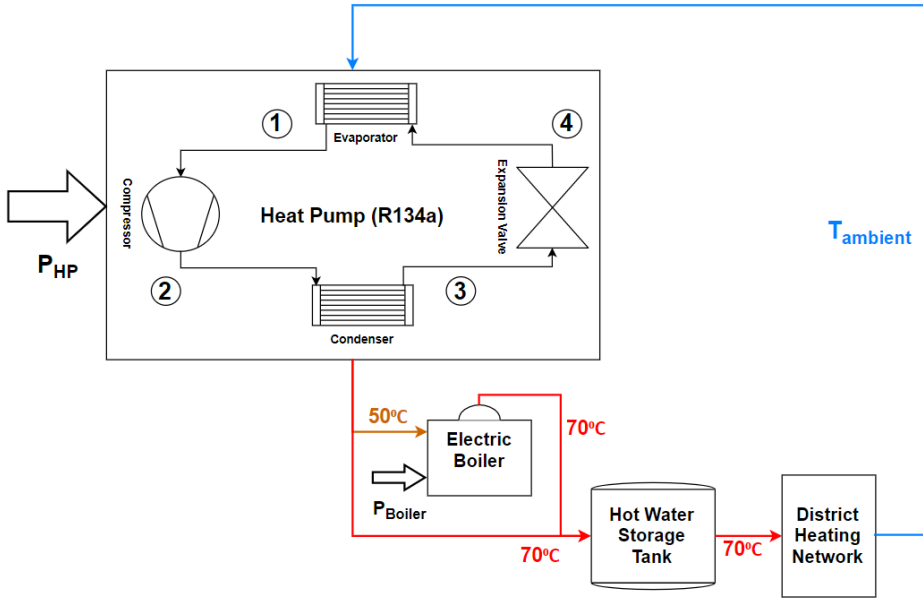


Figure 2.5: Heating Cycle of Water

5 kg/s constant massflow between the heat pump and the storage is assumed for district heating hot water and compressor power of heat pump is controlled with respect to district heating demand. To increase flexibility of MES, a hot water storage tank is connected in PtH to district heating network. It is assumed that the storage tank is able to hold 2400 m³ of 70 °C water without any losses [55].

2.3. Agent Based Hierarchical Control

Hierarchical control is a design approach to provide larger and more complex energy management strategies in order to find the optimum operation of MES. It consists of multi-energy system agents and higher control level. MES agents in this project are power-to-gas, power-to-heat, wind farm and PV farm. Here Modelica MES agents, PtG & PtH, have local objective to supply hydrogen and heat demand profiles, as explained in section 2.4. They also calculate the leveled cost signals for the optimal deployment of flexibility at higher control level, the reader is referred to section 2.4. Active power consumption of PtX for the amount of hydrogen or heat demand is calculated and sent to higher control level via P_{min} output of adjustable power level controller. In addition to this, various physical or technical constraints such as overload, emergency signals, etc. can also be considered for modelling the PtX boundaries. Also, the hourly available active power output of RES is considered for the maximum active power constraint of wind farm and PV farm agents.

Pandapower (PP) optimal power flow solver is used for the energy management of MES at higher control level. Optimal power flow calculation finds the optimal values of active power set points of MES agents to achieve minimum operating cost, as illustrated in figure 2.6. Global objective of the optimal power flow is to minimize operational costs considering leveled cost signals and binding information (flexibility con-

straints) (P_{min}, P_{max}) coming from Modelica agents. In order to do this, built-in optimal power flow solver of Pandapower is enhanced by combining with OM models in Energysim. Pandapower has to communicate with the Modelica agents and learn the operational active power constraints, that is the flexibility constraints, and levelized cost signals, as explained in section 2.4, in order to calculate the optimum operation point within this range.

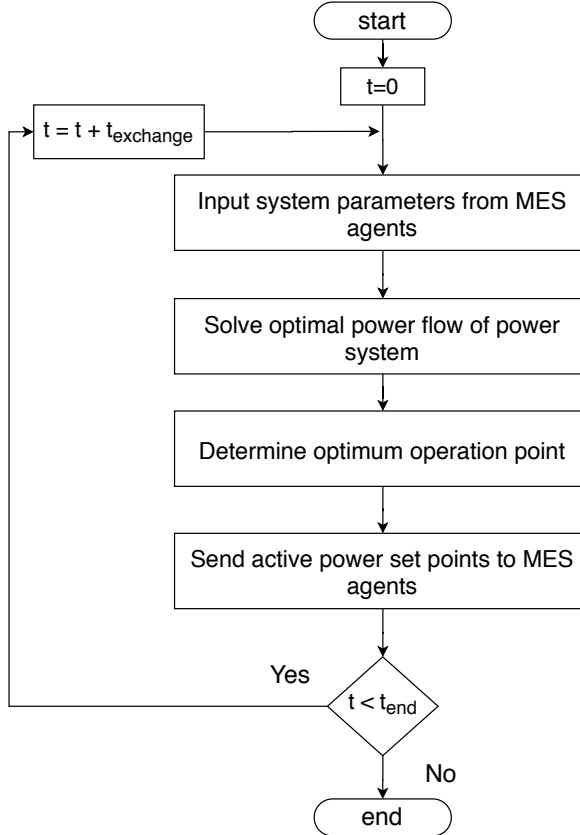


Figure 2.6: Flow chart of higher control level of MES

2.4. Input Data

Renewable Energy Sources

Renewables.ninja [53] models are used in order to analyze the variable power generation of RES. Renewables.ninja allows user to run simulations of the hourly active power output from wind and solar power plants located anywhere in the world. For wind farm model the reader is referred to reference [60], and for PV farm model the reader is referred to reference [54]. For hourly output results of considered RES the reader is referred to appendix B.

Scheduled (Static) Energy Demand Profiles

Energy demand profiles are the scheduled, hourly hydrogen and heat order of PtG and PtH respectively. They define the operational commitment of PtXs in the industrial area. This data was necessary to determine the minimum active power consumption of PtX. Time-series scheduled energy demand profiles also characterize PtX storage flexibility. During normal operation without flexibility, produced hydrogen and heat energy from PtXs are controlled such that they match with the scheduled energy demand data. This helps to maintain stable energy levels in the storage sub-model of PtXs. However, during flexibility, excess RE is utilized in PtX and this increases the stored energy level due to higher hydrogen and heat production than demand profiles.

As can be imagined, time-series heat or hydrogen demand data for industrial networks is exceptionally publicly available. Therefore, model in reference [21] is used to create these energy demand profiles. The benefit of this approach is that it only requires historical ambient temperature data to generate the time-series

scheduled energy demand profiles. Equation 2.1 describes the model in reference [21]. It uses ambient temperature data to determine the share of the dependency of heat demand, Q_{demand} , on ambient temperature. Same equation can also be used to calculate to determine the share of the dependency of hydrogen demand, $H_{2,demand}$, on ambient temperature.

$$Q_{demand}(t) = Q_{base} + \frac{Q_{max} - Q_{base}}{T_{Reference} - T_{min}} \cdot \max(0, T_{Reference} - T(t)) \quad (2.1)$$

Piecewise linear temperature dependency of hydrogen ($H_{2,demand}$) and heat (Q_{demand}) demand in equation 2.1 is illustrated in figure 2.7. Here, Q_{base} and $H_{2,base}$ is the base demand which occurs at temperatures above the reference temperature $T_{Reference}$. Q_{max} , $H_{2,max}$ is the maximum heat and hydrogen demand, respectively, corresponding to the minimum ambient temperature T_{min} . Demand in district heating networks is certainly sensitive to ambient temperature changes. On the other hand, industrial hydrogen demand is expected to be less dependent on the ambient temperature. Therefore, the slope of the linear line in figure 2.7 is larger for power-to-heat than power-to-gas. This means, industrial hydrogen demand has less variations with respect to varying ambient temperature than district heating demand. Values of the parameter are shown in table 2.1.

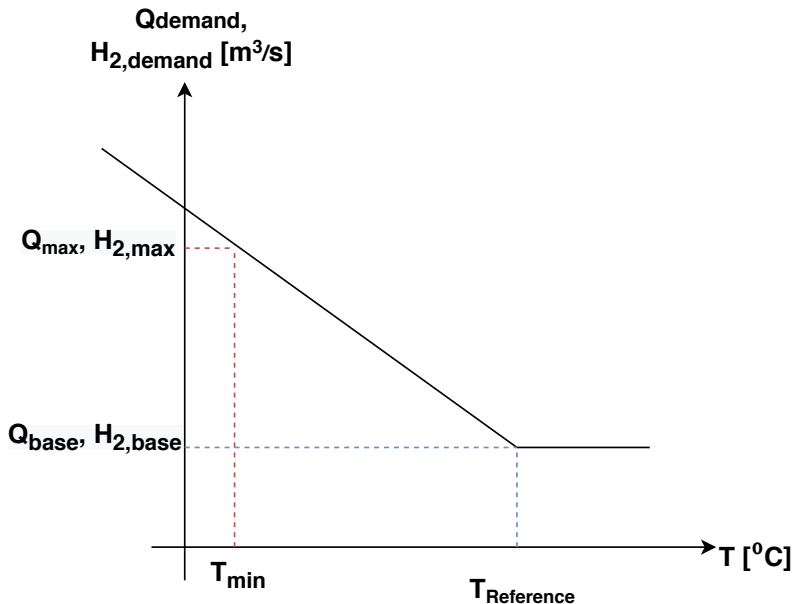


Figure 2.7: The relation between ambient temperature and hydrogen & heat demand [68]

Table 2.1: Ambient temperature - demand relation parameters

	$T_{Reference}$ [°C]	T_{min} [°C]	$Q_{base}, H_{2,base}$ [m^3/s]	$Q_{max}, H_{2,max}$ [m^3/s]
Industrial PtG	25	5	3.1372e-03	3.8502e-03
District Heating PtH	25	5	3	4

Levelized Cost of Energy Production

Levelized cost signals are calculated in PtG and PtX agents taking electrolyser and heat pump efficiency into account. Later, this information is sent to higher control level for optimal power flow calculation. PtG and PtH cost signals are developed to analyze the operational cost savings from the optimal deployment of flexibility and examine the operation of the agent-based hierarchical energy management strategy. Levelized PtX cost signals are particularly considered for the case 2 of power system analysis as explained in the next section 2.5.3.

Linear cost signals [€/MWh] that sent to higher control level, are calculated for PtG and PtH (C_{PtG} , C_{PtH}) as described in equation 2.2, 2.3. Improvements on MES energy production performance and reduction in carbon emissions were the primary concerns for the levelized cost signals. Here, C_{CAP} is the capital cost of the device, C_{OM} is the operations and maintenance cost, LT is the expected lifetime of the device, C_{PEN} is the carbon penalty due to operation in [€/kW] and $\eta_{electrolyser}$, COP_{HP} are electrolyser and heat pump efficiency respectively. Table 2.2, shows the values of the parameters taken from reference [10]. What should be noted from the equations 2.2, 2.3 is, instead of energy produced over lifetime on the denominator, sum of costs are divided by the efficiency output of PtX models. This way cost of energy production of each PtX is compared for the most efficient overall operation.

$$C_{PtG}(t) = \frac{\left(\frac{C_{CAP}+C_{OM}}{LT}\right)_{Electrolyser} + C_{PEN}}{\eta_{electrolyser}(t)} \quad (2.2)$$

$$C_{PtH}(t) = \frac{\left(\frac{C_{CAP}+C_{OM}}{LT}\right)_{HP} + \left(\frac{C_{CAP}+O\&M}{LT}\right)_{Boiler} + C_{PEN}}{COP_{HP}(t)} \quad (2.3)$$

Table 2.2: Cost considerations for PtG & PtH

	Electrolyser	Electric Heat Pump	Electric Boiler
CAPEX(C_{CAP}) [€/kW]	200	1000	70
O & M(C_{OM}) [€/kW]	8	35.5	1.4
Lifetime (LT) [a]	20	20	15
Carbon emission factor($CO_{2,EF}$) [gCO₂/kWh]	16.6	62.3	-
Carbon penalty(C_{PEN}) [€/kW]	16.6	62.3	-
Carbon price (CP) [€/gCO₂]	1	1	1

Equation 2.4 shows the carbon penalty calculation. Considering RES powered water electrolysis and electric heat pump district heating pathways, carbon emission factors, $CO_{2,EF}$ in [gCO₂/kWh], are taken from references [26, 28, 50]. Both PtXs use the same fuel that is the renewable electricity; therefore, fuel price and carbon price (CP) has no effect on cost calculation. Generated RES power is assumed to be the cheapest fuel during excess RE.

$$C_{PEN} = CO_{2,EF} \cdot CP \quad (2.4)$$

2.5. Analysis

For MES and PtX model analysis, the year of 2019 is divided into 8 sections of 45 days. As a result, 8 days from 2019 is selected for to represent the year of 2019. Later, for power system analysis, one of the days is selected in order to have detailed results with smaller step size and convenient co-simulation compile time that is approximately 5-10 minutes. Thus, 24 hours power system analysis is carried out. Table 2.3 shows considered days for historical data.

2.5.1. Multi-Energy System Analysis

MES analysis is implemented in order to investigate the seasonal weather behaviour in the area and investigate the energy balance need of considered power system during a year. This analysis is implemented with available active power output data of RES, as shown in appendix B, and active power output of model B of each PtX. According to the results of this part, one of the considered days is selected for 24 hours power system analysis.

Table 2.3: Selected days for historical data

Selected Days for Historical Data
07.02.2019
23.03.2019
07.05.2019
23.06.2019
07.08.2019
23.09.2019
07.11.2019
23.12.2019

2.5.2. Power-to-X Model Analysis

In PtX model analysis, temperature evolution and its effect on efficiency characteristics of models are compared in order to investigate the model fidelity for accurate device performance characterization. Also, the resulting active power consumption of models are compared. This analysis is implemented with historical data, observing the output of OM models.

2.5.3. Power System Analysis

In this part, flexibility analysis of considered MES is implemented in order to compare the flexibility potential of both PtX options and to evaluate the optimal energy management strategies of MES. Additionally, hydrogen and heat production output of models are compared during flexibility service in order to investigate the model fidelity for such analysis. Flexibility is quantified by the final active power demand of MES as shown in equation 2.5 and this is called "flexible demand of MES ($P_{\text{demand,flexible}}$)". Flexible demand is the difference between the total active power demand ($P_{\text{demand,PtG}}$, $P_{\text{demand,PtH}}$) and the total variable RES generation ($P_{\text{gen,WF}}$, $P_{\text{gen,PV}}$) of MES. This means, final energy demand of an ideal MES would be zero or lower than zero (surplus power) at all times; however, if the RES generation capacity is lower than power demand than final active power demand of MES would be positive, which means MES would need to import energy.

$$P_{\text{demand,flexible}} = P_{\text{demand,PtG}} + P_{\text{demand,PtH}} - P_{\text{gen,WF}} - P_{\text{gen,PV}} \quad (2.5)$$

For this analysis, PtG and PtH OM models are exported as functional mock-up units and combined with hierarchical control using co-simulation environment. Power system analysis is divided into three cases including base case. In base case, it is assumed that none of the PtX is available for flexibility service. Without any flexibility service, flexible demand of MES is plotted and possible holding duration for flexibility service is investigated. In the first case, it is assumed that only one PtX is available for flexibility service. Both PtX options are compared with respect to reduction in flexible demand of MES during flexibility service. Hydrogen and heat production output of models are compared for the same flexibility service in this case. Finally, in the second case, to investigate the optimal deployment of flexibility, it is assumed that both PtX's are available for flexibility service. Optimal active power dispatch during flexibility service is investigated considering leveled cost signals and active power constraints. Savings in total operational cost with respect to two different flexibility dispatch strategies is calculated using equation 2.6. In this equation, i stands for the number of time intervals between the message exchange of models, cost signals explained in section 2.4 are illustrated with $C_{PtX,i}$ and the active power consumption of PtX is shown with P_{PtX} .

$$C_{\text{total}} = \sum_{i=0}^{95} \left(\int_{t_i}^{t_{i+1}} P_{PtX} \cdot C_{PtX,i} dt \right) \quad (2.6)$$

2.6. Simulation Tools

Three different software are used during project. OpenModelica (OM) is used for modelling the physical nature of the PtXs. Python programming language based Pandapower is used for optimal power flow calculations of the electrical network, and these two software are combined using python programming language

based Energysim, for co-simulation and flexibility analysis. A brief description and motivation behind selecting these tools is provided below.

2.6.1. OpenModelica

Modelica is an object-oriented, equation-based programming language which allows for dynamic simulations of multi-domain systems [41]. It supports the combination of models coming from different physical domains in a unified way. Object oriented programming language provides re-use and analysis of large, complex models independent from the application domain. Casual modelling of Modelica provides effortless modelling and fast simulation of complex dynamics. Even small disturbances can be modelled and assessed with Modelica. In addition to these OpenModelica editor (OMEdit) also provides functionality to export models as functional mock-up units (FMUs) for co-simulation. Thus, Modelica language is suitable to simulate coupled energy systems with different levels of detail.

Various OpenModelica (OM) libraries, such as PowerGrids, PowerSystems, PVSystems, WindPowerPlants, AixLib, Buildings etc. have been investigated in order to design PtX systems and their controllers. Among these, iTesla Power Systems Library (iPSL) has found to offer a unique combination of intuitive and simple design leading to computationally cheap models [65]. Additionally, the power electronic converter models of PVSystems Library [51] has found useful for control analysis, but comes with increasing computation time. Consequently, since they require detailed modelling, PtG and PtH with first order dynamics is chosen to be modelled in OM and static generator model from the electrical sub-package of iPSL is preferred for the electrical interface of the developed PtX models. Also, the functionality to export models as FMUs was useful to have hierarchical agent based control structure. PtX models can be further improved for more dynamic/detailed control and energy system analysis of MES.

2.6.2. Pandapower

Pandapower (PP) is a Python based open source tool for power system modeling, analysis and optimization [61]. It supports power flow, optimal power flow, state estimation, topological graph searches and short circuit calculations conforming to IEC 60909. In Pandapower, electrical elements such as transformers, generators, loads, switches, etc. can be described with nameplate parameters and they are internally processed with equivalent circuit models that have been validated with respect to industry standard software tools. The tabular data structure of PP defines networks based on pandas python library that permits simple handling of input and output parameters.

In this study, electrical network of MES is modelled using Pandapower as illustrated in figure 2.1. To determine the optimum operation point of MES agents (PtX & RES), optimal power flow (OPF) solver of Pandapower is used. Operational costs, flexibilities, and network constraints are configured through the element-based Pandapower data structure for optimal power flow. During analysis, Pandapower allows to manage MES agents from higher control level with comprehensive energy management approach. Modelica agents (PtXs) send maximum/minimum active power binding information and cost signals to Pandapower for optimal power flow analysis and the results of OPF are sent back to OM PtX models as active power orders via EnergySim.

2.6.3. EnergySim

To evaluate the flexibility available from PtX and the impact that they can have on power systems, complex simulations need to be set up [23]. Co-simulation is used to combine different models: the heat pump, the electrolyzer, and the control system. Using a co-simulation methodology allows us to integrate the optimal control strategy with the modelled PtX devices as FMU agents to conduct a flexibility analysis.

There exist many co-simulation tools for multi-energy system analysis that allow coupling of models from various energy domains such as Energysim, Mosaik, VirGIL, Mastersim, etc., each with their pros and cons. Energysim (previously, FMUWorld) [23] is used for co-simulation. It is a python-based software tool that was developed specifically to simplify energy system based co-simulations and focus on analysis by conceptualising the setup. What separates Energysim from the other co-simulation tools is that it offers relatively more straightforward approach for particularly MES co-simulation setup. This allows user to maintain the research aim on model development and overall system analysis rather than focusing on simulation time step setup and message exchange algorithm. Energysim allows users to combine:

- Dynamic models packaged as Functional Mockup Units (FMUs)
- Pandapower Networks packaged as pickle files
- PyPSA models (BETA) packaged as Excel workbook
- csv data files

PtX models are tested on OpenModelica (OM) and exported as FMUs, using built-in FMU export function of OM. Pandapower network is exported as pickle file. Later, these two files and input csv data are combined in Energysim for co-simulation.

3

Modelling

3.1. Industrial Loads

In this chapter, we focus exclusively on the modelling of the PtX systems, their interfaces to the grid, and their controllers. Later, we look at the control system and the co-simulation setup.

3.1.1. Power-to-Gas

For power-to-gas, proton-exchange membrane (PEM) electrolyser, compressed hydrogen storage tank and adjustable power level controller modelled in OM, as illustrated in figure 3.1. In order to model large scale electrolyser, it is assumed that electrolyser cells are assembled into stacks and connected in parallel for 50 MW capacity. Electrolyser model and empirical parameters in reference [67] is used for modelling. Physical domains of electrolyser are divided into four domains: electrochemical, pressure, massflow and thermal. Each sub-model has input and output variables that connected to each other. This phenomena is illustrated in figure 2.4. In addition to electrolyser model, storage tank model simply calculates the amount of stored energy assuming constant pressure and temperature inside the tank. Adjustable power level controller model calculates minimum and maximum active power constraints to send higher control level. Finally, the static generator model, in figure 3.1, is from iPSL Modelica library and it provides interface with the electrical network.

Figure 3.1 demonstrates the modelled power-to-gas system. The first input of the model is scheduled industrial hydrogen demand, that defines minimum active power, and the second input of the model is ambient temperature. The third input of the model is active power set point to control electrolyser hydrogen production, this is illustrated with P_{order} input on electrolyser model in figure 3.1. In addition to these inputs, voltage set point for reactive power control can be used. Details of each model are explained below.

Electrolyser

Table 3.1 summarizes the features of electrolyser models. Model "A", operates at constant temperature 60°C while Model "B" calculates the temperature of the electrolyser system with dynamic thermal submodel. Both models are semi-empirical and have static equations but thermal sub-model is dynamic which makes the general behaviour of the electrolyser system dynamic for Model "B". Finally, thermal sub-model equation also includes balance of plant (BOP) elements such as circulation pump or cooling work that affect the temperature evolution and efficiency of electrolyser. Figure 3.2 illustrates the developed electrolyser models.

Table 3.1: Modelling considerations of electrolyser

Model	Physical Domains	Modelling Approach	Dynamic Behaviour	Modelling Scale
A	Electrochemical Electrical	Analytic + Empirical	Static	Cell/Stack
B	Electrochemical Electrical Thermal	Analytic + Empirical	Static + Dynamic (ODE)	Cell/Stack + BOP

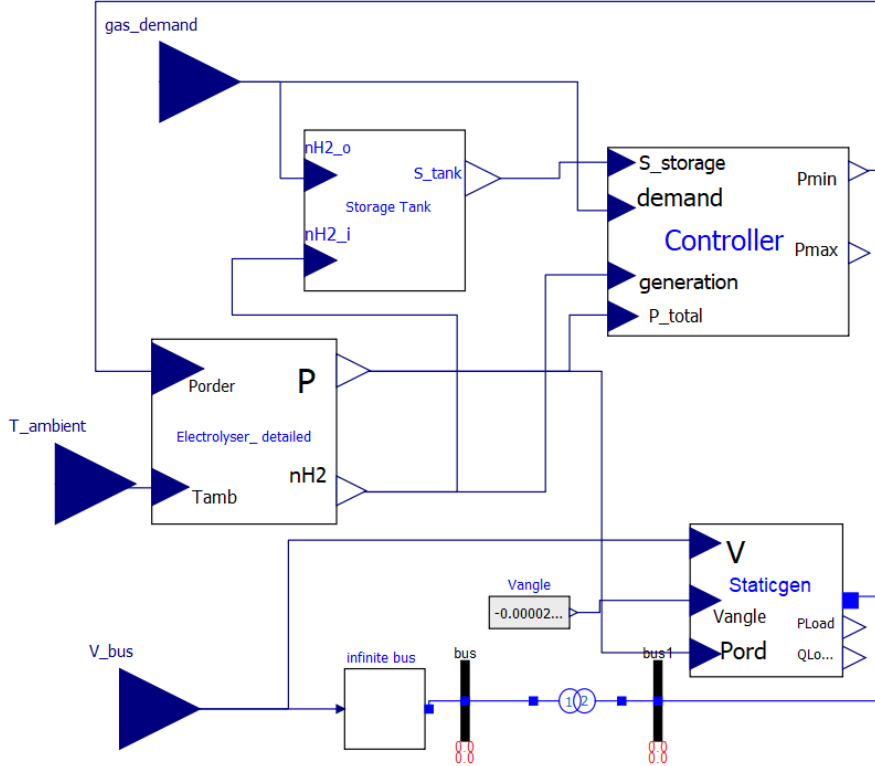


Figure 3.1: Power-to-gas model in OM

PEM electrolyser cell voltage and power is characterized in electrochemical sub-model with equations 3.1-3.9. In equation 3.1, T is the electrolyser's operating temperature. Here, electrolyser cell voltage, V_{cell} , is characterized by the open-circuit voltage, V_{ocv} , activation overpotential, V_{act} , and ohmic overpotential, V_{ohm} . Details are given below.

Electrochemical:

$$V_{cell}(T) = V_{ocv}(T, p) + V_{act}(T) + V_{ohm}(T) \quad [V] \quad (3.1)$$

Open-circuit voltage, V_{ocv} , is the voltage necessary to start the water electrolysis reaction under ideal conditions. It is calculated using Nernst equation 3.2. In this equation, T_{op} is the stack average temperature between the inlet and the outlet of the anode side, pp_{H2O} is the water partial pressure, and pp_{H_2} and pp_{O_2} are the hydrogen and oxygen partial pressures in the hydrogen and oxygen gas separators, respectively. R , F is ideal gas constant and faraday constant, respectively. Reversible cell voltage is calculated as in equation 3.3. V_{std} is 1.23 V for PEM water electrolysis, and standard temperature T_{std} is 298.15 °K. Coefficient of temperature difference is calculated in [20].

$$V_{ocv} = V_{rev} + \frac{R \cdot T_{op}}{2 \cdot F} \cdot \ln \left(\frac{pp_{H_2} \cdot pp_{O_2}^{1/2}}{pp_{H2O}} \right) \quad [V] \quad (3.2)$$

$$V_{rev}(T_{op}) = V_{std} - 0.0009(T_{op} - T_{std}) \quad [V] \quad (3.3)$$

Energy losses within the PEM stack can be modelled as overpotentials. Activation overpotential, V_{act} , is the energy necessary to start the electrochemical reaction. It is dominant at low current densities. Here, i_{dens}

is the current density of stack electrodes in A/m^2 . α_{an} is the charge transfer coefficient of anode side. It is calculated experimentally in [20] to be 0.7353.

$$V_{act} = \frac{R \cdot T_{op}}{2 \cdot \alpha_{an} \cdot F} \cdot \text{asinh} \left(\frac{i_{dens}}{2 \cdot i_{0,an}} \right) \quad [V] \quad (3.4)$$

Ohmic overpotential, V_{ohm} , is the energy loss due to resistance of membrane in cell and it is dominated at medium current densities. Ohmic overpotential is calculated simply by Ohm's Law as shown in equation 3.5. Here, $R_{mem} [\Omega m^2]$ is the membrane resistance, calculated from membrane conductivity $\sigma_{mem} [S/m]$ and membrane thickness $\delta_{mem} [m]$. Nafion 117 membrane, with a δ_{mem} of $178e-6m$. Temperature dependence of membrane conductivity can be modelled using Arrhenius expression [22] in equation 3.7. The values for E_{pro} , activation energy required for the proton transport in membrane, and $\sigma_{mem,std}$, membrane conductivity at the reference temperature and pressure conditions are experimentally calculated in [20].

$$V_{ohm} = R_{mem} \cdot i_{dens} \quad [V] \quad (3.5)$$

$$R_{mem} = \frac{1}{\sigma_{mem}} \delta_{mem} \quad (3.6)$$

$$\sigma_{mem} = \sigma_{mem,std} \cdot \exp \left(\frac{E_{pro}}{R} \cdot \left(\frac{1}{T_{op}} - \frac{1}{T_{std}} \right) \right) \quad (3.7)$$

Additionally, concentration (diffusion) overpotential occurs when electrolysis reaction is fast and the mass transport is relatively slow. Its effect is dominant at high current densities. Concentration overpotential is ignored in this model assuming nominal cell current never reaches high current densities that concentration overpotential is dominant.

Electrolyser cell current and active power consumption is calculated using equations 3.8-3.9. $A_{membrane}$ in equation 3.8 is membrane area in cm^2 , which is 290 according to the technical specifications of the electrolyser in reference [20]. Nominal power of 60 electrolyser cells is considered to be 46 kW according to empirical parameters from [20] and these outputs are scaled according to 50 MW capacity of electrolyser.

$$I_{cell} = A_{membrane} \cdot i_{dens} \quad [A] \quad (3.8)$$

$$P_{cell} = I_{cell} \cdot V_{cell} \quad [W] \quad (3.9)$$

Input of pressure submodel is stack operation temperature T_{op} and the output is the partial pressures of water, hydrogen and oxygen as described in equations 3.10-3.12. Partial pressure of water, pp_{H2O} , is calculated using the empirical equation from [20]. The hydrogen and oxygen partial pressures are calculated using Dalton's law of partial pressures as shown in equations 3.11 - 3.12. P_{cat} and P_{an} are the hydrogen and oxygen storage tank pressures, respectively.

Pressure:

$$pp_{H2O} = 6.1078 \cdot 10^{-3} \cdot \exp \left(17.2694 \cdot \frac{T_{op} - 273.15}{T_{op} - 34.85} \right) \quad [\text{bar}] \quad (3.10)$$

$$pp_{H_2} = p_{cat} - pp_{H2O} \quad [\text{bar}] \quad (3.11)$$

$$pp_{O_2} = p_{an} - pp_{H2O} \quad [bar] \quad (3.12)$$

Massflow sub-model describes the mass transfer phenomena occurring in electrolysis cell with equations 3.13 - 3.15. The input of this submodel is cell current calculated in electrochemical sub-model. η_f is the faraday efficiency assumed to be 1. n_{cells} is the number of electrolyser cells, which is 60 per stack.

Massflow:

$$\dot{n}_{H_2} = \frac{n_{cells} \cdot I}{2 \cdot F} \cdot \eta_f \quad [mol/s] \quad (3.13)$$

$$\dot{n}_{O_2} = \frac{n_{cells} \cdot I}{4 \cdot F} \cdot \eta_f \quad [mol/s] \quad (3.14)$$

$$\dot{n}_{H_2O} = \frac{n_{cells} \cdot I}{2 \cdot F} \cdot \eta_f \quad [mol/s] \quad (3.15)$$

Electrochemical, pressure and massflow sub-models are same for both model A and model B. However, for model B, thermal domain is also created with lumped thermal capacitance model. Temperature of the electrolyser system is simplified with one equation 3.16. The first term on the right side, $Q_{elelctrolysis,heat}$, describes the heat generated by electrolysis reaction and it depends on cell voltage and current, as shown in equation 3.17. $V_{tn} = 1.48V$ is the thermo-neutral voltage of electrolysis in [20]. The second term, $\dot{W}_{pump,loss}$, stands for the work contribution of circulation pump, as shown in equation 3.18. Here, rated electric power consumption of the pump, $\dot{W}_{pump,elec}$, is 1100W for 46 kW electrolyser capacity, and the pump efficiency, $\eta_{motor,elec}$, is assumed to be 0.75. The third term, $Q_{cooling}$, represents for the heat removed by cooling system, it has linear relation with the consumed active power and offset base power. In equation 3.19, P_{offset} is assumed to be 1100 W and a_1 is 70 for 46 kW electrolyser capacity. The fourth term, \dot{Q}_{loss} , is for the heat lost to ambient and it depends on operation and ambient temperature. In equation 3.20, R_{th} is the experimentally calculated thermal resistivity of electrolyser. The last term in equation 3.16 comes from enthalpy lost with the products leaving the system, it has empirical equation that depends on temperature [67]. Considering equations (3.1 - 3.15) adding this dynamic sub-model, equation 3.16, to the system makes the general behavior of the electrolyser dynamic, since each sub-model depends on temperature parameter directly or indirectly.

Thermal:

$$C_{th} \frac{dT}{dt} = \dot{Q}_{elelctrolysis,heat}(V, I) + \dot{W}_{pump,loss} - \dot{Q}_{cooling}(P) - \dot{Q}_{loss}(T) - \sum_j \dot{n}_j \cdot \Delta h_j \quad (3.16)$$

$$\dot{Q}_{elelctrolysis,heat} = (V_{cell} - V_{tn}) \cdot I \cdot n_{cells} \quad (3.17)$$

$$\dot{W}_{pump,loss} = \dot{W}_{pump,elec} \cdot \eta_{motor,elec} \quad (3.18)$$

$$\dot{Q}_{cooling}(P) = P_{offset} + a_1 \cdot P \quad (3.19)$$

$$\dot{Q}_{loss}(T) = \frac{1}{R_{th}} \cdot (T_{op} - T_{amb}) \quad (3.20)$$

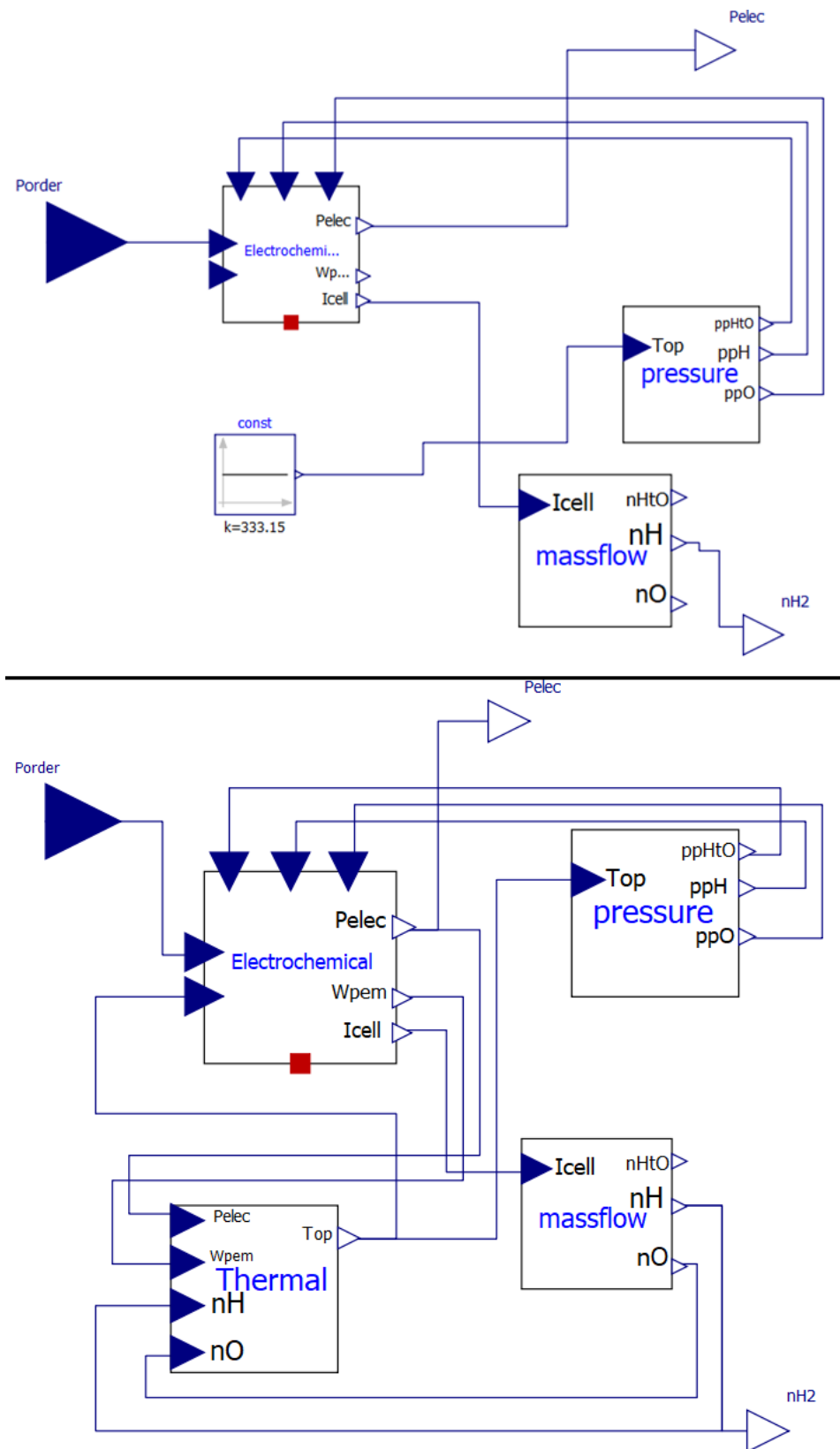


Figure 3.2: Electrolyser model "A" (upper) and model "B" (lower) in OM

Compressed Gas Storage Tank

Occupied storage capacity, S_{PtG} , is modelled with equation 3.21. Storage volume V is assumed to be 100 m^3 . $\dot{H}_{2,prod}$ is the amount of hydrogen in m^3 produced by electrolyser, as described in equation 3.22 and $\dot{H}_{2,demand}$ is the scheduled industrial hydrogen demand profile described in section 2.4. Storage is assumed to be at constant temperature 80 °C with no loss. Units are converted to m^3 using the values in table 3.2.

$$\frac{dS_{PtG}}{dt} = \dot{H}_{2,prod} - \dot{H}_{2,demand} \quad [m^3/s] \quad (3.21)$$

$$\dot{H}_{2,prod} = n_{cells} \frac{M_{H_2}}{\rho_{H_2}} \cdot \frac{I_{cell}}{2 \cdot F} \cdot \eta_f \quad [m^3/s] \quad (3.22)$$

$$\dot{O}_{2,prod} = n_{cells} \frac{M_{H_2}}{\rho_{H_2}} \cdot \frac{I_{cell}}{4 \cdot F} \cdot \eta_f \quad [m^3/s] \quad (3.23)$$

Table 3.2: Hydrogen & Oxygen characteristics at 80 °C

Parameter	Hydrogen	Oxygen
M (molar mass) [kg/mol]	2.016e-3	31.999e-3
ρ (density) [kg/m³]	0.06953	1.104
F (faraday constant)	96485	96485

Adjustable Power Level Controller

Figure 3.3 illustrates the implemented controller model in OM. In a normal operation where there is available space in the storage, minimum active power is controlled such that scheduled energy demand is always balanced by generation. However, when there is no available space in the storage, PtX is forced to work under 10% load until storage energy level is lower than maximum. When the storage energy level is below emergency level, which is assumed to be 50%, PtX is forced to work at nominal power until it reaches normal operation conditions. Maximum active power value is nominal power during normal operation, however it strictly follows minimum active power if storage is in another state.

$$P_{min} = \begin{cases} 0.1 \text{ p.u.} & S_{storage}(t) > S_{max} \\ P(t) - (\dot{n}_{H_2,prod} - \dot{n}_{H_2,demand}) \times K_{gain} & S_{emergency} \leq S_{storage}(t) \leq S_{max} \\ 1.0 \text{ p.u.} & S_{storage}(t) < S_{emergency} \end{cases}$$

$$P_{max} = \begin{cases} 1.0 \text{ p.u.} & \text{if } S_{emergency} \leq S_{storage}(t) \leq S_{max} \\ P_{min} & \text{else} \end{cases}$$

Static Generator

Static generator models in figure 3.1, 3.4 are directly from iPSL library [65]. Their behaviour is similar to current-controlled voltage source converter, and they provide interface with the electrical network.

3.1.2. Power-to-Heat

Figure 3.4 shows created power-to-heat model. The inputs of the model are scheduled district heat demand that defines minimum active power of heat pump and ambient temperature. In addition to these, active power set points to control heat output and/or voltage set point for reactive power control can be used. Details of heat pump and hot water storage tank model are explained below. Adjustable power level controller and static generator models are similar to power-to-gas.

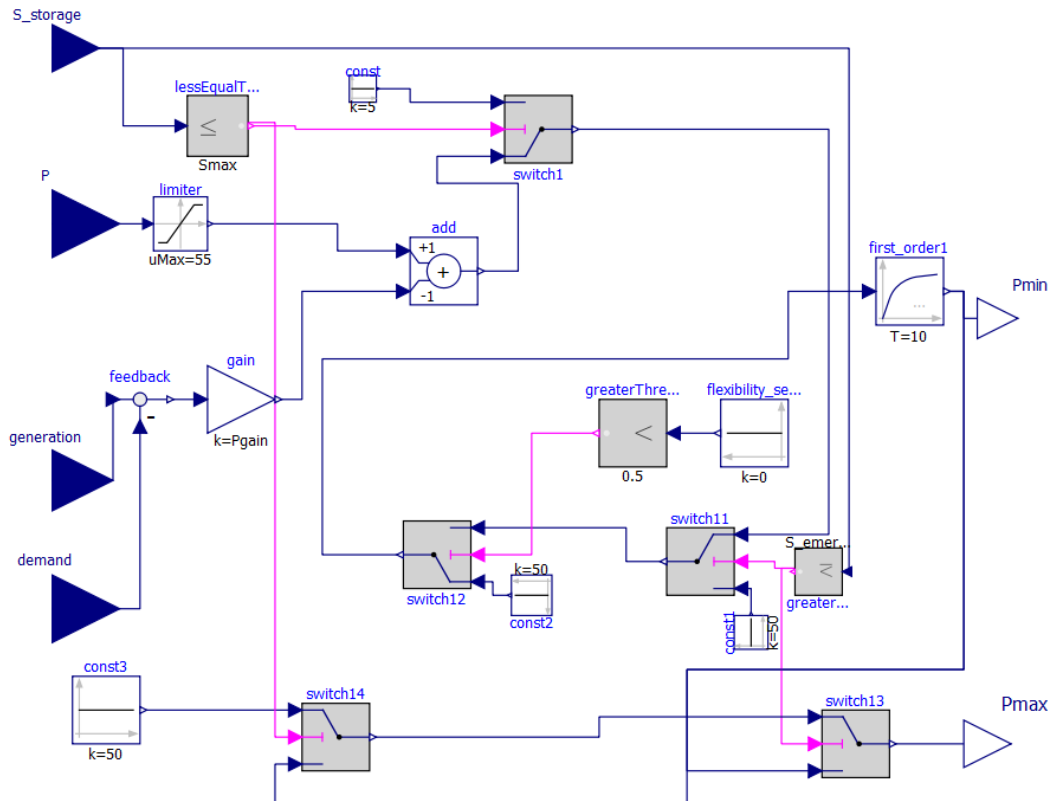


Figure 3.3: Adjustable power level controller in OM

Heat Pump

COP of a heat pump depends on the choice of refrigerant and the rankine cycle efficiency (Carnot efficiency) of that refrigerant inside the heat pump as described in equation 3.24. Using pressure - enthalpy table of refrigerant R134a and Matlab curve fitting tool, fifth order polynomial functions of COP depending on ambient and condenser temperatures are created. In figure 3.5, enthalpy at state 1 and state 3, depends on inlet and outlet temperatures and already known from saturated vapor and liquid table of R134a, the reader is referred to appendix D. Enthalpy at point two, h_2 , calculated by linear interpolation of the super-heat tables for R-134a assuming isentropic compressor work. Rest of the assumptions described in figure 3.5. As a result COP values are calculated for various $T_{ambient}$ and $T_{condenser} = 50, 70^{\circ}\text{C}$ conditions as given in table 3.3 and these results are used to create fifth order polynomial function of COP that depends on ambient and output temperatures.

$$COP = \frac{Q_{produced}}{P_{consumed}} = \frac{Q_{condenser}}{W_{compressor}} = \frac{h_2 - h_3}{h_2 - h_1} \quad (3.24)$$

Table 3.3: COP results for various ambient and condenser temperatures

$T_{ambient}$	-20	-16	-12	-8	-4	0	4
COP @ $T_{cond} = 50^{\circ}\text{C}$	3.3931	3.6429	3.9268	4.2500	4.6251	5.0604	5.5750
COP @ $T_{cond} = 70^{\circ}\text{C}$	2.4174	2.5586	2.7150	2.8887	3.0837	3.3013	3.5476
$T_{ambient}$	8	12	16	20	24	28	32
COP @ $T_{cond} = 50^{\circ}\text{C}$	6.1957	6.9452	7.8660	9.0564	10.5899	12.7115	15.7889
COP @ $T_{cond} = 70^{\circ}\text{C}$	3.8298	4.1514	4.5195	4.9559	5.4618	6.0736	6.8178

Three different models are considered for power-to-heat as explained in table 3.4. In model A, daily av-

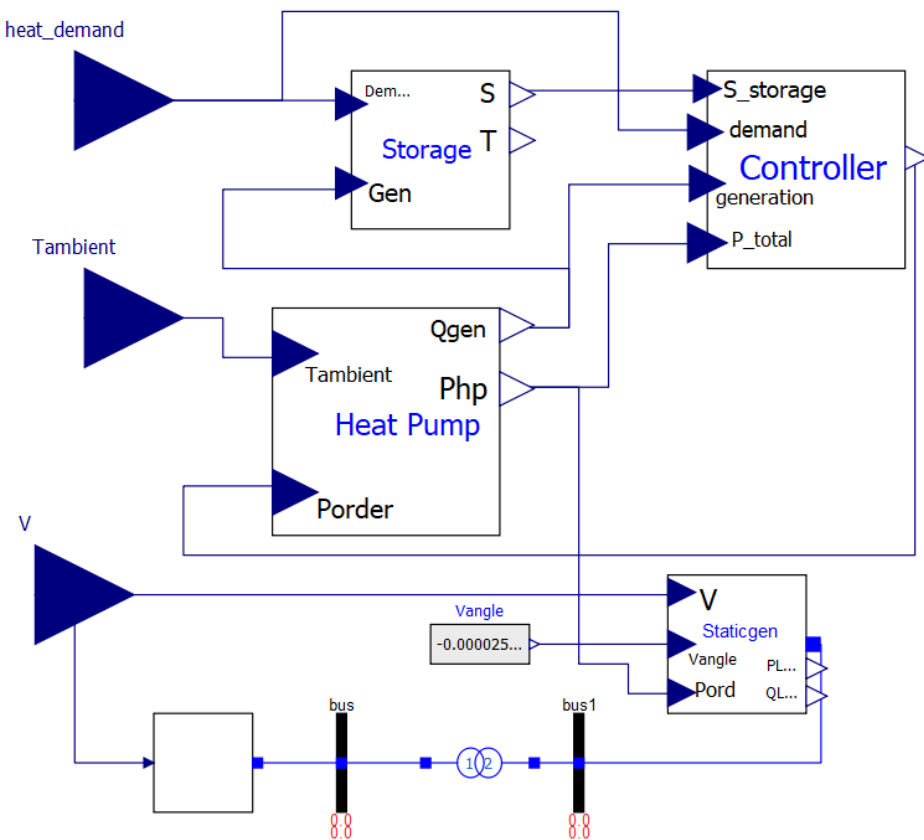
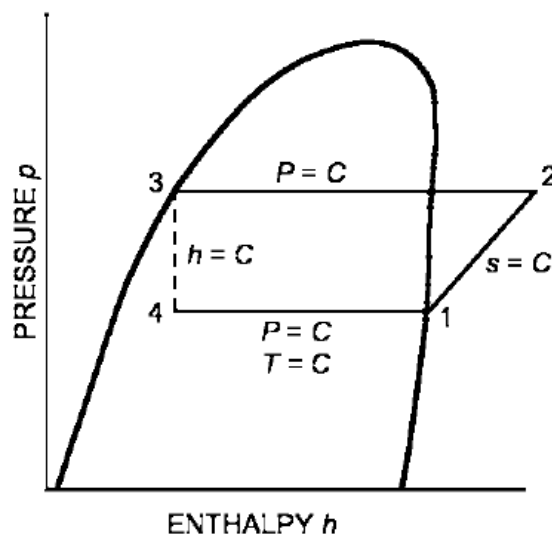


Figure 3.4: Power-to-heat model in OM

Figure 3.5: Theoretical Single-Stage Vapor Compression Refrigeration Cycle ($C = \text{Constant}$) [17]

verage ambient temperature is considered to be the evaporator temperature and it is constant during the day. For model B & C, hourly measured ambient temperature is considered to be the inlet temperature of heat pump. Additionally, for model C, auxiliary electric boiler is connected to the output of electric heat pump in order to increase the efficiency of heat pump. Table 3.4 shows modelling considerations for heat pump.

Figure 2.5 illustrates the heating cycle of PtH. With a return temperature equal to ambient, water is pumped to the evaporator of the heat pump. Here assuming constant mass flow rate for circulation pump, the energy output of heat pump is defined by compressor work and coefficient of performance. Basic approach to model electric heat pump is assuming constant COP and no change in temperature. This approach is considered for model A and described with equation 3.25 in this project. However, in reality COP strongly depends on temperature levels of the energy source. Therefore, regression analysis is carried out in order to create a polynomial function of COP depending on the inlet and outlet temperatures. As a result, COP is modelled as shown in equation 3.26. Additionally, COP increases when temperature difference between the inlet and outlet of the heat pump decreases. Therefore, especially during winter when the weather is cold, heat pump capacity might need to be increased with an auxiliary electric boiler to increase heat pump efficiency. Therefore, for model C, when the ambient temperature is below 15 °C, electric boiler is activated, as explained in equations 3.27-3.29, in order to increase the efficiency and heat capacity.

Table 3.4: Modelling considerations of heat pump

Model	Modelling Approach	Ambient Temperature	Modelling Scale
A	Regression	Daily average	Heat pump
B	Regression	Hourly measured	Heat pump
C	Regression	Hourly measured	Heat pump with auxiliary electric boiler

Model A:

$$P_t = \frac{\dot{Q}_t^{HP}}{COP^{average}} \quad \forall t \quad (3.25)$$

Model B & C:

$$P_t = \frac{\dot{Q}_t^{HP}}{COP_t^{real}(T_{inlet}, T_{outlet})} \quad \forall t \quad (3.26)$$

For Model C:

if $T_{amb} \leq 15^\circ\text{C}$:

$$Q_{boiler} = \dot{m} \cdot c \cdot \Delta T \quad (3.27)$$

$$\eta_{boiler} = 99\% \quad (3.28)$$

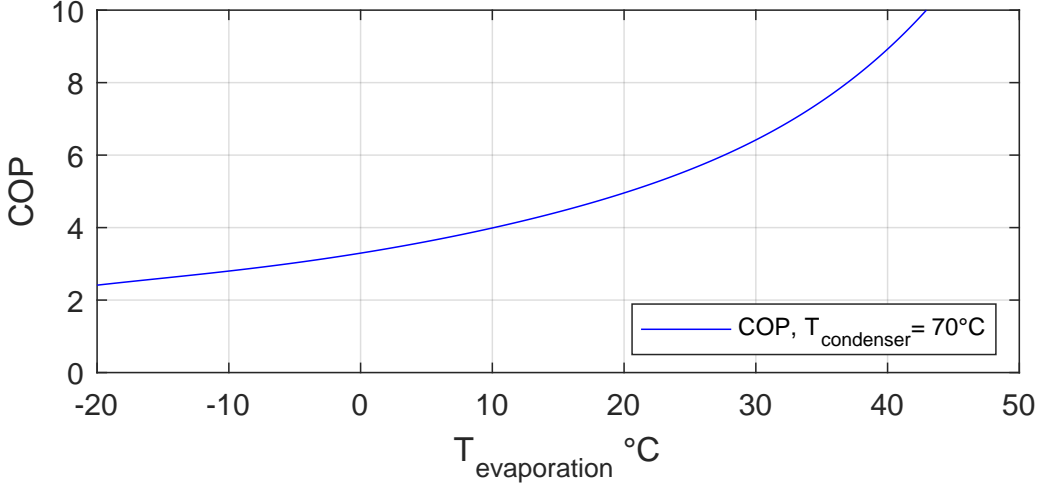
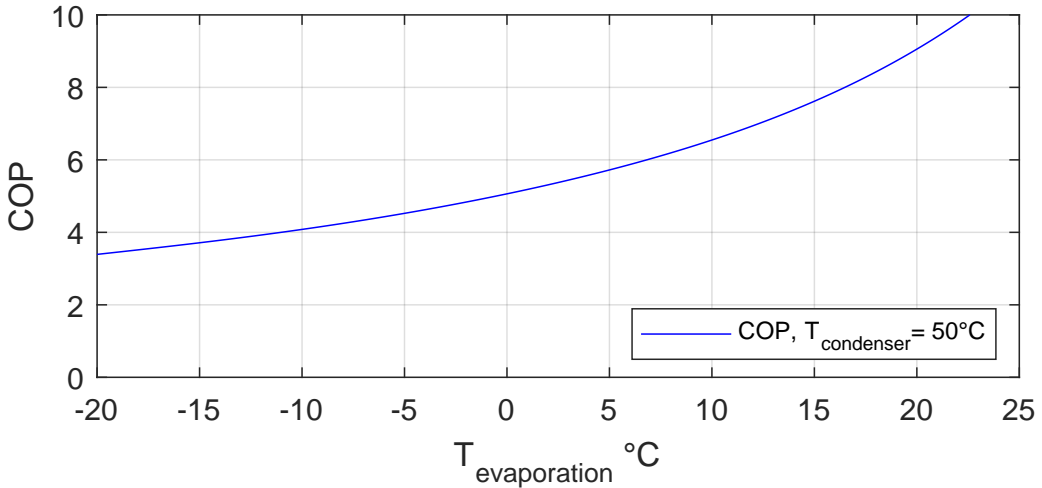
$$P_{boiler} = \frac{Q_{boiler}}{\eta_{boiler}} \quad (3.29)$$

Fifth order polynomial function of COP is shown in equation 3.30. Matlab curve fitting results are shown in figure 3.6, 3.7 and calculated coefficient results of fifth order polynomial function is shown in table 3.5. Two different COP equation coefficients are created for $T_{condenser} = 50$ and 70°C . This is because, for model C, when the ambient temperature drops below 15°C , heat pump output temperature is switched to 50°C to increase heat pump efficiency and the rest of the energy is supplied by electric boiler in order to increase supply temperature to 70°C .

$$COP(T_{amb}) = a_1 T_{amb}^5 + a_2 T_{amb}^4 + a_3 T_{amb}^3 + a_4 T_{amb}^2 + a_5 T_{amb} + a_6 \quad (3.30)$$

Table 3.5: 5th order polynomial fuction parameters for $T_{condenser} = 50, 70^\circ\text{C}$

$T_{condenser} (\text{ }^\circ\text{C})$	a_1	a_2	a_3	a_4	a_5	a_6
50	3.46e-8	1.29e-6	4.35e-5	2.387e-3	1.186e-1	5.063
70	1.46e-8	-9.66e-8	6.61e-6	1.01e-3	5.864e-2	3.295

Figure 3.6: COP vs. $T_{ambient}$, $T_{condenser} = 70^\circ\text{C}$ Figure 3.7: COP vs. $T_{ambient}$, $T_{condenser} = 50^\circ\text{C}$

Hot Water Storage Tank

Occupied storage capacity is modelled with equation 3.31. Storage volume V is assumed to be 2400 m^3 . Q_{prod} is the the amount of heat energy in m^3/s produced by heat pump, It is converted to from kg/s to m^3/s as described in equation 3.32, using specific heat and density of water at 70 °C. Values of equation 3.32 is given in table 3.6. Q_{demand} is the scheduled ditrict heatind demand profile described in section 2.4.

$$\frac{dS_{PtH}}{dt} = \dot{Q}_{prod} - \dot{Q}_{demand} \quad [\text{m}^3/\text{s}] \quad (3.31)$$

$$\dot{m} \cdot Q_{prod, [\text{kJ/kg}]} = c_p \cdot \rho \cdot (70 - T_{amb}) \cdot Q_{prod, [\text{m}^3/\text{s}]} \quad (3.32)$$

Table 3.6: Power-to-Heat storage parameters

Parameter	Value
m (massflow) [kg/s]	5
Q	[kj/kg] (t)
c_p (specific heat) [kj/(K kg)]	4.190
ρ (density) [kg/m3]	977.74
Storage Volume [m3]	2400

3.1.3. Electrical Base Load

20 MW constant electrical base load connected in pandapower, as illustrated in figure 2.1, to represent the constant base load in the industrial area.

3.2. Electrical Network & Optimal Power Flow

Higher level control is called community energy management system (CEMS). The role of CEMS is to minimize the operational costs of MES. For this purpose, a constrained, single objective, economic active power dispatch optimization problem was need to be created. A major advantage of pandapower is its capability to calculate optimal power flow (OPF) with cost functions. Therefore, it perfectly fit to create such optimization problem. The inputs of CEMS is the active power constraints coming from MES agents and the cost signals of PtXs. The outputs are the active power dispatch results for PtXs after the OPF. Additionally, bus voltage and/or reactive power can be considered depending on the nature of the study.

Figure 3.8 illustrates the co-simulation flowchart. Red dashed line, CEMS, represents the higher control level that is Pandapower and blue dashed line represents, lower control level, that is MES agents. At $t = 0$, optimal power flow (OPF) solver in pandapower calculates the optimum operation point with the objective of minimizing operational cost. After that the results of the OPF are sent to MES agents. Here PtX models simulate until the next exchange time and send out the adjustable power level and cost binding information to higher control level for the next calculations.

3.2.1. Formulation of the Optimization Problem

Python-based tool Pandapower is used for the energy management of MES. Pandapower optimal power flow solver has objective function to minimize operational cost, as shown in equation 3.33. Linear cost signals are calculated depending on the efficiency of device in Modelica, as explained in section 2.4 and sent to pandapower as the c_1 value of the polynomial cost function in equation 3.34.

Objective function:

$$\min \sum_{i \in load} f_i(P_i) \quad (3.33)$$

Cost function:

$$f_{pol}(p) = c_n p^n + \dots + c_1 p + c_0 \quad (3.34)$$

Optimal power flow problem of pandapower considers the constraints shown in table 3.7. Bus constraint contains maximum and minimum voltage magnitude, branch constraints contain maximum loading percentage and, attention of this project, operational power constraints contains the active and reactive power generation of generators or loads as operational flexibility for the OPF. This means, higher control level which is pandapower has to communicate with modelica agents and obtain the adjustable power level, which is P_{min} and P_{max} , in order to calculate the optimum operating point within this range. Optimal power flow solver calculates the exact operation point for the next time step considering cost signals within the available range defined by the physical situation of the agents. Thus, existing OPF problem of Pandapower is enhanced by adding OM agents and controlling these boundaries depending on the storage situation of agents.

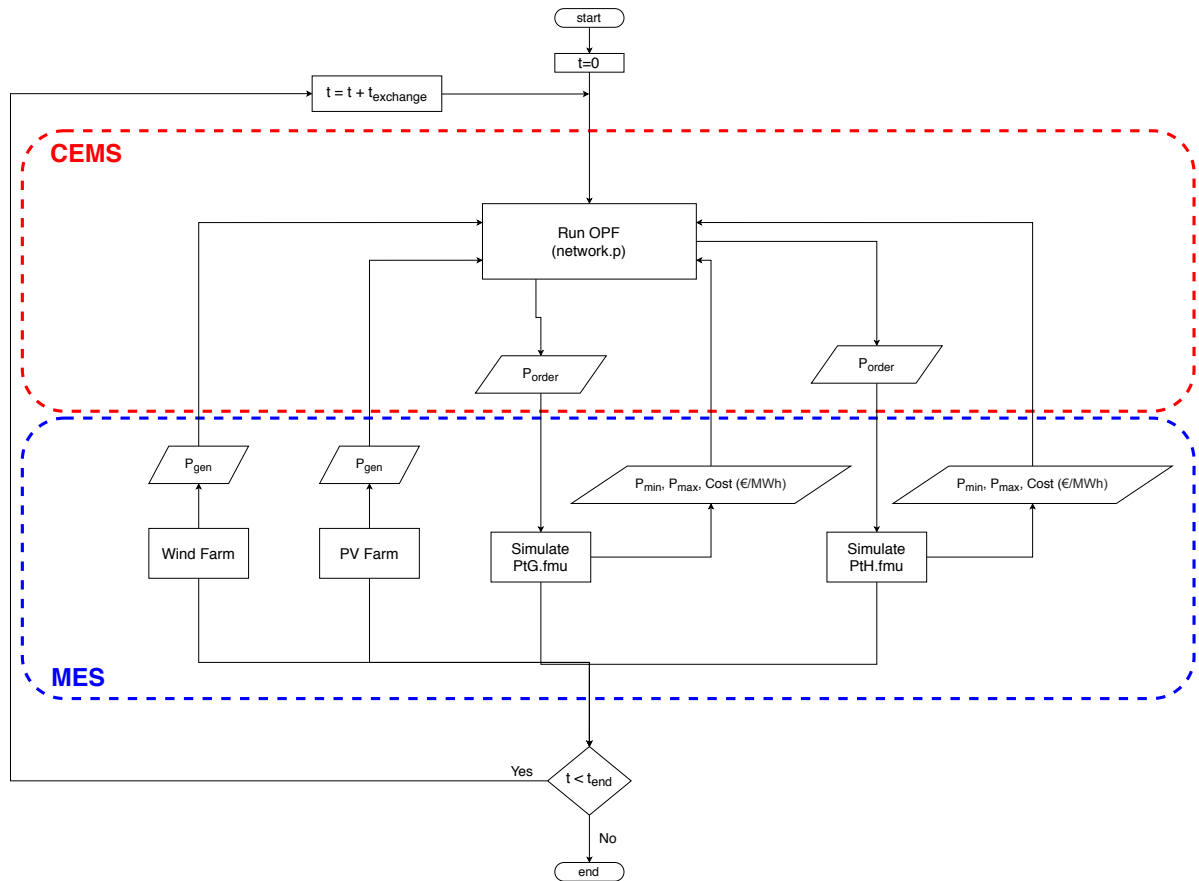


Figure 3.8: Co-simulation flow chart

Table 3.7: Constraints

Element	Constraint	Remarks
Load Static Generator External Grid	$P_{min,i} \leq P_i \leq P_{max,i}$ $Q_{min,i} \leq Q_i \leq Q_{max,i}$	Operational power constraints (Device flexibility)
Transformer	$L_i \leq L_{max,i}$	Branch constraint (maximum loading percentage)
Line	$L_i \leq L_{max,i}$	Branch constraint (maximum loading percentage)
Bus	$V_{min,i} \leq V_i \leq V_{max,i}$	Network constraint

3.3. Co-simulation Setup

Co-simulation was essential for this study as a result of multi-domain nature of MES and hierarchical control. Electrolyser model in gas domain and heat pump model in heat domain have different physical characteristics. Therefore, they modelled separately to have accurate representation of both energy domains. Electrical network and optimized control is modelled by a optimal power flow solver. These three files can not be combined with a single software tool. Thus, they are connected by means of co-simulation. Co-simulation inputs and outputs can be seen in figure 3.8 and parameters are given in table 3.8.

Table 3.8: Co-simulation parameters

Parameter	Value
Simulation duration [s]	3600*24
Exchange time [s]	900
Step time PtG [s]	3
Step time PtH [s]	3
Step time OPF [s]	300

Python-based tool Energysim is used to combine Modelica FMU's for PtX agents and Pandapower file for optimal power flow; and implement this complex simulation in a relatively simple way by exchanging only necessary variables. Figure 3.9 shows the macro step time that optimal power flow solver and Modelica agents exchange information, and micro step time that the agents simulate. With the considered exchange time and duration, simulation takes approximately 8 minutes.

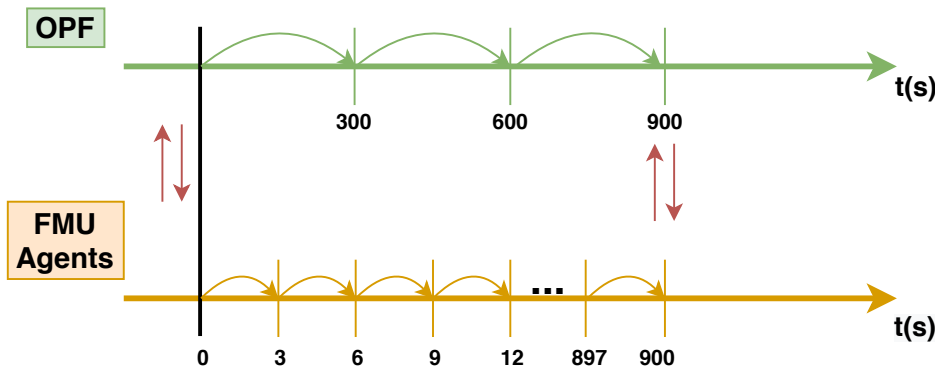


Figure 3.9: Co-simulation synchronization

4

Results & Discussions

4.1. Model Validation

Cell characteristic of PEM electrolyser model and coefficient of performance of refrigerant R134a cycle are validated in this section comparing with reference [11, 20]. To validate the electrolyser model, cell voltage response to cell current densities from 0 to 1.5 A/cm^2 is compared with the reference [20] in figure 4.1. During this analysis anode side pressure is set to 35 bar and operating temperature is set to 50 °C in order to be consistent with reference's result. Voltage curve above is from the reference and the curve below is the modelled electrolyser's cell voltage response. -0.02V offset found for the developed model with respect to reference for any value of cell current density, but overall characteristic is similar with increasing current density as can be seen in the figure. Small offset in the I-V curve of electrolyser model may be explained by rounding of parameter values. This effect is ignored during simulations. Additionally, anode and cathode side operating pressures are assumed to be kept constant at 30 bar during simulations to be compatible with reference [20]. Electrolyser efficiency varies around 70%. For 50 MW active power input, hydrogen molar production rate is calculated as 146.74 mol/s and 4.25 m³/s. Values of the model parameters can be seen in appendix F, and key modelling assumptions are explained in appendix E.

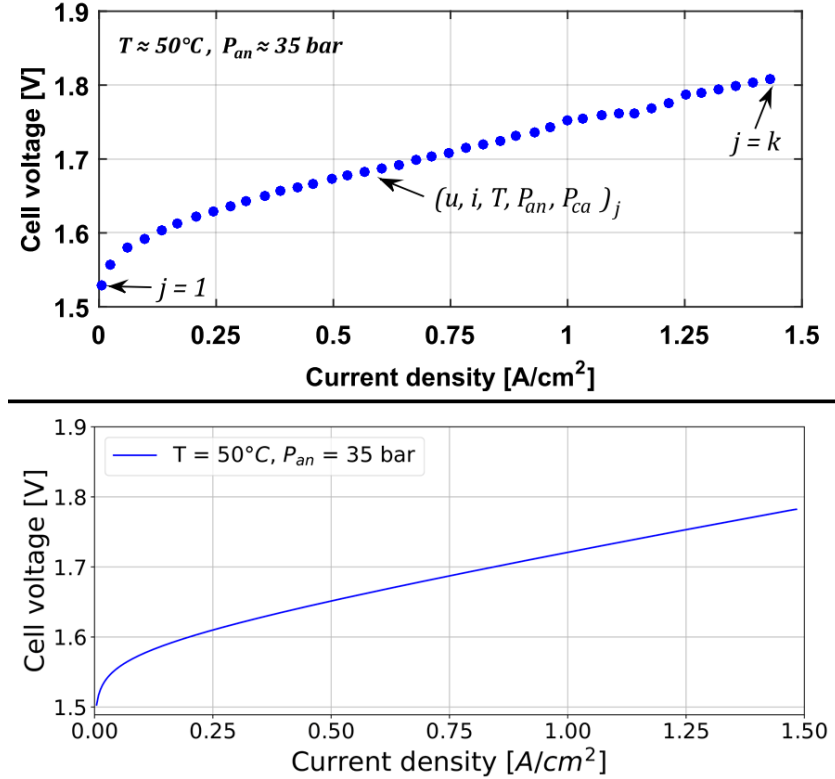
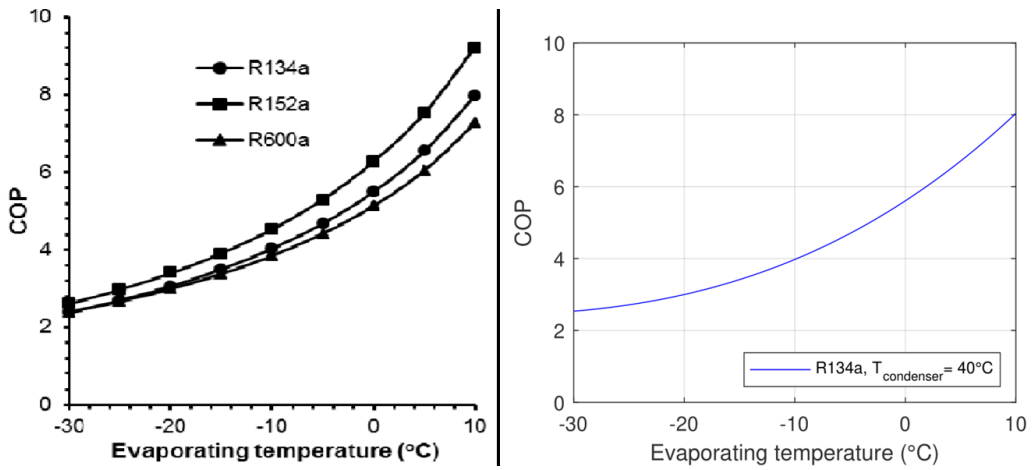


Figure 4.1: PEM Electrolyser cell voltage vs. current density

To validate the heat pump model, COP output of the model is compared with COP curve of refrigerant R134a cycle at varying evaporator temperature and at $T_{condenser} = 40^\circ\text{C}$ using result in reference [11]. Figure 4.2 compares both curves. COP curve on the left side is from reference [11] and curve on the right side is the calculated MATLAB curve fitting result of COP. No significant difference between two curves are observed. This was expected since model is derived from the ideal Carnot cycle efficiency of refrigerant using pressure-enthalpy table. During simulations, heat pump COP varies around four when $T_{condenser} = 70^\circ\text{C}$ and around seven when auxiliary electric boiler is activated. For 50 MW active power input, heat production rate of the model varies around $4.5 \text{ m}^3/\text{s}$ for $T_{condenser} = 70^\circ\text{C}$. Values of the model parameters can be seen in appendix G, and key modelling assumptions are shown in appendix E.

Figure 4.2: Coefficient of performance (COP) vs. evaporating temperature for $T_{cond} = 40^\circ\text{C}$

4.2. Analysis

Implementation of analysis is already explained in section 2.5. Considered days of 2019 are distinguished by yellow vertical dashed lines in figures 4.3 - 4.11. Results are shown below.

4.2.1. Multi-Energy System Analysis

Figure 4.3 illustrates the wind and solar farm capacity in the area. The sum of these two curves is considered as the total generation of MES. Figure 4.4 compares the total generation and demand of MES. Blue line is the sum of the power output of WF and PV farm and red line is the sum of active power consumption of model B of each PtX as illustrated in figure 4.11. Flexibility opportunities or needs due to variable RES can easily be identified from this figure. Figure 4.4 reveals that, in this area, energy can be stored during summer season and this stored energy can be used during winter, spring or in the second half of fall. Longer sun hours during summer not only increases the magnitude of excess RE but also increases the duration of it. Thus, summer season provides opportunity for longer flexibility services. Extreme wind conditions during winter can also provide opportunity to take the advantage of excess RE. But this should be considered for shorter flexibility services due to smaller time duration of excess RE. Thus, according to this figure 07.02.2019 is selected to be suitable for 24 hour simulations in power system analysis.

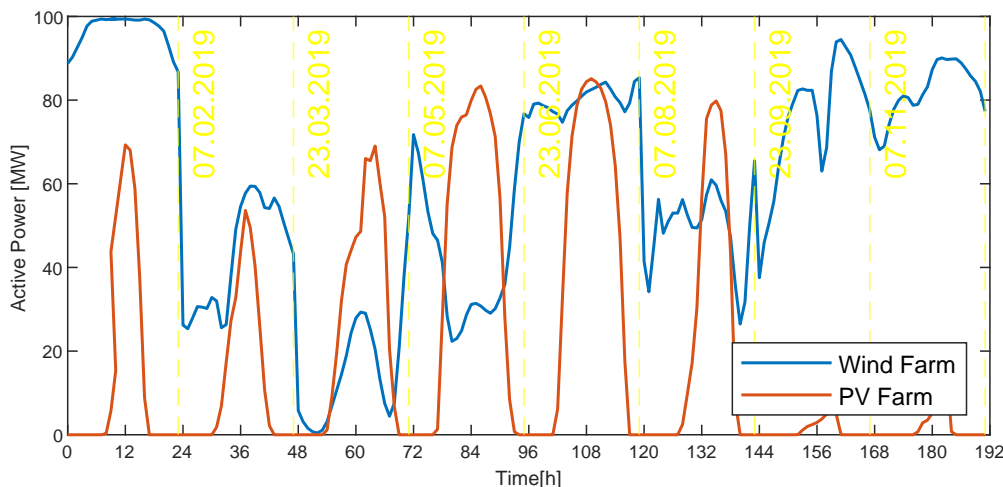


Figure 4.3: Power capacity of renewable energy sources

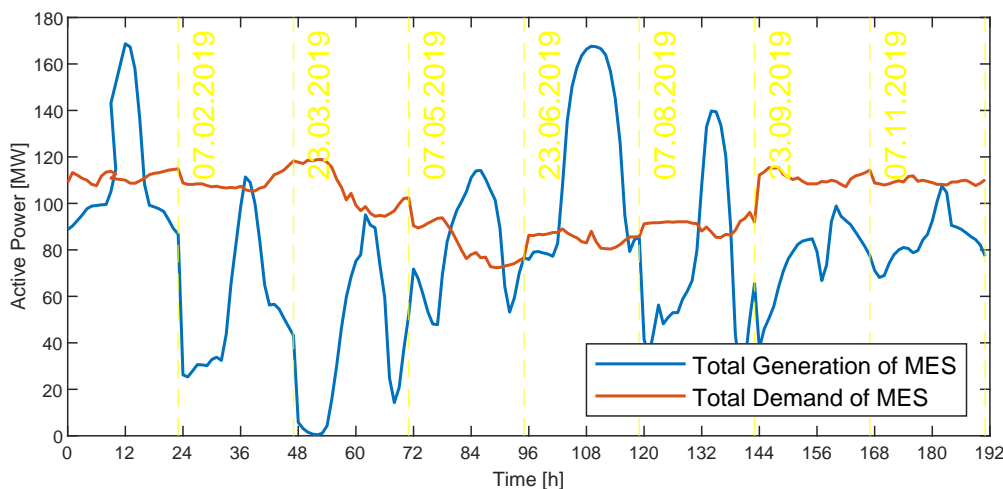


Figure 4.4: Flexible capacity of multi-energy system

4.2.2. Power-to-X Model Analysis

The effect of operational temperature evolution on efficiency curve of electrolyser and ambient temperature evolution on COP of heat pump can be observed in figures 4.6 and 4.9 respectively. For electrolyser model A temperature is constant at 60 °C and model B it varies between 52 to 65 °C as illustrated in figure 4.5. With respect to temperature deviation, maximum efficiency difference is 0.6% between model A and B in figure 4.6. This is not a significant difference. However, thermal sub-model is necessary to analyse the required capacity of auxiliary units for temperature regulation. If the cooling capacity of the system would assumed to be less than required, this would lead to larger temperature differences; therefore, bigger variations in efficiency results.

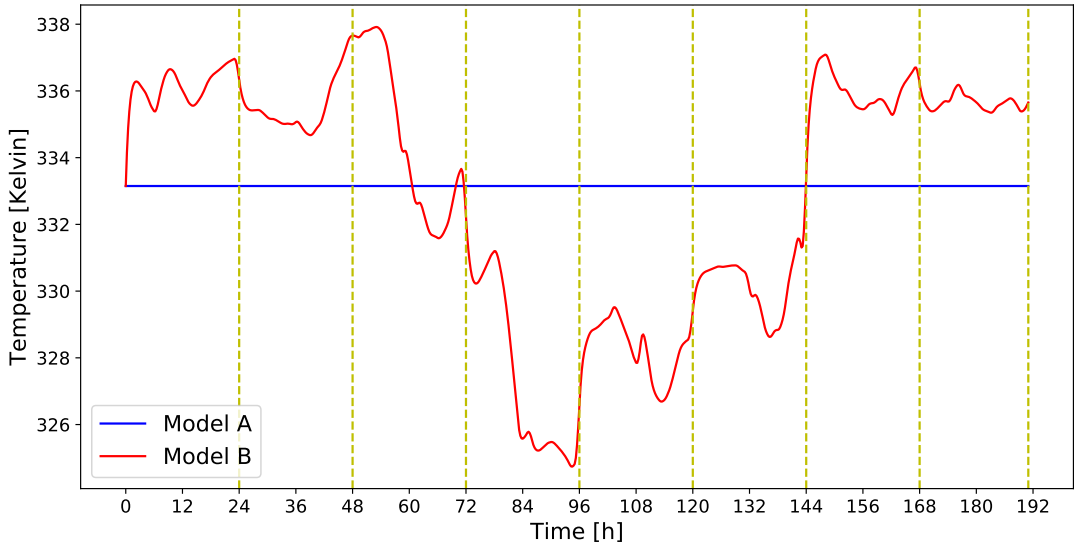


Figure 4.5: Operational temperature comparison of electrolyser models vs. time

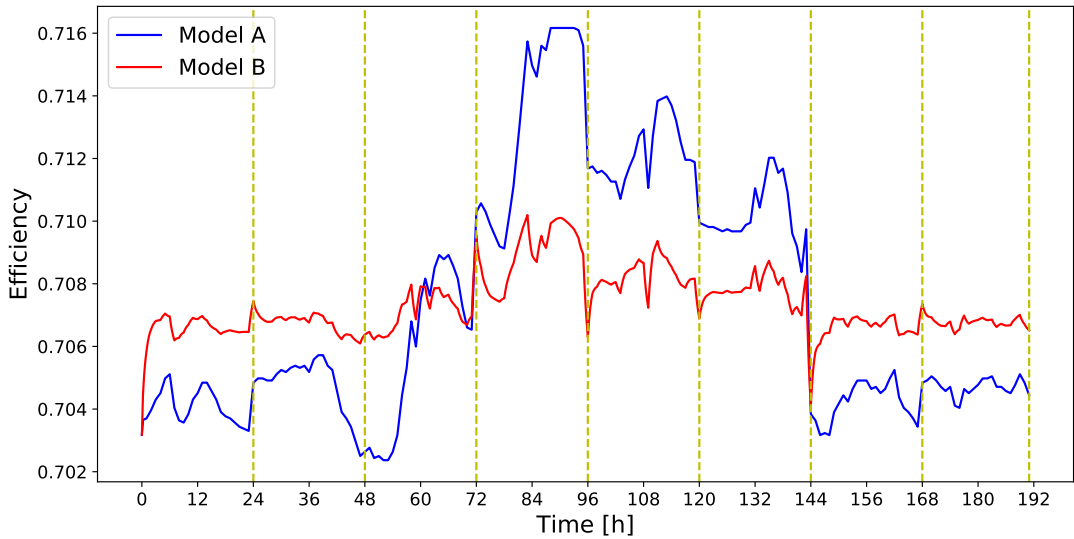


Figure 4.6: Efficiency comparison of electrolyser models vs. time

Figure 4.7 reveals the difference between the active power consumption of PtG models. Maximum power consumption difference between model A and B is 0.4 MW for 50 MW electrolyser system. This corresponds to 0.8% of the total capacity. The number is not significant in this case. However, as the electrolyser capacity increased, this percentage would lead to larger active power difference between models that may be critical to understand the available capacity of electrolyser.

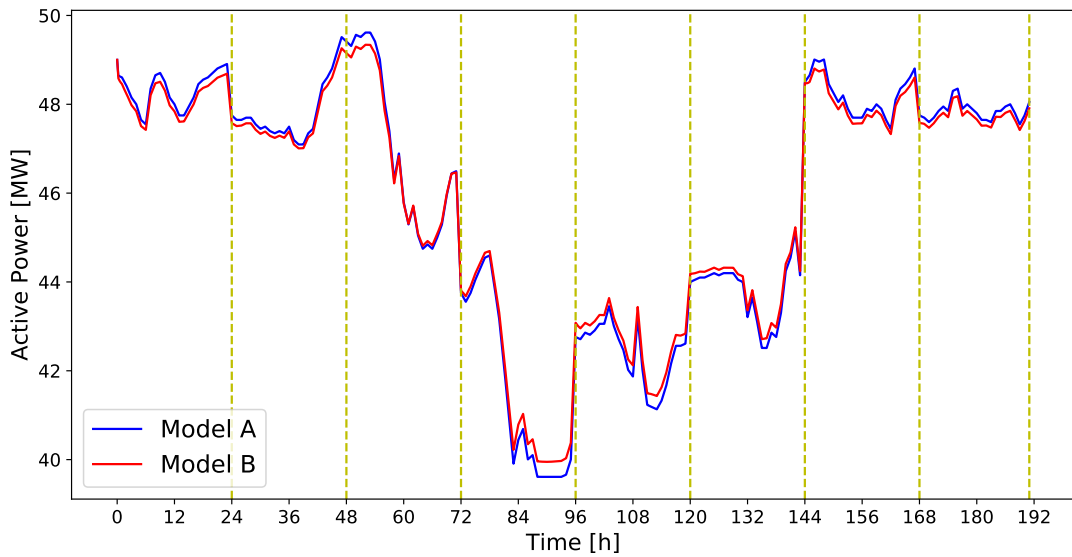
Figure 4.7: $P_{Load,PtG}$ of electrolyser models vs. time

Figure 4.8 illustrates the daily average and hourly ambient temperature data during the 8 days and figure 4.9 compares the COP output of models. For heat pump model A, COP is calculated from daily average temperature; therefore, it is constant during a day. For model B and C hourly measured temperature is used for COP calculations. Maximum COP difference between model A and B is 1.4 and model B and C is 3 . Results show that temperature considerations have significant effect on COP characterization of heat pump. Model C revealed that auxiliary boilers are able to improve efficiency of a heat pump considerably.

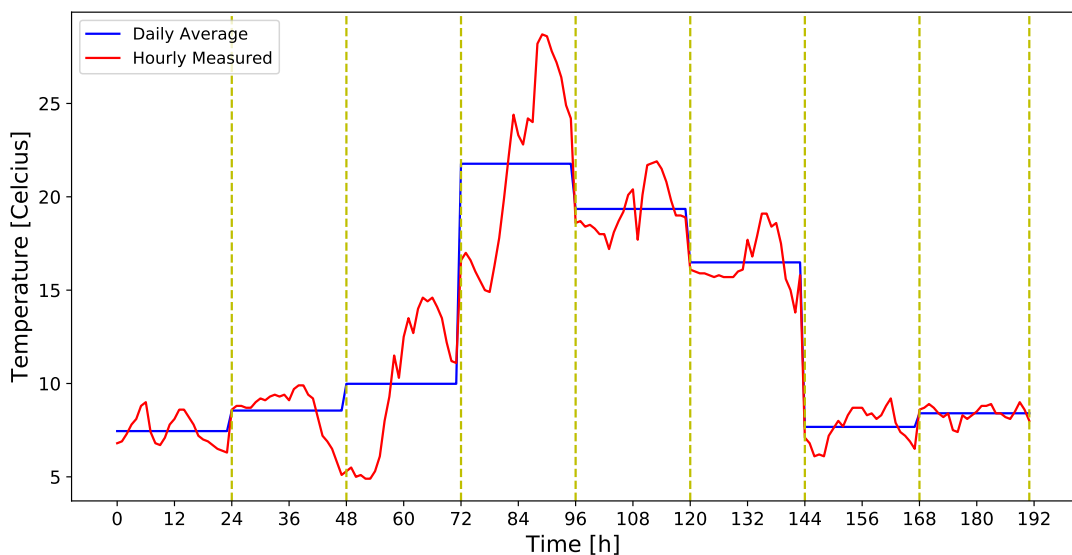


Figure 4.8: Ambient temperature vs. time

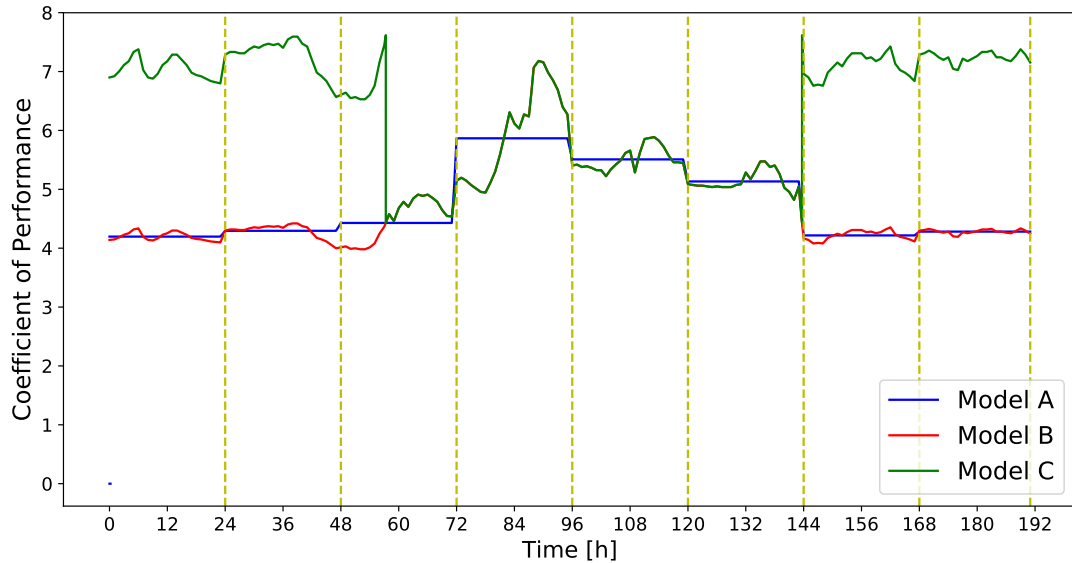


Figure 4.9: COP results of heat pump models vs. time

Figures 4.10 compares the active power consumption of PtH models. Maximum power consumption difference between model A and B is 9 MW and model B and C is 4.55 MW. This is equal to 18% and 9% maximum error for 50 MW electric heat pump system respectively. These are significant numbers. Therefore, COP of a heat pump can be assumed constant if inlet and outlet temperatures remain stable during operation. Otherwise, COP must be calculated with respect to temperature levels of the energy source.

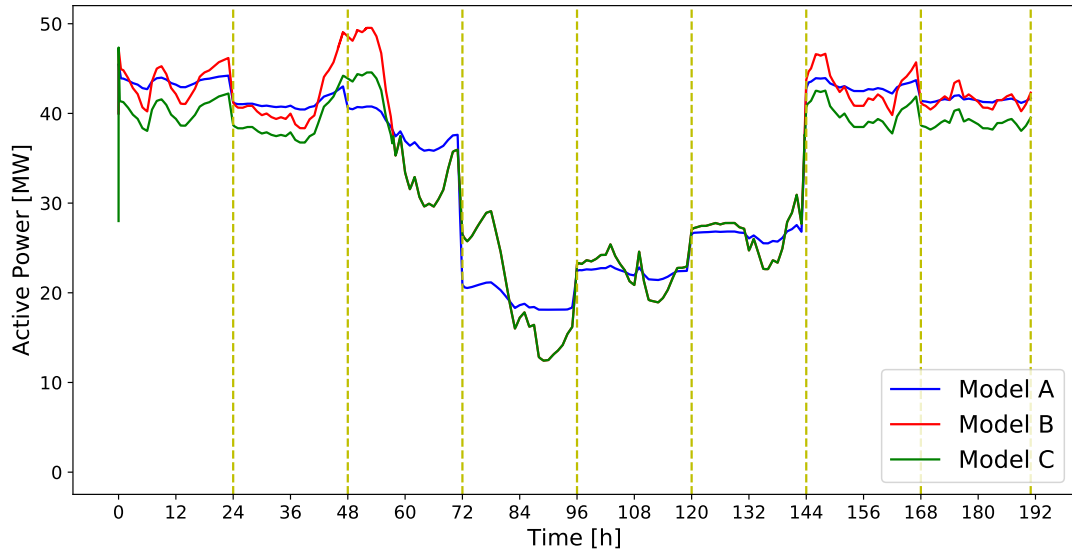
Figure 4.10: $P_{Load,PtH}$ of heat pump models vs. time

Figure 4.11 shows the demand curves of model B of each PtX. This figure validates that industrial hydrogen demand has less variations with respect to changing ambient temperature than district heating demand as expected from section 2.4.

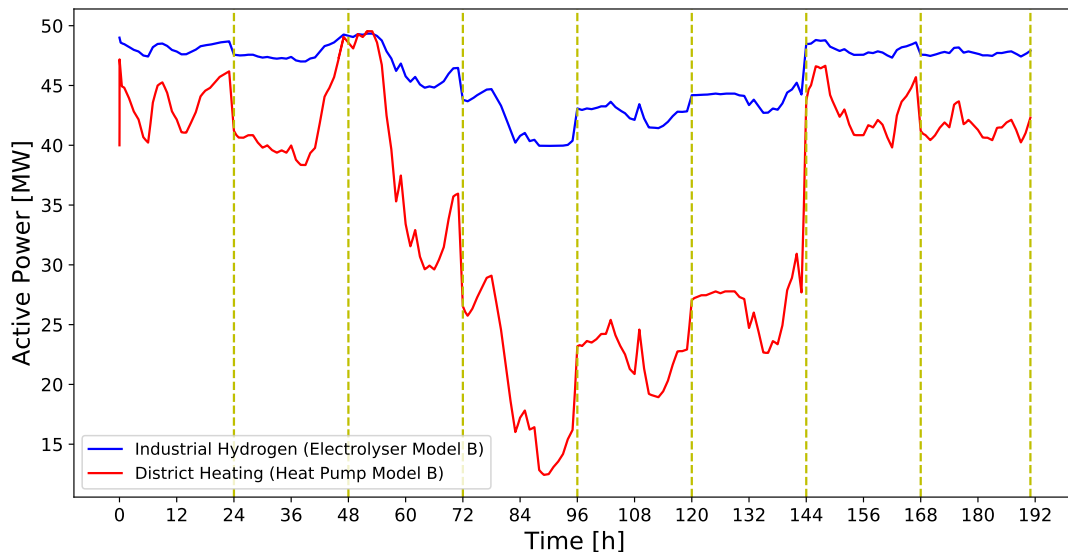


Figure 4.11: Active power consumption for Model "B" of PtG & PtH vs. time

4.2.3. Power System Analysis

This analysis is carried out in three cases as explained in section 2.5.3.

Base Case

Figure 4.12 shows the flexible active power demand of MES for base case. In this case, flexible demand of MES varies between +25 to (-60) MW. Results show that a flexibility service to store excess RE can be applied between 10:00 to 16:00 in this day. According to this flexibility service, resulting flexible demand curves are calculated for the first case.

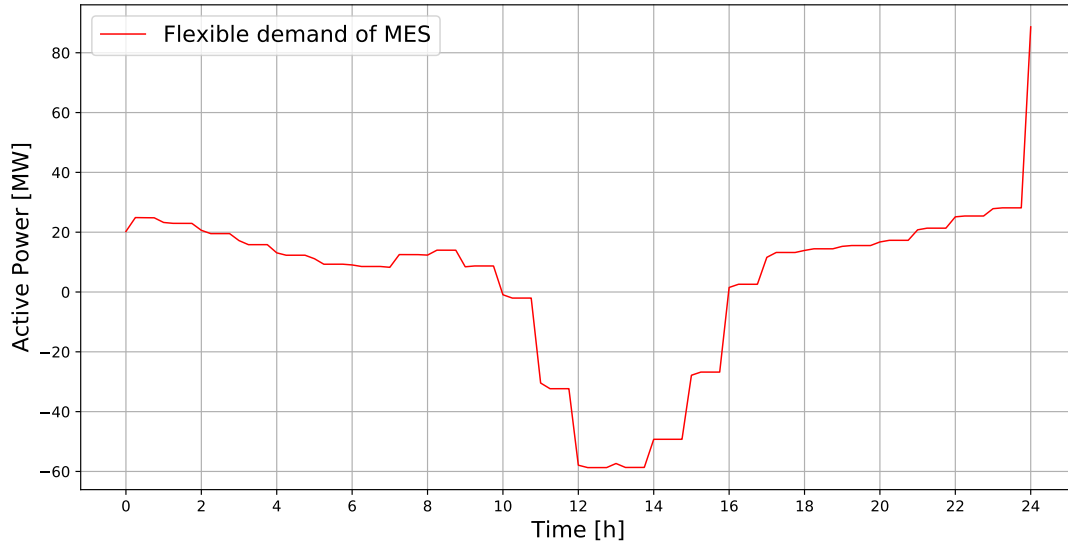


Figure 4.12: Flexible active power demand of MES on 07.02.2019 for base case

Case 1

Figure 4.13 compares the flexible demand of MES when only one of the PtXs is available for flexibility service. PtX is controlled such that, during excess RE, available capacity is used to store surplus energy. Green line is for comparison. It is the same curve in figure 4.12. Blue line is the active power consumption of model B of PtG, when only PtG is available for flexibility service. Red line is the active power consumption of model B of PtH, when only PtH is available for flexibility service. As can be seen from figure 4.13, during excess RE, active power set-point of available PtX is controlled such that the amount of excess RE is reduced and the

flexible demand curve is approached closer to zero. Since industrial demand is more stable at values close to nominal, it offers less flexibility. Therefore the maximum difference between base case and PtG case is 2 MW. On the other hand, PtH operates at lower demands due to higher rate of change of heat demand. Therefore, it is able to provide more flexible capacity to MES. Maximum difference between the base case and PtH case is 10 MW.

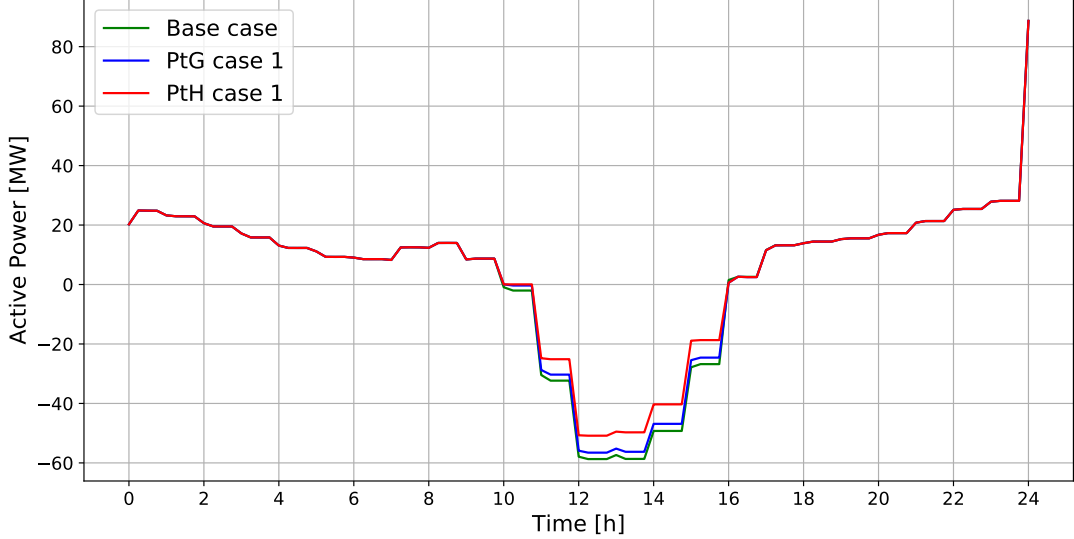


Figure 4.13: Flexible active power demand of MES on 07.02.2019 for case 1

Figure 4.14 compares the hydrogen production output of electrolyser models for the same flexibility service in figure 4.13. Increasing hydrogen production using excess RE can be observed between 10:00 to 16:00 in figure 4.14. For the other hours production curves follow the demand profile. Maximum difference between the hydrogen production output of model A and B is $0.032 \text{ m}^3/\text{s}$.

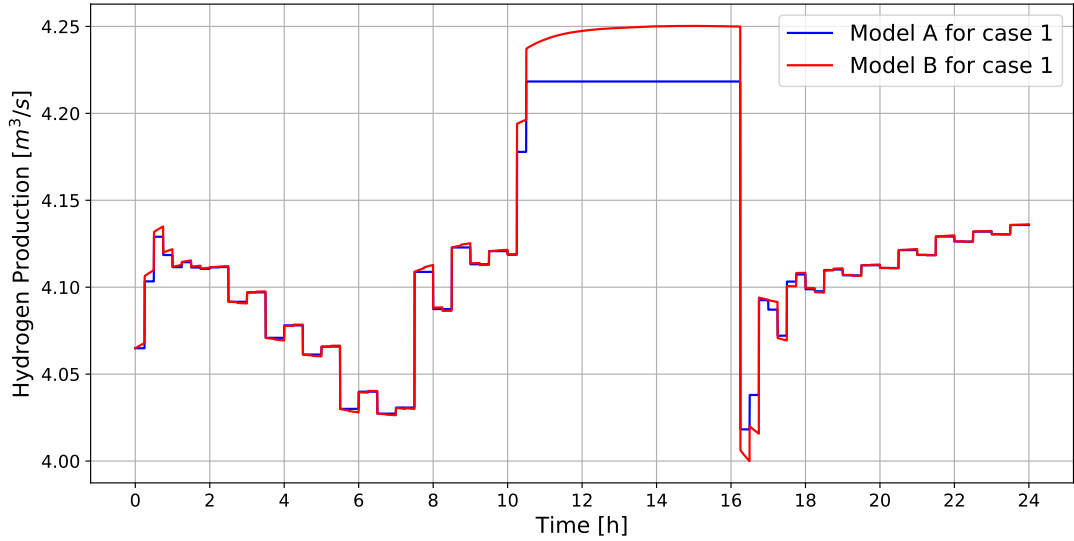


Figure 4.14: Hydrogen production of PtG models on 07.02.2019 for case 1

Figure 4.15 compares the heat production of heat pump models for the same flexibility service in figure 4.13. Blue curve illustrates heat pump model A with constant daily average temperature input. Red curve illustrates heat pump model B with hourly measured temperature input and green curve illustrates the heat pump model C with auxiliary electric boiler. COP is constant for model A; therefore, blue curve has less

volatility during the day. Maximum difference between model A and B is $0.20 \text{ m}^3/\text{s}$. During 07.02.2019, ambient temperature is below 15°C ; therefore, auxiliary boiler is activated for model C. It is obvious from the figure that auxiliary electric boiler increases the heat pump capacity significantly for heat pump. Maximum difference between model B and C is $0.96 \text{ m}^3/\text{s}$. Additionally, green curve reveals that the proportional gain of the adjustable power level controller of PtH, explained in section 3.1.1, is too small for Model C to return back to normal state after flexibility service. Therefore, it takes approximately 2 hours, between 16:00 - 18:00, for model C to follow the demand again. However, this has no effect on the results of this work since the aim is on the time horizon for flexibility service that is between 10:00 - 16:00.

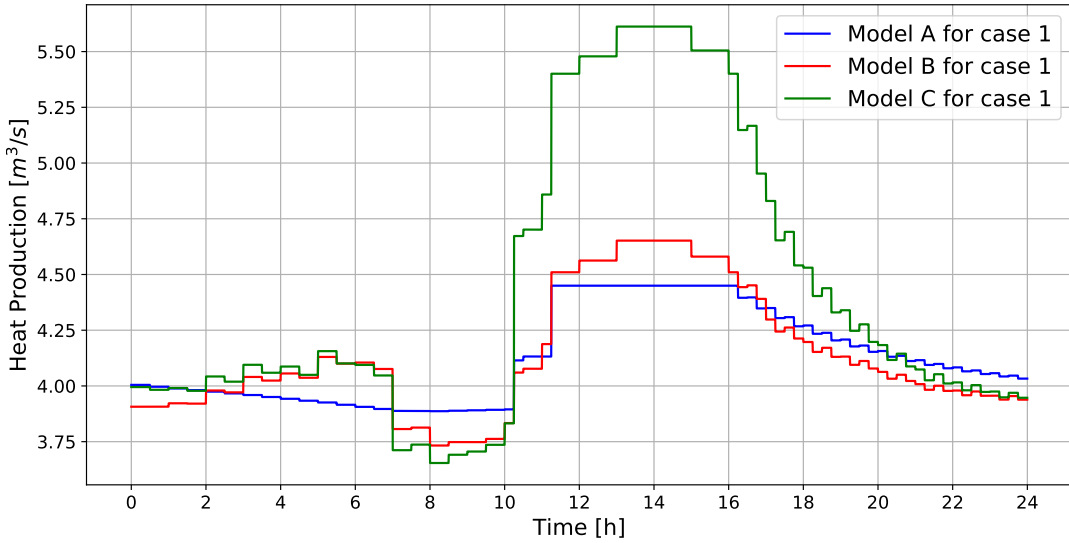


Figure 4.15: Heat production of PtH models on 07.02.2019 for case 1

Case 2

In this case, PtX load profiles explained in section 2.4 are lowered to half in order to observe the effects clearly. Figure 4.16 shows the leveled cost signals of PtG and PtH as explained in section 2.4. Blue curve shows PtG signals and red curve shows the PtH cost signals. From 10:00 to 10:15, PtG costs less than PtH. However, between 10:15 - 16:00 PtH costs less than PtG. These signals are used for the active power dispatch of available flexibility from 10:00 to 16:00.

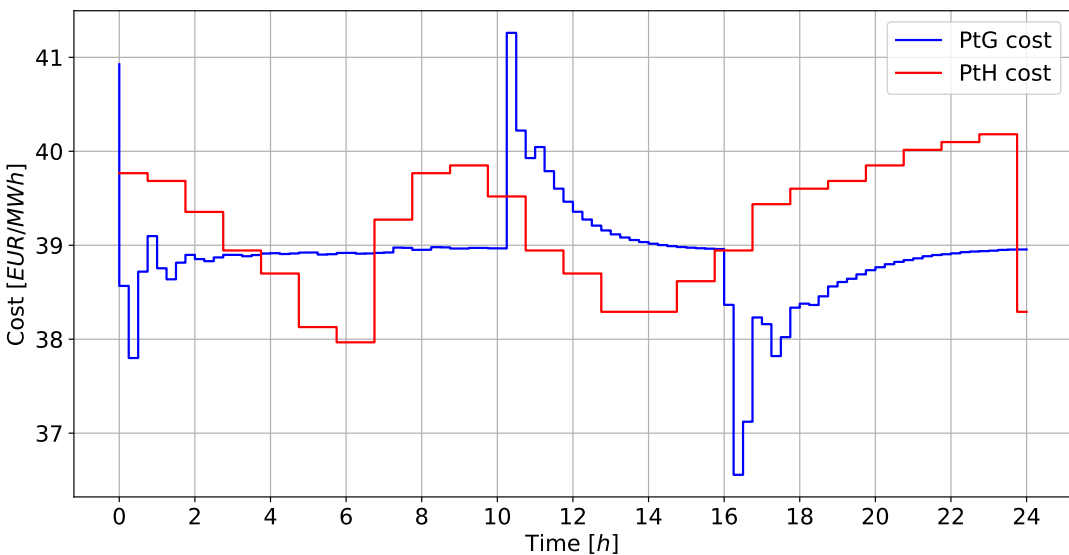


Figure 4.16: Levelized cost of PtX for case 2

Figure 4.17 presents the resulting active power consumption of PtXs and the amount of excess RE. The effect of flexibility service from 10:00 to 16:00 can be observed in figure 4.17. During this time, active power consumption of PtX is increased in order to take the advantage of excess RE. Figure 4.17 shows that flexibility of MES is able to compensate surplus power between 10:00 to 10:45. However, after 45 minutes the amount of surplus power is larger than the total flexible capacity of available PtXs; therefore, excess RE linearly increases from 0 to 23 MW between 10:45 - 11:00 and both PtX operates at 50 MW from 11:00 to 15:45. Between 15:45 and 16:00, active power output of PV farm drops to zero; therefore, flexible capacity of PtXs is able to compensate excess RE again, without operating both PtX options at nominal power.

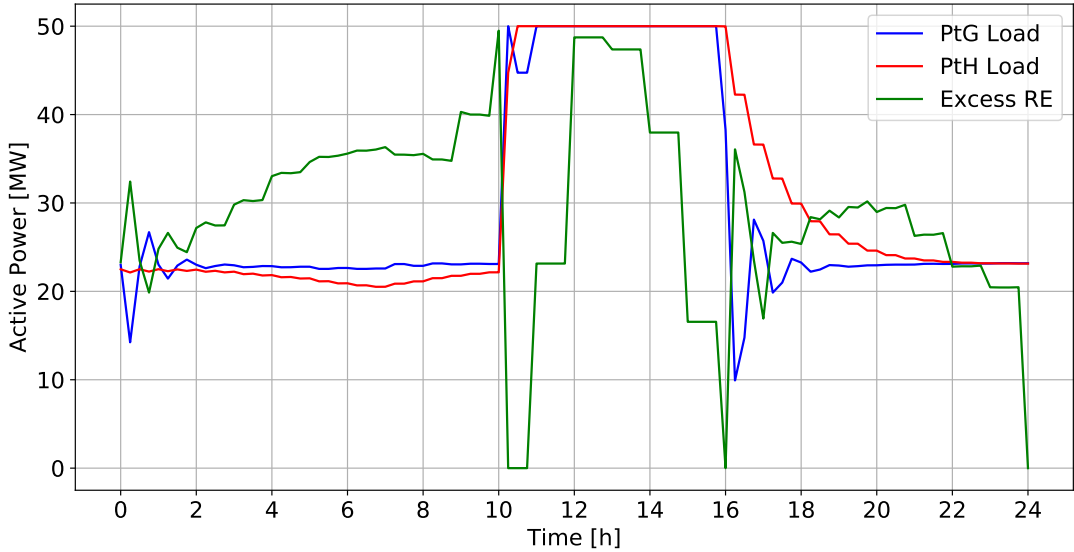


Figure 4.17: PtX active power consumption and Excess RE for case 2

The effect of cost signals on optimal flexibility deployment can be observed between 10:00 to 11:00 and 15:45 - 16:00. The exact values of blue and red curves in figure 4.17 are given in the first two column of table 4.1 which is the optimal deployment of flexibility. According to this result, two different flexibility dispatch strategies are compared in order to see the benefits of optimization. In 50% equal priority of flexibility scenario, that is the third and fourth column in table 4.1, it is assumed that both PtX has balanced priority for active power dispatch. Therefore available power is always shared equally between PtXs. In 100% PtG priority of flexibility scenario, that is the fifth and sixth column in table 4.1, it is assumed that PtG has priority to use surplus power at all times. Therefore, maximum available power is always used for PtG. The values for 11:00 to 15:45 are not given since operating point is 50 MW for both PtXs, and this has no effect on results.

As the amount of excess RE is smaller than flexible capacity of PtX during 10:00 to 10:45, this excess energy needs to be optimally distributed between PtXs. As can be seen from figure 4.16, in the beginning of the flexibility service at 10:00, PtG cost is cheaper than PtH for 15 minutes; therefore, PtG active power consumption is set to nominal value 50 MW initially while PtH is set to 44.74 MW. However, after 15 minutes, PtH cost becomes cheaper than PtG cost for the rest of the flexibility service. This results with higher active power consumption of PtH than PtG after 23 minutes. This effect is observed in figure 4.17 from 10:00 to 10:30, as the blue line that represents the PtG load crosses the red line that represents the PtH load between 10:15 to 10:30.

Table 4.1: Active power dispatch for optimal deployment of flexibility & priority assumptions

Time	Optimal Deployment		50% Equal Priority		100% PtG Priority	
	PtG [MW]	PtH [MW]	PtG [MW]	PtH [MW]	PtG [MW]	PtH [MW]
10:00	23.10	22.15	23.09	22.15	23.10	22.15
10:15	50.00	44.74	47.37	47.37	50.00	44.74
10:30	44.74	50.00	47.37	47.37	50.00	44.74
10:45	44.74	50.00	47.37	47.37	50.00	44.74
11:00	50.00	50.00	50.00	50.00	50.00	50.00
—						
16:00	38.27	49.98	44.13	44.13	49.98	38.27

Table 4.2 shows the total operational costs between 10:00 to 16:00 with respect to three presented flexibility deployment strategies in table 4.1. Optimal deployment of flexibility is able to save 2.75 € with respect to 100% PtG priority and 0.99 € with respect to 50% equal priority. Results show that optimal energy management of MES is able to provide significant cost savings annually. Therefore, with accurate market models, implemented co-simulation method is able to bring detailed results for the optimum energy management of MES, considering physical constraints of agents and market signal simultaneously.

Table 4.2: Total operational cost for optimal deployment of flexibility priority assumptions

Time	Optimal Deployment [€]	50% Equal Priority [€]	100% PtG Priority [€]
10:00 - 10:15	686.47	686.67	686.48
10:15 - 10:30	956.61	956.62	957.76
10:30 - 10:45	943.84	944.30	944.76
10:45 - 11:00	959.64	959.96	960.28
11:00 - 11:15	987.37	987.37	987.37
—			
15:45 - 16:00	916.58	916.59	916.61
Total Cost	22932.0294	22933.0185	22934.7779

5

Conclusion & Future Work

5.1. Conclusion

This thesis has provided a deeper insight into multi-energy system flexibility. The findings will be of interest to grid operators, industrial PtX owners and researchers of the subject. The aim of this research was to examine the model fidelity of PtX devices for flexibility analysis and to assess comprehensive energy management strategies to optimally control MES. This study has shown that the flexibility analysis requires correct efficiency characterization of models and operating temperature of PtX has substantial influence on performance of the device. Therefore, detailed thermal models are necessary to accurately represent the efficiency of PtX otherwise flexibility analysis may result with defective outcomes on active power consumption or energy production output of PtX. Additionally, detailed modelling of physical conditions of PtX might not be necessary if operating conditions are assured to be ideal or close to ideal during application. The second major finding was that the agent based hierarchical energy management is able to optimally operate the considered MES. This approach reveals a multi-layer structure for the energy management that enables the implementation of local control objectives for the agents individually and a global objective for MES that constrained by the information coming from agents. Lastly, the relevance of co-simulation and Energysim for flexibility analysis of MES is clearly supported by the current methodology. Co-simulation is especially advantageous to represent the multi energy domain nature of MES and Energysim facilitates the development of co-simulation.

In response to the first research question: '**which technologies have the highest potential to provide flexibility?**', it was found that power-to-hydrogen for industrial processes and power-to-heat for district heating has the most potential for providing flexibility. Power-to-hydrogen and water electrolysis is advantageous due to versatility of hydrogen and its multiple utilization. Despite this, the electrolysis process requires water conditioning and this makes the hydrogen production more expensive than other fuels. Power-to-heat is profitable, because high efficiency of PtH makes the generation costs extremely low with respect to other PtX options. Also PtH has low storage costs with respect to others. Comparing both PtG and PtH, latter is more volatile relative to ambient temperature. This means, when the weather is warm, PtH is able to provide more adjustable power margin to balance the surplus energy. As the weather gets cold, district heating demand would increase and this would lead to less flexible capacity for PtH. On the other hand, hydrogen itself is already flexible as an energy carrier because it can be used directly as a fuel or converted into synthetic gas, methane or LPG. Also, compared the other storage units, hydrogen storage has significantly less losses than other storage options. This makes hydrogen storage convenient for seasonal storage purposes. Therefore, PtG with storage offers more alternatives for demand-side management along side with flexibility.

In response to the second research question: '**to what extent does model fidelity impact flexibility analysis?**', precision of flexibility analysis is bounded by the efficiency characterization of PtX and correct efficiency characterization of PtX highly depends on operating temperature or pressure conditions. Therefore, physical conditions of PtX must be modelled in detail for flexibility analysis.

In response to the third research question: '**how to manage optimal deployment of flexibility consider-**

ing individual resource constraints?", it was found that demand response is crucial to increase flexibility of power system. Particularly market demand response, that is the price signals, and physical demand response that is PtX conditions necessary for the optimal management of MES. A comprehensive control approach can be achieved by hierarchical agent based energy management systems. This new understanding should help to improve predictions of the optimum operating point of the MES.

5.2. Contributions

This study makes the following contributions to the current literature:

1. Power-to-Gas with PEM electrolyser and power-to-heat with electric heat pump models are developed in OpenModelica to represent the "X" side of power-to-X. The models can be further improved for detailed gas side, heat side or control analysis.
2. Current optimal power flow problem of Pandapower is enhanced by the developed OpenModelica models. Flexibility constraints and cost signals of optimal power flow are modelled in OM and sent to Pandapower. By this way, a simple approach to consider physical effects and cost signals for the optimal energy management of MES is introduced.
3. A co-simulation setup for detailed MES control and flexibility analysis is created. Co-simulation provides endless opportunities for analysis of MES with various details according to the needs of study. The method used for flexibility analysis may be applied to larger scale MES models in the future .
4. A method to calculate levelized cost signals is developed to examine the operational cost saving potential of optimal deployment of flexibility.

5.3. Recommendations for future work

Findings of this study provide the following insights for future research:

- The focus of this project was on the demand side. However, a greater focus on variable renewable energy sources could produce interesting findings. In particular, renewable forecast models can be developed for investigating their effect on flexibility results and comparing with the results of this study. Also, virtual inertia need from RES power electronic converters can be analyzed by combining the active and reactive power outputs with the inertia model of MES.
- Considerably more work will need to be done to determine intelligent demand response of MES. Specifically, demand response of industrial systems (peak shaving, demand shifting, etc.) require more sophisticated analysis because of many factors such as production constraints, maintenance schedules, storage constraints, etc. Further research may consider these limitations of industrial systems for the optimal demand response.
- Very little was found in the literature for experimental data or modelling of industrial power-to-X. This makes the validation of the model almost impossible for the large-scale PtX devices. Therefore characteristics of industrial PtX must be experimentally investigated, by researcher or manufacturer, in order to correctly validate the developed models in the literature.
- It has been proven that price signals are crucial to optimally control MES. Thus, further work on MES market modelling could produce interesting findings that account for the most economic operation of MES.

A

Historical Data Processing & Probabilistic Weather

Historical data process is summarized in figure A.1. 2019 historical wind speed and solar irradiation data of RES location is divided into 8 regions that consists of 45 days. For every hour of each 45 day group a histogram table is created [24]. Then parameters of the Weibull and Beta PDF (shape, scale) are calculated by curve fitting in MATLAB using these tables.

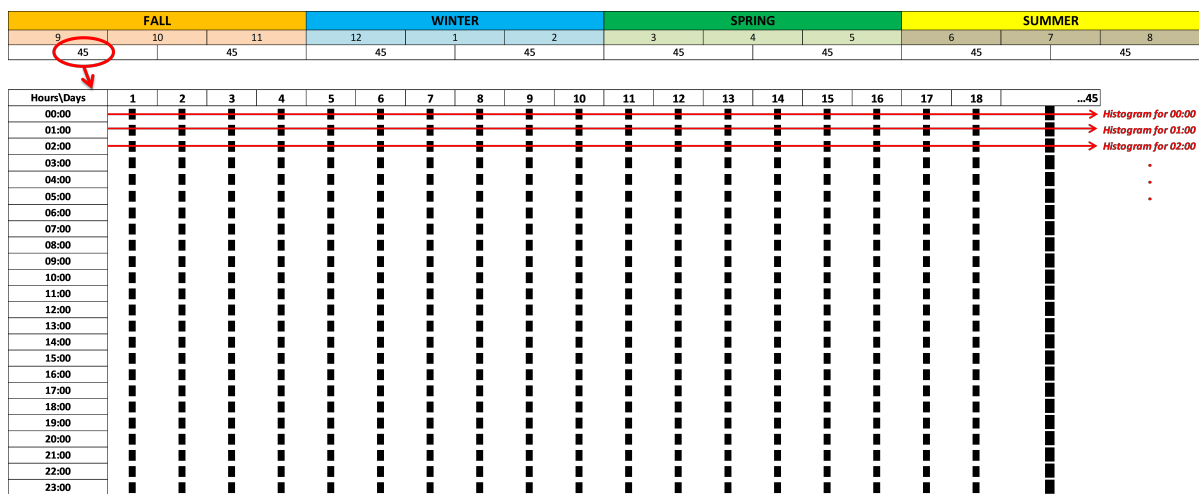


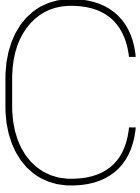
Figure A.1: Historical data processing

It was considered that probabilistic density function (PDF) of weibull and beta distribution for wind speed and solar irradiation generation, respectively, would be modelled based on historical data processing in order to investigate the effect of renewable energy generation models (Probabilistic vs. Historical data). However, it is observed that these models increase the simulation time significantly due to random generation of renewable energy sources with large amount of equations. Therefore, these models currently not in use and this part is excluded from the project.

B

Wind Farm & PV Farm Data

Hour\Day	7.02.2019			23.03.2019			7.05.2019			23.06.2019			7.08.2019			23.09.2019			7.11.2019			23.12.2019		
	Power (kW)	Speed (m/s)																						
0:00	88750.949	11.357	26222.646	6.026	5778.91	3.742	71760.561	9.325	75839.049	9.693	41444.907	7.124	37547.003	6.861	71138.664	9.271								
01:00	90293.251	11.659	25343.918	5.952	3129.872	3.145	67431.457	8.964	79043.579	10.029	34188.088	6.619	45931.625	7.431	68130.061	9.02								
02:00	92691.445	12.187	27907.221	6.161	1549.057	2.609	60889.148	8.451	79285.795	10.055	44850.676	7.359	50252.668	7.736	68972.071	9.089								
03:00	94943.193	12.897	30633.557	6.365	716.795	2.153	53278.167	7.929	78669.285	9.989	56283.77	8.138	55714.664	8.094	74136.082	9.539								
04:00	97679.965	14.228	30509.491	6.354	413.059	1.879	48115.306	7.575	78198.107	9.934	48165.889	7.577	64016.641	8.689	77557.683	9.896								
05:00	98850.022	15.322	30188.681	6.328	1095.603	2.39	46490.986	7.47	77243.433	9.838	50929.367	7.763	70894.933	9.245	79975.279	10.131								
06:00	99100.837	15.721	32822.538	6.529	3165.853	3.155	41149.653	7.102	76661.851	9.782	52996.879	7.91	76095.485	9.726	81036.2	10.253								
07:00	99382.052	16.694	31590.499	6.46	6867.586	3.937	28384.259	6.192	74697.25	9.591	52895.806	7.904	79305.323	10.057	80584.682	10.196								
08:00	99238.043	17.523	25590.066	5.971	10553.679	4.499	22338.246	5.702	77480.106	9.864	56227.548	8.134	82310.382	10.397	78760.55	9.998								
09:00	99349.675	17.157	26332.091	6.037	14436.677	4.951	23008.658	5.768	78786.739	10.001	52567.046	7.881	82674.717	10.451	78973.695	10.021								
10:00	99356.365	16.46	38080.872	6.89	18870.301	5.4	24853.248	5.921	79793.231	10.111	49573.244	7.668	82333.159	10.399	81306.589	10.284								
11:00	99333.389	16.334	49167.86	7.641	24356.035	5.88	28608.043	6.209	80934.875	10.241	49429.618	7.659	82348.441	10.406	83172.51	10.515								
12:00	99383.457	16.864	54587.354	8.017	27905.152	6.161	31151.452	6.407	81937.291	10.36	51394.572	7.802	76273.889	9.736	87300.527	11.106								
13:00	99278.348	17.416	57749.304	8.235	29307.875	6.265	31415.206	6.418	82505.947	10.429	57369.278	8.214	63028.409	8.624	89706.955	11.532								
14:00	99128.934	17.749	59427.451	8.357	29040.348	6.241	30777.014	6.371	83062.074	10.497	60948.575	8.47	68626.596	9.051	90078.552	11.616								
15:00	99122.275	17.76	59391.34	8.349	25193.696	5.945	29767.001	6.304	83750.64	10.59	59644.62	8.376	86850.573	11.038	89703.55	11.541								
16:00	99375.851	16.978	57832.151	8.249	20474.632	5.538	29044.578	6.247	84292.071	10.663	56074.862	8.117	93921.445	12.568	89807.618	11.561								
17:00	99195.918	15.915	54297.25	7.995	13290.124	4.832	30128.316	6.326	82669.919	10.445	53408.634	7.939	94476.638	12.737	89856.165	11.571								
18:00	98507.267	14.914	54086.295	7.983	7482.077	4.035	32681.769	6.519	80757.825	10.217	47225.525	7.512	92628.803	12.201	88915.665	11.39								
19:00	97685.474	14.232	56603.001	8.155	4426.706	3.456	35892.824	6.738	79381.122	10.066	35734.21	6.728	90811.928	11.767	87427.67	11.121								
20:00	96489.627	13.546	54587.368	8.017	7583.19	4.056	44830.193	7.349	77206.858	9.828	26468.626	6.045	87753.325	11.186	85747.873	10.864								
21:00	92980.903	12.297	50634.278	7.743	20709.728	5.559	58727.891	8.307	79324.886	10.059	31732.329	6.446	84581.58	10.703	84459.467	10.686								
22:00	89190.383	11.442	46900.932	7.489	37600.406	6.863	70017.108	9.168	84478.143	10.688	50210.49	7.721	81326.929	10.287	82105.607	10.375								
23:00	86740.936	11.014	43229.483	7.25	51959.945	7.835	76733.954	9.789	85345.637	10.811	65482.238	8.802	77500.611	9.866	77335.324	9.85								



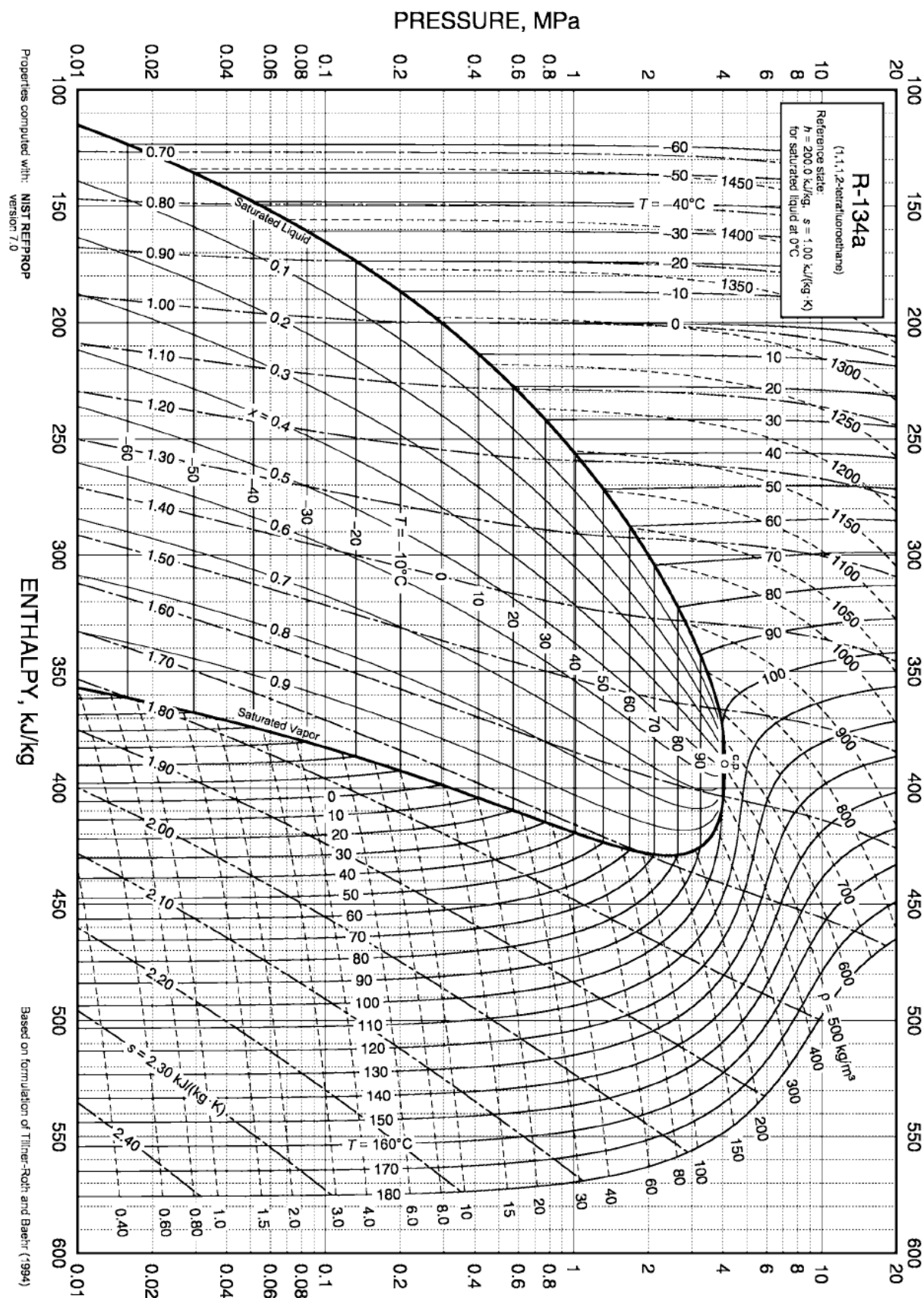
Ambient Temperature & Energy Demand Data

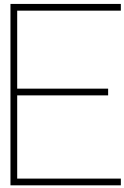
Hour\Day	7.02.2019			23.03.2019			7.05.2019			23.06.2019		
	Tamb (°C)	Industrial Hydrogen Demand (m³/s)	DHN Demand (m³/s)	Tamb (°C)	Industrial Hydrogen Demand (m³/s)	DHN Demand (m³/s)	Tamb (°C)	Industrial Hydrogen Demand (m³/s)	DHN Demand (m³/s)	Tamb (°C)	Industrial Hydrogen Demand (m³/s)	DHN Demand (m³/s)
00:00	6.8	0.00378603	4.82	8.6	0.003721860	4.64	5.3	0.0038395050	4.97	16.6	0.003436660	3.84
01:00	6.9	0.00378247	4.81	8.8	0.003714730	4.62	5.5	0.0038323750	4.95	17	0.003422400	3.8
02:00	7.3	0.00376821	4.77	8.8	0.003714730	4.62	5	0.0038502000	5	16.6	0.003436660	3.84
03:00	7.8	0.00375038	4.72	8.7	0.003718295	4.63	5.1	0.0038466350	4.99	16	0.003458050	3.9
04:00	8.1	0.00373969	4.69	8.7	0.003718295	4.63	4.9	0.0038537650	5.01	15.5	0.003475875	3.95
05:00	8.8	0.00371473	4.62	9	0.003707600	4.6	4.9	0.0038537650	5.01	15	0.003493700	4
06:00	9	0.00370760	4.6	9.2	0.003700470	4.58	5.3	0.0038395050	4.97	14.9	0.003497265	4.01
07:00	7.4	0.00376464	4.76	9.1	0.003704035	4.59	6.1	0.0038109850	4.89	16.3	0.003447355	3.87
08:00	6.8	0.00378603	4.82	9.3	0.003696905	4.57	8	0.0037432500	4.7	17.8	0.003393880	3.72
09:00	6.7	0.00378960	4.83	9.4	0.003693340	4.56	9.3	0.0036969050	4.57	19.9	0.003319015	3.51
10:00	7.1	0.00377534	4.79	9.3	0.003696905	4.57	11.5	0.0036184750	4.35	22.2	0.003237020	3.28
11:00	7.8	0.00375038	4.72	9.4	0.003693340	4.56	10.3	0.0036612550	4.47	24.4	0.003158590	3.06
12:00	8.1	0.00373969	4.69	9.1	0.003704035	4.59	12.5	0.0035828250	4.25	23.3	0.003197805	3.17
13:00	8.6	0.00372186	4.64	9.7	0.003682645	4.53	13.5	0.0035471750	4.15	22.8	0.003215630	3.22
14:00	8.6	0.00372186	4.64	9.9	0.003675515	4.51	12.7	0.0035756950	4.23	24.2	0.003165720	3.08
15:00	8.2	0.00373612	4.68	9.9	0.003675515	4.51	14	0.0035293500	4.1	24	0.003172850	3.1
16:00	7.8	0.00375038	4.72	9.4	0.003693340	4.56	14.6	0.0035079600	4.04	28.2	0.003137200	3
17:00	7.2	0.00377177	4.78	9.2	0.003700470	4.58	14.4	0.0035150900	4.06	28.7	0.003137200	3
18:00	7	0.00377890	4.8	8.2	0.003736120	4.68	14.6	0.0035079600	4.04	28.6	0.003137200	3
19:00	6.9	0.00378247	4.81	7.2	0.003771770	4.78	14.1	0.0035257850	4.09	27.8	0.003137200	3
20:00	6.7	0.00378960	4.83	6.9	0.003782465	4.81	13.5	0.0035471750	4.15	27.2	0.003137200	3
21:00	6.5	0.00379673	4.85	6.5	0.003796725	4.85	12.2	0.0035935200	4.28	26.4	0.003137200	3
22:00	6.4	0.00380029	4.86	5.8	0.003821680	4.92	11.2	0.0036291700	4.38	24.9	0.003140765	3.01
23:00	6.3	0.00380386	4.87	5.1	0.003846635	4.99	11.1	0.0036327350	4.39	24.2	0.003165720	3.08
Average	7.45	0.003762858	4.76	8.55	0.003723643	4.65	9.98	0.0036725	4.50	21.77	0.003277423	3.39

Hour\Day	7.08.2019			23.09.2019			7.11.2019			23.12.2019		
	Tamb (°C)	Industrial Hydrogen Demand (m³/s)	DHN Demand (m³/s)	Tamb (°C)	Industrial Hydrogen Demand (m³/s)	DHN Demand (m³/s)	Tamb (°C)	Industrial Hydrogen Demand (m³/s)	DHN Demand (m³/s)	Tamb (°C)	Industrial Hydrogen Demand (m³/s)	DHN Demand (m³/s)
00:00	18.6	0.003365360	3.64	16.1	0.003454485	3.89	7.1	0.003775335	4.79	8.6	0.00372186	4.64
01:00	18.7	0.003361795	3.63	16	0.00345805	3.9	6.8	0.00378603	4.82	8.7	0.003718295	4.63
02:00	18.4	0.003372490	3.66	15.9	0.003461615	3.91	6.1	0.003810985	4.89	8.9	0.003711165	4.61
03:00	18.5	0.003368925	3.65	15.9	0.003461615	3.91	6.2	0.00380742	4.88	8.7	0.003718295	4.63
04:00	18.3	0.003376055	3.67	15.8	0.00346518	3.92	6.1	0.003810985	4.89	8.4	0.00372899	4.66
05:00	18	0.003386750	3.7	15.7	0.003468745	3.93	7.2	0.00377177	4.78	8.2	0.00373612	4.68
06:00	18	0.003386750	3.7	15.8	0.00346518	3.92	7.6	0.00375751	4.74	8.4	0.00372899	4.66
07:00	17.2	0.003415270	3.78	15.7	0.003468745	3.93	8	0.00374325	4.7	7.5	0.003761075	4.75
08:00	18.1	0.003383185	3.69	15.7	0.003468745	3.93	7.7	0.003753945	4.73	7.4	0.00376464	4.76
09:00	18.7	0.003361795	3.63	15.7	0.003468745	3.93	8.3	0.003732555	4.67	8.3	0.003732555	4.67
10:00	19.2	0.003343970	3.58	16	0.00345805	3.9	8.7	0.003718295	4.63	8.1	0.003739685	4.69
11:00	20.1	0.003311885	3.49	16.1	0.003454485	3.89	8.7	0.003718295	4.63	8.3	0.003732555	4.67
12:00	20.4	0.003301190	3.46	17.7	0.003397445	3.73	8.7	0.003718295	4.63	8.5	0.003725425	4.65
13:00	17.7	0.003397445	3.73	16.8	0.00342953	3.82	8.3	0.003732555	4.67	8.8	0.00371473	4.62
14:00	20.1	0.003311885	3.49	17.9	0.003390315	3.71	8.4	0.00372899	4.66	8.8	0.00371473	4.62
15:00	21.7	0.003254845	3.33	19.1	0.003347535	3.59	8.1	0.003739685	4.69	8.9	0.003711165	4.61
16:00	21.8	0.003251280	3.32	19.1	0.003347535	3.59	8.3	0.003732555	4.67	8.4	0.00372899	4.66
17:00	21.9	0.003247715	3.31	18.4	0.00337249	3.66	8.8	0.00371473	4.62	8.4	0.00372899	4.66
18:00	21.5	0.003261975	3.35	18.6	0.00336536	3.64	9.2	0.00370047	4.58	8.2	0.00373612	4.68
19:00	20.8	0.003286930	3.42	17.5	0.003404575	3.75	7.9	0.003746815	4.71	8.1	0.003739685	4.69
20:00	19.8	0.003322580	3.52	15.6	0.00347231	3.94	7.4	0.00376464	4.76	8.5	0.003725425	4.65
21:00	19	0.003351100	3.6	15	0.0034937	4	7.2	0.00377177	4.78	9	0.0037076	4.6
22:00	19	0.003351100	3.6	13.8	0.00353648	4.12	6.9	0.003782465	4.81	8.6	0.00372186	4.64
23:00	18.9	0.003354665	3.61	15.8	0.00346518	3.92	6.5	0.003796725	4.85	8	0.00374325	4.7
Average	19.35	0.003338623	3.57	16.49	0.003440671	3.85	7.68	0.003754836	4.73	8.40	0.00372884	4.66

D

R134a Pressure - Enthalpy Table





Key Modelling Assumptions

E.1. Power-to-Gas

- Electrolyser
 - Electrolyser cells are assembled into stacks and connected in parallel for 50 MW capacity.
 - Concentration overpotential of electrolyser cell is ignored.
 - Ideal gas behaviour is assumed.
 - Temperature of the water in contact with the cell membrane is assumed to be uniform in the stack.
 - Operational pressure effects are ignored.
- Storage
 - Constant temperature and pressure inside compressed hydrogen storage tank is assumed.
 - Static and dynamic losses are ignored.
 - Charging/discharging rate is assumed to be large enough.

E.2. Power-to-Heat

- Heat Pump
 - Influence of part load efficiency is ignored.
 - Heat exchangers are supposed at hot start in equilibrium with the external sources and heat exchange is ideal.
 - Refrigerant massflow inside heatpump is assumed to be constant.
 - Isenthalpic flow across the expansion valve; and isentropic efficiency for the compressor.
- Storage
 - Constant temperature and pressure inside the hydrogen storage tank.
 - Static and dynamic losses are ignored.
 - Uniform temperature in the hot water reservoir (stratification is not considered)
 - No external heat loss from the reservoir wall
 - The total amount of hot water in the reservoir is conserved (No water consumption during heating process).
 - Charging/discharging rate is assumed to be large enough.

E.3. Multi-Energy System

- Power electronic converters are assumed to be ideal.
- Grid is able to provide flexible capacity when it is necessary.

F

Modelica Power-to-Gas Model Parameters

Parameter	Value	Remark
V_{std}	1.23 V	Cell voltage at standard conditions
T_{std}	298.15 °C	Standard Temperature
F	96485 C/mol	Faraday constant
R	8.314 JK ⁻¹ mol ⁻¹	Ideal gas constant
P_{cat}	30 bar	Pressure at cathode side
P_{an}	30 bar	Pressure at anode side
α_{an}	0.7353	Charge transfer coefficient at anode
$\sigma_{mem,std}$	10.31	Membrane conductivity at standard temperature
C_{th}	162116 J/K	Thermal capacitance of electrolyser
R_{th}	0.0668 K/W	Thermal resistance of electrolyser
V_{tn}	1.48 V	Minimum energy in electricity to heat to perform electrolysis(V)
n_{cells}	60	Number of cells per stack
V	100 m ³	Storage capacity
S_{base}	50 MW	Base power of system
$A_{membrane}$	290 cm ²	Membrane area
δ_{mem}	178e-6 m	Membrane thickness
K_{gain}	18000	Controller gain

G

Modelica Power-to-Heat Model Parameters

Parameter	Value	Remark
\dot{m}	5 kg/s	Water massflow rate
c_p	4.190 kJ/(Kkg)	Specific heat of water at 70 °C
ρ	977.74 kg/m³	Water density at 70 °C
V	2400 m³	Storage capacity
S_{base}	50 MW	Base power of system
K_{gain}	3	Controller gain
$a_{1,T_{50}}$	3.46e-8	First coefficient
$a_{2,T_{50}}$	1.29e-6	Second coefficient
$a_{3,T_{50}}$	4.35e-5	Third coefficient
$a_{4,T_{50}}$	2.387e-3	Fourth coefficient
$a_{5,T_{50}}$	1.186e-1	Fifth coefficient
$a_{6,T_{50}}$	5.063	Sixth coefficient
$a_{1,T_{70}}$	1.46e-8	First coefficient
$a_{2,T_{70}}$	-9.66e-8	Second coefficient
$a_{3,T_{70}}$	6.61e-6	Third coefficient
$a_{4,T_{70}}$	1.01e-3	Fourth coefficient
$a_{5,T_{70}}$	5.864e-2	Fifth coefficient
$a_{6,T_{70}}$	3.295	Sixth coefficient

Bibliography

- [1] Zon op de slufter: exploitant gezocht voor grootste drijvende zonnepark van nederland, May 2019. URL <https://www.portofrotterdam.com/nl/nieuws-en-persberichten/zon-op-de-slufter>.
- [2] The Future of Hydrogen. *The Future of Hydrogen*, (June), 2019. doi: 10.1787/1e0514c4-en.
- [3] World Energy Outlook 2019. *International Energy Agency*, 2019. ISSN 1387-1811. doi: DOE/EIA-0383(2012)U.S. URL <https://www.eia.gov/outlooks/aoe/pdf/aoe2019.pdf>.
- [4] Alliander; ECN. Demand and supply of flexibility in the power system of the Netherlands, 2015-2050. *Summary report of the FLEXNET project*, (November 2017):70, 2017.
- [5] P K S Ayivor, J L Rueda Torres, and Mart A M M van der Meijden. Modelling of Large Size Electrolyser for Electrical Grid Stability Studies - A Hierarchical Control Approach. *17th International Wind Integration Workshop*, (October), 2018.
- [6] Bjarne Bach, Jesper Werling, Torben Ommen, Marie Münster, Juan M. Morales, and Brian Elmegaard. Integration of large-scale heat pumps in the district heating systems of Greater Copenhagen. *Energy*, 107:321–334, 2016. ISSN 03605442. doi: 10.1016/j.energy.2016.04.029. URL <http://dx.doi.org/10.1016/j.energy.2016.04.029>.
- [7] John Barton, Sikai Huang, David Infield, Matthew Leach, Damiete Ogunkunle, Jacopo Torriti, and Murray Thomson. The evolution of electricity demand and the role for demand side participation, in buildings and transport. *Energy Policy*, 52:85–102, 2013. ISSN 03014215. doi: 10.1016/j.enpol.2012.08.040. URL <http://dx.doi.org/10.1016/j.enpol.2012.08.040>.
- [8] Morten B. Blarke. Towards an intermittency-friendly energy system: Comparing electric boilers and heat pumps in distributed cogeneration. *Applied Energy*, 91(1):349–365, 2012. ISSN 03062619. doi: 10.1016/j.apenergy.2011.09.038. URL <http://dx.doi.org/10.1016/j.apenergy.2011.09.038>.
- [9] Andreas Bloess, Wolf Peter Schill, and Alexander Zerrahn. Power-to-heat for renewable energy integration: A review of technologies, modeling approaches, and flexibility potentials. *Applied Energy*, 212 (December 2017):1611–1626, 2018. ISSN 03062619. doi: 10.1016/j.apenergy.2017.12.073.
- [10] Carsten Bode and Gerhard Schmitz. Dynamic simulation and comparison of different configurations for a coupled energy system with 100% renewables. *Energy Procedia*, 155:412–430, 2018. ISSN 18766102. doi: 10.1016/j.egypro.2018.11.037. URL <https://doi.org/10.1016/j.egypro.2018.11.037>.
- [11] B. O. Bolaji and Z. Huan. Energy performance of eco-friendly RE170 and R510A refrigerants as alternatives to R134a in vapour compression refrigeration system. *Proceedings of the 9th Conference on the Industrial and Commercial Use of Energy, ICUE 2012*, (July):139–146, 2012.
- [12] Kenneth Bruninx, Dieter Patteeuw, Erik Delarue, Lieve Helsen, and William D’Haeseleer. Short-term demand response of flexible electric heating systems: The need for integrated simulations. *International Conference on the European Energy Market, EEM*, (March), 2013. ISSN 21654077. doi: 10.1109/EEM.2013.6607333.
- [13] Van Hai Bui, Akhtar Hussain, and Hak Man Kim. A multiagent-based hierarchical energy management strategy for multi-microgrids considering adjustable power and demand response. *IEEE Transactions on Smart Grid*, 9(2):1323–1333, 2018. ISSN 19493053. doi: 10.1109/TSG.2016.2585671.
- [14] Marwan Chamoun, Romuald Rulliere, Philippe Haberschill, and Jean Francois Berail. Dynamic model of an industrial heat pump using water as refrigerant. *International Journal of Refrigeration*, 35(4):1080–1091, 2012. ISSN 01407007. doi: 10.1016/j.ijrefrig.2011.12.007. URL <http://dx.doi.org/10.1016/j.ijrefrig.2011.12.007>.

- [15] Xinyu Chen, Xi Lu, Michael B. McElroy, Chris P. Nielsen, and Chongqing Kang. Synergies of wind power and electrified space heating: Case study for Beijing. *Environmental Science and Technology*, 48(3):2016–2024, 2014. ISSN 0013936X. doi: 10.1021/es405653x.
- [16] Yongbao Chen, Peng Xu, Jiefan Gu, Ferdinand Schmidt, and Weilin Li. Measures to improve energy demand flexibility in buildings for demand response (DR): A review. *Energy and Buildings*, 177:125–139, 2018. ISSN 03787788. doi: 10.1016/j.enbuild.2018.08.003. URL <https://doi.org/10.1016/j.enbuild.2018.08.003>.
- [17] Tullie Circle. *2013 ASHRAE Handbook—Fundamentals*. 2013. ISBN 1936504472.
- [18] Jonathan M. Cullen and Julian M. Allwood. The efficient use of energy: Tracing the global flow of energy from fuel to service. *Energy Policy*, 38(1):75–81, 2010. ISSN 03014215. doi: 10.1016/j.enpol.2009.08.054. URL <http://dx.doi.org/10.1016/j.enpol.2009.08.054>.
- [19] Michael Diekerhof, Antonello Monti, and Sebastian Schwarz. *Demand-side management- recent aspects and challenges of optimization for an efficient and robust demand-side management*. Elsevier Inc., 2018. ISBN 9780128124420. doi: 10.1016/B978-0-12-812441-3.00012-4. URL <http://dx.doi.org/10.1016/B978-0-12-812441-3.00012-4>.
- [20] Manuel Espinosa-López, Christophe Darras, Philippe Poggi, Raynal Glises, Philippe Baucour, André Rakotondrainibe, Serge Besse, and Pierre Serre-Combe. Modelling and experimental validation of a 46 kW PEM high pressure water electrolyzer. *Renewable Energy*, 119:160–173, 2018. ISSN 18790682. doi: 10.1016/j.renene.2017.11.081.
- [21] Björn Felten, Jan Paul Baginski, and Christoph Weber. KWK-Mindest- und Maximaleinspeisung - Die Erzeugung von Zeitreihen für die Energiesystemmodellierung. (10), 2017.
- [22] R. García-Valverde, N. Espinosa, and A. Urbina. Simple PEM water electrolyser model and experimental validation. *International Journal of Hydrogen Energy*, 37(2):1927–1938, 2012. ISSN 03603199. doi: 10.1016/j.ijhydene.2011.09.027.
- [23] Digvijay Gusain, Miloš Cvetković, and Peter Palensky. Energy flexibility analysis using FMUWorld. *2019 IEEE Milan PowerTech, PowerTech 2019*, 2019. doi: 10.1109/PTC.2019.8810433.
- [24] Kofi E. Hagan, Olufemi O. Oyebajo, Tarek Medalel Masaud, and Rajab Challoo. A probabilistic forecasting model for accurate estimation of PV solar and wind power generation. *2016 IEEE Power and Energy Conference at Illinois, PECon 2016*, pages 1–5, 2016. doi: 10.1109/PECI.2016.7459241.
- [25] Karsten Hedegaard, Brian Vad Mathiesen, Henrik Lund, and Per Heiselberg. Wind power integration using individual heat pumps - Analysis of different heat storage options. *Energy*, 47(1):284–293, 2012. ISSN 03605442. doi: 10.1016/j.energy.2012.09.030. URL <http://dx.doi.org/10.1016/j.energy.2012.09.030>.
- [26] Bongghi Hong and Robert W. Howarth. Greenhouse gas emissions from domestic hot water: Heat pumps compared to most commonly used systems. *Energy Science and Engineering*, 4(2):123–133, 2016. ISSN 20500505. doi: 10.1002/ese3.112.
- [27] Iea. Clean and efficient heat for industry – analysis. URL <https://www.iea.org/commentaries/clean-and-efficient-heat-for-industry>.
- [28] Intelligent Energy Europe. Guidelines for technical assessment of District Heating systems. URL www.ecoheat4cities.eu.
- [29] IRENA. *Hydrogen From Renewable Power: Technology outlook for the energy transition*. Number September. 2018. ISBN 9789292600778. URL www.irena.org.
- [30] Huiyong Kim, Mikyoung Park, and Kwang Soon Lee. One-dimensional dynamic modeling of a high-pressure water electrolysis system for hydrogen production. *International Journal of Hydrogen Energy*, 38(6):2596–2609, 2013. ISSN 03603199. doi: 10.1016/j.ijhydene.2012.12.006. URL <http://dx.doi.org/10.1016/j.ijhydene.2012.12.006>.

- [31] Jan Christian Koj, Christina Wulf, and Petra Zapp. Environmental impacts of power-to-X systems - A review of technological and methodological choices in Life Cycle Assessments. *Renewable and Sustainable Energy Reviews*, 112(November 2018):865–879, 2019. ISSN 18790690. doi: 10.1016/j.rser.2019.06.029. URL <https://doi.org/10.1016/j.rser.2019.06.029>.
- [32] Fabian Levihn. CHP and heat pumps to balance renewable power production: Lessons from the district heating network in Stockholm. *Energy*, 137:670–678, 2017. ISSN 03605442. doi: 10.1016/j.energy.2017.01.118. URL <https://doi.org/10.1016/j.energy.2017.01.118>.
- [33] Francisco Da Costa Lopes and Edson H. Watanabe. Experimental and theoretical development of a PEM electrolyzer model applied to energy storage systems. *2009 Brazilian Power Electronics Conference, COBEP2009*, (2):775–782, 2009. doi: 10.1109/COBEP.2009.5347619.
- [34] Introduction Low-carbon. Netherlands Government Strategy on Hydrogen. *Report*, (387):1–14, 2020.
- [35] Peter D. Lund, Juuso Lindgren, Jani Mikkola, and Jyri Salpakari. Review of energy system flexibility measures to enable high levels of variable renewable electricity. *Renewable and Sustainable Energy Reviews*, 45:785–807, 2015. ISSN 13640321. doi: 10.1016/j.rser.2015.01.057. URL <http://dx.doi.org/10.1016/j.rser.2015.01.057>.
- [36] Pierluigi Mancarella. MES (multi-energy systems): An overview of concepts and evaluation models. *Energy*, 65:1–17, 2014. ISSN 03605442. doi: 10.1016/j.energy.2013.10.041. URL <http://dx.doi.org/10.1016/j.energy.2013.10.041>.
- [37] Pierluigi Mancarella and Gianfranco Chicco. Integrated energy and ancillary services provision in multi-energy systems. *Proceedings of IREP Symposium: Bulk Power System Dynamics and Control - IX Optimization, Security and Control of the Emerging Power Grid, IREP 2013*, (ii), 2013. doi: 10.1109/IREP.2013.6629423.
- [38] Luis Gabriel Marín, Mark Sumner, Diego Muñoz-Carpintero, Daniel Köbrich, Seksak Pholboon, Doris Sáez, and Alfredo Núñez. Hierarchical energy management system for microgrid operation based on robust model predictive control. *Energies*, 12(23), 2019. ISSN 19961073. doi: 10.3390/en12234453.
- [39] B. V. Mathiesen and H. Lund. Comparative analyses of seven technologies to facilitate the integration of fluctuating renewable energy sources. *IET Renewable Power Generation*, 3(2):190–204, 2009.
- [40] G. Migoni, P. Rullo, F. Bergero, and E. Kofman. Efficient simulation of Hybrid Renewable Energy Systems. *International Journal of Hydrogen Energy*, 41(32):13934–13949, 2016. ISSN 03603199. doi: 10.1016/j.ijhydene.2016.06.019. URL <http://dx.doi.org/10.1016/j.ijhydene.2016.06.019>.
- [41] Modelica Association. Modelica Language Specification. 2017.
- [42] Mohammad Mohammadi, Younes Noorollahi, Behnam Mohammadi-ivatloo, and Hossein Yousefi. Energy hub: From a model to a concept – A review. *Renewable and Sustainable Energy Reviews*, 80 (December 2016):1512–1527, 2017. ISSN 18790690. doi: 10.1016/j.rser.2017.07.030.
- [43] Theresa Müller and Dominik Möst. Demand Response Potential: Available when Needed? *Energy Policy*, 115(February 2017):181–198, 2018. ISSN 03014215. doi: 10.1016/j.enpol.2017.12.025. URL <https://doi.org/10.1016/j.enpol.2017.12.025>.
- [44] Pierre Olivier, Cyril Bourasseau, and Pr Belkacem Bouamama. Low-temperature electrolysis system modelling: A review. *Renewable and Sustainable Energy Reviews*, 78(February):280–300, 2017. ISSN 18790690. doi: 10.1016/j.rser.2017.03.099.
- [45] Kazuo Onda, Toshio Murakami, Takeshi Hikosaka, Misaki Kobayashi, Ryouhei Notu, and Kohei Ito. Performance Analysis of Polymer-Electrolyte Water Electrolysis Cell at a Small-Unit Test Cell and Performance Prediction of Large Stacked Cell. *Journal of The Electrochemical Society*, 149(8):A1069, 2002. ISSN 00134651. doi: 10.1149/1.1492287.
- [46] Poul Alberg Østergaard. Comparing electricity, heat and biogas storages' impacts on renewable energy integration. *Energy*, 37(1):255–262, 2012. ISSN 03605442. doi: 10.1016/j.energy.2011.11.039. URL <http://dx.doi.org/10.1016/j.energy.2011.11.039>.

- [47] Peter Palensky and Dietmar Dietrich. Demand side management: Demand response, intelligent energy systems, and smart loads. *IEEE Transactions on Industrial Informatics*, 7(3):381–388, 2011. ISSN 15513203. doi: 10.1109/TII.2011.2158841.
- [48] G. Papaefthymiou, B. Hasche, and C. Nabe. Potential of heat pumps for demand side management and wind power integration in the German electricity market. *IEEE Transactions on Sustainable Energy*, 3(4): 636–642, 2012. ISSN 19493029. doi: 10.1109/TSTE.2012.2202132.
- [49] Position Paper. *Flexibility concepts for the German power supply in 2050*. Number February. 2016. ISBN 9783804735491.
- [50] B. Parkinson, P. Balcombe, J. F. Speirs, A. D. Hawkes, and K. Hellgardt. Levelized cost of CO₂ mitigation from hydrogen production routes. *Energy and Environmental Science*, 12(1):19–40, 2019. ISSN 17545706. doi: 10.1039/c8ee02079e. URL <http://dx.doi.org/10.1039/C8EE02079E>.
- [51] Raul Rodríguez Pearson. Pvsystems: A modelica library for photovoltaic system and power converter design. URL <https://raulrpearson.github.io/PVSystems/index.html#PVSystems>.
- [52] M. K. Petersen, K. Edlund, L. H. Hansen, J. Bendtsen, and J. Stoustrup. A taxonomy for modeling flexibility and a computationally efficient algorithm for dispatch in Smart Grids. *Proceedings of the American Control Conference*, pages 1150–1156, 2013. ISSN 07431619. doi: 10.1109/acc.2013.6579991.
- [53] Stefan Pfenninger and Iain Staffell. URL <http://www.renewables.ninja/>.
- [54] Stefan Pfenninger and Iain Staffell. Long-term patterns of European PV output using 30 years of validated hourly reanalysis and satellite data. *Energy*, 114:1251–1265, 2016. ISSN 03605442. doi: 10.1016/j.energy.2016.08.060. URL <http://dx.doi.org/10.1016/j.energy.2016.08.060>.
- [55] Heat Pumps, I N Combination, With District, Increases Energy, and Efficiency At. Heat pumps in combination with district heating increases energy efficiency at hammarbyverket.
- [56] Jonathan Reynolds, Muhammad Waseem Ahmad, and Yacine Rezgui. Holistic modelling techniques for the operational optimisation of multi-vector energy systems. *Energy and Buildings*, 169:397–416, 2018. ISSN 03787788. doi: 10.1016/j.enbuild.2018.03.065. URL <https://doi.org/10.1016/j.enbuild.2018.03.065>.
- [57] Rijkswaterstaat. Nieuw windpark maasvlakte 2, Mar 2020. URL <https://www.rijkswaterstaat.nl/nieuws/2020/03/ministerie-infrastructuur-en-waterstaat-verduurzaamt-met-nieuw-windpark-tweede-maasvlakte.aspx>.
- [58] Jyri Salpakari, Jani Mikkola, and Peter D. Lund. Improved flexibility with large-scale variable renewable power in cities through optimal demand side management and power-to-heat conversion. *Energy Conversion and Management*, 126:649–661, 2016. ISSN 01968904. doi: 10.1016/j.enconman.2016.08.041. URL <http://dx.doi.org/10.1016/j.enconman.2016.08.041>.
- [59] Paul Schott, Johannes Sedlmeir, Nina Strobel, Thomas Weber, Gilbert Fridgen, and Eberhard Abele. A generic data model for describing flexibility in power markets. *Energies*, 12(10):1–29, 2019. ISSN 19961073. doi: 10.3390/en12101893.
- [60] Iain Staffell and Stefan Pfenninger. Using bias-corrected reanalysis to simulate current and future wind power output. *Energy*, 114:1224–1239, 2016. ISSN 03605442. doi: 10.1016/j.energy.2016.08.068. URL <http://dx.doi.org/10.1016/j.energy.2016.08.068>.
- [61] Leon Thurner, Alexander Scheidler, Florian Schafer, Jan Hendrik Menke, Julian Dollichon, Friederike Meier, Steffen Meinecke, and Martin Braun. Pandapower - An Open-Source Python Tool for Convenient Modeling, Analysis, and Optimization of Electric Power Systems. *IEEE Transactions on Power Systems*, 33(6):6510–6521, 2018. ISSN 08858950. doi: 10.1109/TPWRS.2018.2829021.
- [62] Bart W. Tuinema, Ebrahim Adabi, Patrick K.S. Ayivor, Víctor García Suárez, Lian Liu, Arcadio Perilla, Zameer Ahmad, José Luis Rueda Torres, Mart A.M.M. Van Der Meijden, and Peter Palensky. Modelling of large-sized electrolyzers for realtime simulation and study of the possibility of frequency support by electrolyzers. *IET Generation, Transmission and Distribution*, 14(10):1985–1992, 2020. ISSN 17518687. doi: 10.1049/iet-gtd.2019.1364.

- [63] Andreas Ulbig, Matthias A Bucher, and Göran Andersson. Operational Flexibility of Power Systems. In *Renewable Energy Integration*, pages 201–216. Elsevier, 2017. ISBN 9780128095928. doi: 10.1016/B978-0-12-809592-8.00015-9. URL <https://linkinghub.elsevier.com/retrieve/pii/B9780128095928000159>.
- [64] United Nations. Summary of the Paris Agreement. *United Nations Framework Convention on Climate Change*, pages 27–52, 2015. URL <http://bigpicture.unfccc.int/#content-the-paris-agreement>.
- [65] L. Vanfretti, T. Rabuzin, M. Baudette, and M. Murad. iTesla Power Systems Library (iPSL): A Modelica library for phasor time-domain simulations. *SoftwareX*, 5(September 2007):84–88, 2016. ISSN 23527110. doi: 10.1016/j.softx.2016.05.001. URL <http://dx.doi.org/10.1016/j.softx.2016.05.001>.
- [66] Clara Verhelst, Filip Logist, Jan Van Impe, and Lieve Helsen. Study of the optimal control problem formulation for modulating air-to-water heat pumps connected to a residential floor heating system. *Energy and Buildings*, 45:43–53, 2012. ISSN 03787788. doi: 10.1016/j.enbuild.2011.10.015. URL <http://dx.doi.org/10.1016/j.enbuild.2011.10.015>.
- [67] John Webster and Carsten Bode. Implementation of a Non-Discretized Multiphysics PEM Electrolyzer Model in Modelica. *Proceedings of the 13th International Modelica Conference, Regensburg, Germany, March 4–6, 2019*, 157:833–840, 2019. doi: 10.3384/ecp19157833.
- [68] Jens Weibezahl. Data Documentation 92: Electricity, Heat, and Gas Sector Data for Modeling the German System. *DIW Berlin*, 2017, (ISSN 1861-1532), 2017.
- [69] Edmund Widl, Tobias Jacobs, Daniel Schwabeneder, Sebastien Nicolas, Daniele Basciotti, Sawsan Henein, Tae Gil Noh, Olatz Terreros, Anett Schuelke, and Hans Auer. Studying the potential of multi-carrier energy distribution grids: A holistic approach. *Energy*, 153:519–529, 2018. ISSN 03605442. doi: 10.1016/j.energy.2018.04.047. URL <https://doi.org/10.1016/j.energy.2018.04.047>.
- [70] W. Yang, M.A. Wilkinson, and P.J. Tavner. Condition monitoring and fault diagnosis of a wind turbine synchronous generator drive train. *IET Renewable Power Generation*, 3(1):1–11, 2003. doi: 10.1049/iet-rpg.